70-20,683

MORRIS, Jr., Charles Franklin, 1942-
   THE EFFECTS OF PARTIALLY COHERENT RADIATION
   ON THE PERFORMANCE OF AN OPTICAL HETERODYNE
   RECEIVER.

   Georgia Institute of Technology, Ph.D., 1970
   Engineering, electrical

University Microfilms, A XEROX Company, Ann Arbor, Michigan

THE EFFECTS OF PARTIALLY COHERENT RADIATION ON THE

PERFORMANCE OF AN OPTICAL HETERODYNE RECEIVER

A THESIS

Presented to

The Faculty of the Graduate Division

by

Charles Franklin Morris, Jr.

In Partial Fulfillment

of the Requirements for the Degree

Doctor of Philosophy

in the School of Electrical Engineering

Georgia Institute of Technology

January, 1970

In presenting the dissertation as a partial fulfillment of
the requirements for an advanced degree from the Georgia
Institute of Technology, I agree that the Library of the
Institute shall make it available for inspection and
circulation in accordance with its regulations governing
materials of this type. I agree that permission to copy
from, or to publish from, this dissertation may be granted
by the professor under whose direction it was written, or,
in his absence, by the Dean of the Graduate Division when
such copying or publication is solely for scholarly purposes
and does not involve potential financial gain. It is under-
stood that any copying from, or publication of, this dis-
sertation which involves potential financial gain will not
be allowed without written permission.

Charles F. Mound

7/25/68

THE EFFECTS OF PARTIALLY COHERENT RADIATION ON THE

PERFORMANCE OF AN OPTICAL HETERODYNE RECEIVER

Approved:

_____
Chairman

_____
Ray H. Pettit

_____

Date approved by Chairman: _____

ACKNOWLEDGMENTS

Dr. William B. Jones, Jr. was my thesis advisor for the initial stages of my Doctoral research and provided much helpful guidance. Many worthwhile discussions with Bill Mayo, at the time a Ph.D. student and now graduated, contributed a great deal to the formulation of the problem and the statistical approach presented in Appendix II. When Dr. Jones left Georgia Tech, Dr. Aubrey M. Bush became my advisor. He provided many helpful suggestions and much guidance during the intermediate and final stages of the research. Dr. F. Kenneth Hurd also provided much assistance during this period and he with Dr. Bush helped me in getting all the equipment necessary for the experimental work. Dr. Albert P. Sheppard and Dr. Ray H. Pettit served as members of my reading committee and provided many worthwhile suggestions for the experimental work.

My first three years of graduate school were financed by a NASA fellowship; the last two by a Teaching and Research Assistantship provided by Dr. B. J. Dasher, then Director of the School of Electrical Engineering and continued by Dr. D. T. Paris, the present Director. The experimental facilities were provided by the School of Electrical Engineering. The computer facilities were provided by the Rich Electronic Computer Center. The staff of the computer center, and in particular Mr. S. P. Lenoir, Mr. Jerry Segers, and Mr. Leon Kinard were

always very considerate in assisting me with the problems that arose in this area.

My wife, Elizabeth, spent many long hours typing rough drafts; Betty Sims typed the final version of the thesis.

My wife, Elizabeth, and daughter, Martha, shared with me the life of a graduate student.

To these people, I express my deepest appreciation and most heartfelt thanks.

TABLE OF CONTENTS

LIST OF TABLES

LIST OF ILLUSTRATIONS

Figure   Page

ix

Figure   Page

35. A Plot of $v_{DC}/v_{DC_{max}}$ Versus R_A/a
     for an Ideal Gaussian Beam. 116

36. The Experimental Arrangement for
     Measuring Local Oscillator Coherence. 117

37. Data from the Coherence Measurements. 117

38. A Plot of κ Versus R_A/a for
     Gaussian I_L and Constant I_s 121

39. Photographs of the LDSV Experimental Setup. 123

40. Typical Scope Waveforms 125

41. The Experimental Setup for Determining. 128

42. Plots of the Data for Case 1. 130

43. Plots of the Data for Case 2. 132

44. Plots of the Data for Case 3. 134

45. Plots of the Data for Case 4. 136

46. Error Bounds for Case 1 137

47. Error Bounds for Case 2 138

48. Error Bounds for Case 3 139

49. Error Bounds for Case 4 140

50. Photographs of the LDF Experimental Setup 142

51. Typical Scope Waveforms 144

52. Plots of the Data for Cases 1 and 2 148

53. Plots of the Data for Case 3. 150

54. Photomultiplier Gain Curve. 151

55. Error Bounds for Case 1 153

56. Error Bounds for Case 2 154

Reproduced with permission of the copyright owner. Further reproduction prohibited without permission.

SUMMARY

Heterodyne detection of optical signals offers, potentially, several advantages over other methods of detection, including inherent gain and high discrimination against noise. In many cases, to realize these advantages, the optical heterodyning must be done efficiently. This places some rather stringent requirements on the alignment of the optical system and the coherence of the signal and local oscillator fields.

This research is a study of the effects of partial coherence of the signal and local oscillator fields on the performance of an optical heterodyne receiver; the heterodyne receiver efficiency and signal-to-noise ratio are taken as performance indicators. An analytical approach is taken where the heterodyne receiver efficiency and signal-to-noise ratio are defined mathematically for a general heterodyne system. Each is, then, related to the signal and local oscillator field coherence in a single expression. These expressions are applied to three specific heterodyne systems: (1) a communications link through a turbulent atmosphere, (2) a laser heterodyne rough surface velocity measuring system, and (3) a laser heterodyne fluid flow velocity measuring system. In each system, the signal field coherence function is derived based on a statistical description of the system, and the heterodyne efficiency and signal-to-noise ratio are calculated and studied as functions of the receiver variables such as receiver aperture size and shape, local

oscillator field intensity distribution, and local oscillator coherence.

From this study, the conclusions made are that for the heterodyne systems studied, efficient operation and good signal-to-noise ratios cannot be obtained simultaneously; the most important parameters are the size of the local oscillator intensity distribution and the size of the receiver aperture. The shape of the local oscillator intensity distribution and the shape of the receiver aperture have little effect on system performance, nor do slight reductions in local oscillator coherence.

The performance of the surface velocity and fluid flow velocity measuring systems was studied experimentally. The experimentally measured efficiency and signal-to-noise ratio were compared to that predicted theoretically and found to be in close agreement.

CHAPTER I

INTRODUCTION

Heterodyne detection has been used in many communication and measurement systems for some time and its principles and advantages have long been understood. Prior to the availability of a coherent light source, the use of heterodyning was confined to RF and microwave frequencies. With the development of the laser, a coherent source of light, an almost immediate extension of heterodyne principles to optical frequencies was attempted by many in the hope of realizing the advantages heterodyning has in certain applications. It was soon apparent, however, that heterodyning at optical frequencies presented many unexpected and previously unencountered problems. These problems lay primarily in the stringent requirements made on the alignment of the optical system and on the incoming signal field coherence. In some systems, these problems were severe enough to make heterodyning impractical.

These problems originate from the fact that heterodyning at optical frequencies is basically a distributed phenomenon; an incoming signal and a locally produced signal (called a local oscillator) exist as fields that are superimposed over a photoelectric detector surface. The heterodyne signal in the photodetector output current arises from the mutual interference of the signal and local oscillator fields on the photosurface. The interference pattern formed will fluctuate in intensity at a rate equal to the frequency difference in the two fields.

The output current is proportional to the intensity and will likewise fluctuate at the difference frequency.

The total photodetector current is the sum of contributions from each elemental area of the photosurface. Therefore, for a maximum heterodyne signal, these currents and hence the intensity fluctuations at each point on the photosurface must all be exactly in phase. This requires the two interfering fields to have the same relative phase relationship over the photosurface; that is, the wavefronts of both fields must be coincident. This, in turn, requires two things:

1. The signal and local oscillator fields must have the same direction of propagation.

2. The signal and local oscillator fields must be individually spatially coherent over the photosurface.[*]

The first condition is met by proper alignment of the two fields. The second is met by the use of spatially coherent signal and local oscillator fields. Due to the smallness of an optical wavelength, both conditions are frequently very difficult if not impossible to achieve.

The alignment problems have been extensively studied and by now are very well understood. The coherence problems have received only minor attention, however, and none using the terminology of coherence theory. There are many systems where the signal field coherence is a limiting factor in the performance of the system: in an earthbound optical communications link or radar system where the signal field

---

[*]Except in a special case where both beams are distorted in the same way, i.e. individually incoherent but coherent with each other.

coherence is degraded by propagating through a turbulent atmosphere;
in a measurement system employing light scattering from a random medium
as a signal. Because heterodyning can provide improved signal-to-noise
ratios in the communication uses and improved sensitivity and selec-
tivity in certain measurement systems, it is important to know the
effects of signal field coherence on the heterodyne system operation.

This research is a study of the effects of partial coherence of
the signal and local oscillator fields on the performance of an optical
heterodyne detector. The heterodyne system efficiency and the output
signal-to-noise ratio serve as performance indicators. An analytical
approach is taken where the heterodyne efficiency and signal-to-noise
ratio are each defined for a general system and related to the signal
and local oscillator field coherence in single expressions. These
expressions are applied to three specific systems in which coherence is
a problem: (1) an optical communications link through a turbulent
atmosphere, (2) a laser heterodyne fluid flow measuring system, and
(3) a laser heterodyne rough surface measuring system. In each system,
the signal field coherence function is derived based on a statistical
description of the system and the heterodyne efficiency and signal-to-
noise ratio are calculated and studied as functions of receiver vari-
ables such as receiver aperture size and shape, local oscillator inten-
sity function, etc.

Some of these results are studied experimentally in the fluid
flow and rough surface measuring systems. The principle objective is
to verify the applicability of the analytical work.

The organization is as follows: The necessary background material on coherence, interference, and heterodyne detection theory is presented in Chapter II. The derivation of the heterodyne efficiency and signal-to-noise ratio expressions in terms of the signal and local oscillator coherence functions is made in Chapter III. The three systems mentioned above are studied as examples in Chapter IV, the experimental work is presented in Chapter V, and general conclusions as well as some suggestions for future work are presented in Chapter VI.

CHAPTER II

BACKGROUND

Introduction

The interrelation of the coherence of radiation, its inter-
ference, and heterodyne detection form the basis of this study. In
this chapter, the central concepts of the coherence and interference
of radiation and optical heterodyne detection are presented and dis-
cussed. The theory of coherence is first discussed, then the theory
of interference and its relation to coherence theory. Finally hetero-
dyne detection is discussed in terms of interference and coherence
theory. Only the theory necessary to the understanding of this problem
and its development is presented. For a more detailed study, the
reader is referred to the literature cited.

The Coherence of Optical Fields

The concept of a monochromatic wave is very useful in electro-
magnetic field theory and optics. A necessary starting point in many
problems is the examination of the monochromatic case. For such fields,
the amplitude and phase of the wave are deterministic functions of
space and time.

Every physical optical field, however, has some fluctuations
associated with it. These fluctuations may be small and slow so that
the field is essentially constant in amplitude and phase over several

optical periods. In this case, the field looks like a monochromatic field except for small fluctuations about an average amplitude and phase. For this reason, this type of field is called quasi-monochromatic. On the other hand, these fluctuations may be large and rapid. In this case, no average amplitude or phase is discernible. This type of field is called polychromatic.

Optical coherence theory is concerned, in general, with a statistical description of these fields. Most of the work to date has been on second order effects, that is, on the correlation between these fluctuations in the field at two different points. These second order effects are related to the interference phenomenon and, therefore, are of central importance in this work.

Consider a real classical wave function $\bar{V}(\bar{R},t)$ characterizing the field at a point $\bar{R}$ in space at time t. $\bar{V}$ can describe, for example the electric field, the magnetic field, or the vector potential of the field. $\bar{V}(\bar{R},t)$ will be a fluctuating function of time due to random effect in the source, along its path of propagation, or both. It can, therefore, be considered as a member of the ensemble of all possible realizations of the field. Now, as is usually done in electromagnetic field theory, we can associate a complex field $\tilde{V}(\bar{R},t)$ with this field for which $\bar{V} = \text{Re}\{\tilde{V}\}$.[*] Generally for quasi-monochromatic fields

$$\bar{V}(\bar{R},t) = \bar{A}(\bar{R},t)\cos(\bar{\omega}t + \phi(\bar{R},t))$$

---

[*] In most approaches, the complex analytic signal is used here for which $\bar{V} = 2\,\text{Re}\{\tilde{V}\}$ but this simpler notation is used here.

and

$$\bar{V}(\bar{R},t) = \bar{A}(\bar{R},t)e^{j\bar{\omega}t},$$

where

$$\bar{A}(\bar{R},t) = \bar{A}(\bar{R},t)e^{j\phi(\bar{R},t)}$$

is the complex envelope of $\bar{V}$ and $\bar{\omega}$ is the average of center radian frequency of the wave. The field, thus, looks like a narrow band random process in $\bar{R}$ and t. No such simple characterization exists for polychromatic fields in general but they may still be represented by the more general form $\bar{V}(\bar{R},t)$.

Next, for simplicity, consider a linearly polarized field so that it may be represented as

$$\bar{V}(\bar{R},t) = \bar{a}_u V(\bar{R},t),$$

where $\bar{a}_u$ is a unit vector in the direction of $\bar{V}$ and $V(\bar{R},t)$ is a scalar quantity. The correlation* in the fluctuations of the field at two space-time points $\bar{R}_1,t_1$ and $\bar{R}_2,t_2$ then is

$$\Gamma_e(\bar{R}_1,\bar{R}_2,t_1,t_2) = E[V(\bar{R}_1,t_1)V^*(\bar{R}_2,t_2)], \qquad (2-1)$$

---

*The definition varies and depends on what literature source is used.

where E[ ] denotes the expectation or ensemble average over all possible realizations of the field. This function is called the mutual coherence function.[1-3] For the case of quasi-monochromatic fields, the mutual coherence function can be written more simply as the correlation of the complex envelopes

$$\Gamma_e(\bar{R}_1,\bar{R}_2,t_1,t_2) = E[A(\bar{R}_1,t_1)A^*(\bar{R}_2,t_2)].$$

One is often concerned with stationary fields in which case, the ensemble average is independent of time origin. For such fields

$$\Gamma_e(\bar{R}_1,\bar{R}_2,t_1,t_2) = E[V(\bar{R}_1,t_1)V^*(\bar{R}_2,t_1-\tau)] = \Gamma_e(\bar{R}_1,\bar{R}_2,\tau),$$

where $\tau = t_1 - t_2$.

A normalized coherence function can be defined as

$$\gamma_e(\bar{R}_1,\bar{R}_2,\tau) = \frac{\Gamma_e(\bar{R}_1,\bar{R}_2,\tau)}{[\Gamma_e(\bar{R}_1,\bar{R}_1,0)\Gamma_e(\bar{R}_2,\bar{R}_2,0)]^{\frac{1}{2}}}, \qquad (2-2)$$

for which $0 \leq |\gamma_e| \leq 1$. This function is called the complex degree of coherence or sometimes just the degree of coherence and provides a measure of the correlation in the field at the two space-time points. Values of γ_e near one indicate good correlation in the field at the two points, values near zero indicate poor correlation. For mono-chromatic fields, the correlation will be perfect for all points and $|\gamma_e| = 1$ since the amplitude and phase are completely deterministic.

A monochromatic field is, therefore, completely coherent.[3] For most practical fields, however, there will be a region of space-time points $\bar{R}_2, t_2$ about the point $\bar{R}_1, t_1$ for which $|\gamma|$ will be significantly greater than zero. The size of this region depends on the characteristics of the fluctuations and the random effects producing them. But within this region, the fluctuations are correlated to some degree while outside the region, the fluctuations are in general uncorrelated.

For each member of the ensemble of wave functions, a time correlation can be defined as

$$\Gamma_t(\bar{R}_1, \bar{R}_2, \tau) = \langle V(\bar{R}_1, t) V^{*}(\bar{R}_2, t-\tau) \rangle, \qquad (2-3)$$

where the brackets $\langle\ \rangle$ indicate an infinite time average defined as

$$\langle f(t) \rangle = \lim_{T \to \infty} \frac{1}{2T} \int_{-T}^{T} f(t) dt.$$

In normalized form, the time correlation is

$$\gamma_t(\bar{R}_1, \bar{R}_2, \tau) = \frac{\Gamma_t(\bar{R}_1, \bar{R}_2, \tau)}{[\Gamma_t(\bar{R}_1, \bar{R}_1, 0) \Gamma_t(\bar{R}_2, \bar{R}_2, 0)]^{\frac{1}{2}}},$$

where again $0 \le |\gamma_t| \le 1$.

They are referred to as the time mutual coherence function and degree of coherence, respectively. If the fields are ergodic then

$$\Gamma_e(\bar{R}_1, \bar{R}_2, \tau) = \Gamma_t(\bar{R}_1, \bar{R}_2, \tau)$$

and

$$\gamma_e(\bar{R}_1,\bar{R}_2,\tau) = \gamma_t(\bar{R}_1,\bar{R}_2,\tau).$$

This is useful in physical situations where it may be easier to measure one average, but more convenient to work analytically with the other.

The results for a linearly polarized wave are easily generalized to non-linearly polarized fields.[2,3] The mutual coherence function and degree of coherence can be defined to represent the correlation between various Cartesian components of the vector fields. For the purposes of this work, however, the scalar definition is suitable since linearly polarized fields will be used for the most part. Also, the electric field will be used throughout rather than the H field or vector potential so the coherence functions will be defined in terms of the E field. That is

$$\Gamma_e(\bar{R}_1,\bar{R}_2,\tau) = E[E(\bar{R}_1,t)E^*(\bar{R}_2,t-\tau)],$$

etc., where E is the complex representation of the real field E.

The Interference of Two Waves

The concept of second order coherence has long been associated with the interference phenomenon, for it is from interference that coherence can best be understood and physically described. The correlation in two fields can best be exhibited in an interference experiment. To see this, let us examine the interference between two waves;

first, consider the ideal case of monochromatic waves to establish some

basic results, then, the more practical case of quasi-monochromatic

waves.

Interference of Monochromatic Waves

Consider the superposition of two linearly polarized monochromatic

waves whose electric fields at some observation point $\bar{R}$ are

$$E_1(\bar{R},t) = \bar{A}_1(\bar{R})\cos(\omega_1 t - \bar{k}_1(\bar{R})\cdot\bar{R})$$

and

$$E_2(\bar{R},t) = \bar{A}_2(\bar{R})\cos(\omega_2 t - k_2(\bar{R})\cdot\bar{R}), \qquad (2\text{-}4)$$

where $\bar{k}_1$ and $\bar{k}_2$ are the wave vectors of magnitudes ω_1/c and ω_2/c,

respectively, and in the direction of the propagation of $\bar{E}_1$ and $\bar{E}_2$,

respectively. The associated magnetic fields are

$$\bar{H}_1(\bar{R},t) = \frac{\bar{k}_1 \times \bar{E}_1(\bar{R},t)}{\omega_1 \mu}$$

and

$$\bar{H}_2(\bar{R},t) = \frac{\bar{k}_2 \times \bar{E}_2(\bar{R},t)}{\omega_2 \mu} . \qquad (2\text{-}5)$$

The total fields resulting from the superposition of these fields are

$$\bar{E}(\bar{R},t) = \bar{E}_1(\bar{R},t) + \bar{E}_2(\bar{R},t) \tag{2-6}$$

and

$$\bar{H}(\bar{R},t) = \bar{H}_1(\bar{R},t) + \bar{H}_2(\bar{R},t). \tag{2-7}$$

The intensity at the observation point $\bar{R}$ is defined in terms of the average power flow per unit time to be[1]

$$I(\bar{R},t) = <\bar{S}(\bar{R},t)_T> \cdot \bar{n}. \tag{2-8}$$

$\bar{S}(\bar{R},t)$ is the Poynting vector at $\bar{R}$ and $\bar{n}$ is a unit vector normal to the observation surface. The brackets $< >_T$ represent an average over a resolving time T of the observer which is long compared to a period, $2\pi/\omega_1$ or $2\pi/\omega_2$. The exact nature of this average depends on the observer but will, in general, be approximately of the form

$$<f(t)>_T \cong \frac{1}{T} \int_t^{t+T} f(t')dt'.$$

The vectors $\bar{k}_1$, $\bar{k}_2$, and $\bar{n}$ are illustrated in Figure 1.

Substituting equations 2-6 and 2-7 into equation 2-8 results in

$$I(\bar{R},t) = <(\bar{E}_1+\bar{E}_2) \times (\bar{H}_1+\bar{H}_2)>_T \cdot \bar{n} \tag{2-9}$$

$$= <\bar{E}_1 \times \bar{H}_1 + \bar{E}_1 \times \bar{H}_2 + \bar{E}_2 \times \bar{H}_1 + \bar{E}_2 \times \bar{H}_2>_T \cdot \bar{n}.$$
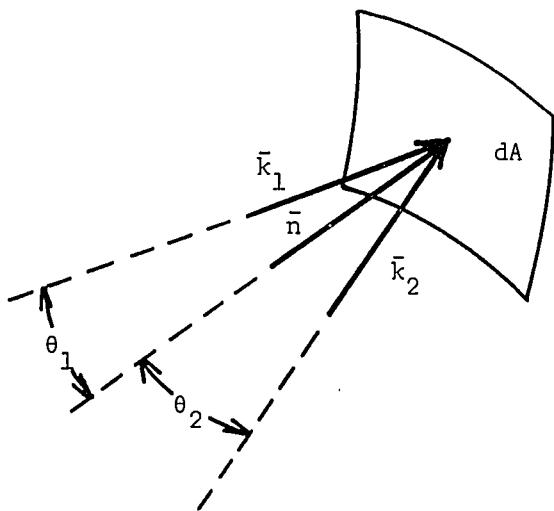
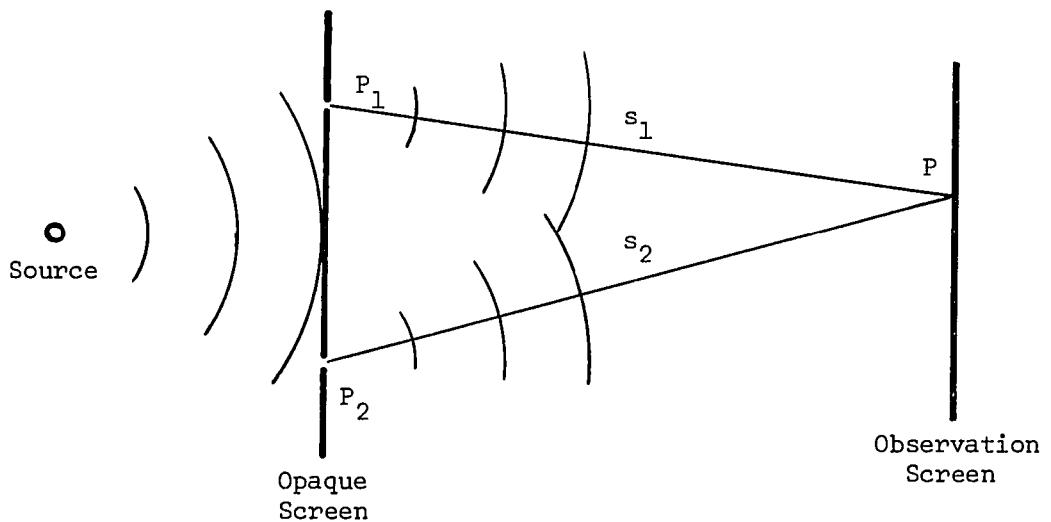Figure 1. An Illustration of the Vectors $\bar{k}_1$, $\bar{k}_2$, and $\bar{n}$

Figure 2. Young's Interference Experiment

Using equations 2-5 for the $\bar{H}$ fields along with the vector identity,[4]

$$\bar{A} \times (\bar{B} \times \bar{C}) = (\bar{A} \cdot \bar{C})\bar{B} - (\bar{A} \cdot \bar{B})\bar{C},$$

we can simplify equation 2-9 to

$$I(\bar{R},t) = \langle \bar{E}_1 \cdot \bar{E}_1 + \bar{E}_1 \cdot \bar{E}_2 \rangle_T \frac{\bar{k}_1 \cdot \bar{n}}{\omega_1 \mu} + \left\langle \frac{(\bar{k}_2 \cdot \bar{E}_1)(\bar{E}_2 \cdot \bar{n})}{\omega_2 \mu} \right\rangle_T$$

$$+ \left\langle \frac{(\bar{k}_1 \cdot \bar{E}_2)(\bar{E}_1 \cdot \bar{n})}{\omega_1 \mu} \right\rangle_T + \langle \bar{E}_2 \cdot \bar{E}_1 + \bar{E}_2 \cdot \bar{E}_2 \rangle_T \frac{\bar{k}_2 \cdot \bar{n}}{\omega_2 \mu} . \qquad (2\text{-}10)$$

In general, $\bar{k}_1$, $\bar{k}_2$, $\bar{E}_1$, and $\bar{E}_2$ are all functions of $\bar{R}$. For small θ_1 and θ_2 (see Figure 1), however, the quantities

$$k_1 \cdot \bar{E}_2 \cong 0, \qquad \bar{E}_2 \cdot \bar{n} \cong 0,$$

$$\bar{k}_2 \cdot \bar{E}_1 \cong 0, \qquad \bar{E}_1 \cdot \bar{n} \cong 0,$$

$$\bar{k}_1 \cdot \bar{n} \cong \frac{\omega_1}{c}, \qquad \bar{k}_2 \cdot \bar{n} \cong \frac{\omega_2}{c} . \qquad (2\text{-}11)$$

Using equations 2-11 in equation 2-10, we can simplify

$$I(\bar{R},t) \cong \frac{1}{c} \langle \bar{E}_1 \cdot \bar{E}_1 + 2\bar{E}_1 \cdot \bar{E}_2 + \bar{E}_2 \cdot \bar{E}_2 \rangle_T$$

$$= \sqrt{\epsilon/\mu} \, \langle \bar{E}(\bar{R},t) \cdot \bar{E}(\bar{R},t) \rangle_T . \qquad (2\text{-}12)$$

Now, let us look for the moment at the use of a complex representation for $\bar{E}$. That is,

$$\bar{E}_1(\bar{R},t) = \tfrac{1}{2}[\bar{E}_1(\bar{R},t) + \bar{E}_1^*(\bar{R},t)]$$

or

$$\bar{E}_1(\bar{R},t) = \text{Re}\{\bar{E}_1(\bar{R},t)\},$$

where

$$\bar{E}_1(\bar{R},t) = \bar{A}_1(\bar{R})e^{j\omega_1 t}$$

and

$$\bar{A}_1(\bar{R}) = \bar{A}_1(\bar{R})e^{j\bar{k}_1(\bar{R})\cdot\bar{R}},$$

and similarly for $\bar{E}_2$. Using these in equation 2-12, we get

$$I(\bar{R},t) = \sqrt{\epsilon/\mu}\,\left\langle \left(\frac{\bar{E}_1+\bar{E}_1^*+\bar{E}_2+\bar{E}_2^*}{2}\right) \cdot \left(\frac{\bar{E}_1+\bar{E}_1^*+\bar{E}_2+\bar{E}_2^*}{2}\right)\right\rangle_T$$

$$= \sqrt{\epsilon/\mu}\,\left\langle \frac{\bar{E}_1\cdot\bar{E}_1^*}{2} + \frac{\bar{E}_2\cdot\bar{E}_2^*}{2} + \frac{\bar{E}_1\cdot\bar{E}_2^*}{2} + \frac{\bar{E}_1^*\cdot\bar{E}_2}{2}\right.$$

$$+ \frac{\bar{E}_1\cdot\bar{E}_1}{4} + \frac{\bar{E}_1^*\cdot\bar{E}_1^*}{4} + \frac{\bar{E}_2\cdot\bar{E}_2}{4} + \frac{\bar{E}_2^*\cdot\bar{E}_2^*}{4}$$

$$\left. + \frac{\bar{E}_1\cdot\bar{E}_2}{2} + \frac{\bar{E}_1^*\cdot\bar{E}_2^*}{2}\right\rangle_T .$$

Examination of the first four terms shows that they are of zero, zero, $\omega_1 - \omega_2$, and $-(\omega_1 - \omega_2)$ frequency variation, respectively, while the last six are of $2\omega_1, -2\omega_1, 2\omega_2, -2\omega_2, \omega_1 + \omega_2$, and $-(\omega_1 + \omega_2)$ frequency variation. The averaging process will eliminate the last six terms but not affect the first four if $2\pi/|\omega_1 - \omega_2| \gg T$. This equation can be rewritten as

$$I(\bar{R},t) = \tfrac{1}{2}\sqrt{\epsilon/\mu}\ (\bar{E}_1 + \bar{E}_2)\cdot(\bar{E}_1^* + \bar{E}_2^*) = \tfrac{1}{2}\sqrt{\epsilon/\mu}\ \bar{E}(\bar{R},t)\cdot\bar{E}^*(\bar{R},t). \qquad (2\text{-}13)$$

The use of the complex representation for the fields, therefore, eliminates the need to retain the time average if

$$\frac{2\pi}{|\omega_1 - \omega_2|} \gg T \gg \frac{2\pi}{\omega_1} \text{ or } \frac{2\pi}{\omega_2}\ .$$

The results of equations 2-12 and 2-13 are approximately the same.

Substituting the complex forms of equation 2-4 into equation 2-13, we get

$$I(\bar{R},t) = \tfrac{1}{2}\sqrt{\epsilon/\mu}\ [\bar{E}_1 \cdot \bar{E}_1^* + \bar{E}_2 \cdot \bar{E}_2^* + 2\text{Re}\{\bar{E}_1 \cdot \bar{E}_2^*\}]$$

$$= I_1(\bar{R}) + I_2(\bar{R}) + \sqrt{\epsilon/\mu}\ \text{Re}\{\bar{E}_1(\bar{R},t)\cdot\bar{E}_2^*(\bar{R},t)\}, \qquad (2\text{-}14)$$

where I_1 and I_2 are the intensity at R due to $\bar{E}_1$ and $\bar{E}_2$ alone, respectively. Looking just at the last term in this equation, we can simplify it to

$$\sqrt{\epsilon/\mu} \; Re\{\bar{E}_1 \cdot \bar{E}_2^*\} = \sqrt{\epsilon/\mu} \; Re\{\bar{A}_1 \cdot \bar{A}_2 e^{j[(\omega_1 - \omega_2)t + (\bar{k}_2 - \bar{k}_1) \cdot \bar{R}]}\}$$

$$= \sqrt{\epsilon/\mu} \; \bar{A}_1 \cdot \bar{A}_2 \cos[(\omega_1 - \omega_2)t + (\bar{k}_2 - \bar{k}_1) \cdot \bar{R}].$$

This is a time varying term of radian frequency $\omega_1 - \omega_2$. The amplitude depends on $\bar{A}_1 \cdot \bar{A}_2$. If $\bar{E}_1$ and $\bar{E}_2$ are mutually orthogonal, then $\bar{A}_1 \cdot \bar{A}_2 = 0$. On the other hand, if $\bar{E}_1$ and $\bar{E}_2$ are both polarized in the same direction, then $\bar{A}_1 \cdot \bar{A}_2 = A_1 A_2$. For this case, we have

$$\sqrt{\epsilon/\mu} \; A_1 A_2 = \sqrt{\sqrt{\epsilon/\mu} \; (\bar{E}_1 \cdot \bar{E}_1^*) \; \sqrt{\epsilon/\mu} \; (\bar{E}_2 \cdot \bar{E}_2^*)} = 2\sqrt{I_1(\bar{R}) I_2(\bar{R})}.$$

Two monochromatic waves linearly polarized in the same direction, will therefore interact or interfere to produce a time varying intensity of

$$I(\bar{R},t) = I_1(\bar{R}) + I_2(\bar{R}) + 2\sqrt{I_1(\bar{R}) I_2(\bar{R})} \; \cos[(\omega_1 - \omega_2) + (\bar{k}_2 - \bar{k}_1) \cdot \bar{R}]$$

at a frequency of $\omega_1 - \omega_2$ about an average of $I_1 + I_2$. Since the amplitude and phase of this term are functions of $\bar{R}$ only, the complex amplitude

$$A_1(\bar{R}) A_2^*(\bar{R})$$

is a stationary function.

When the interfering waves are of the same frequency ($\omega_1 = \omega_2$), the intensity expression becomes

$$I(\bar{R}) = I_1(\bar{R}) + I_2(\bar{R}) + 2\sqrt{I_1(\bar{R})I_2(\bar{R})} \cos[(\bar{k}_2-\bar{k}_1)\cdot\bar{R}] \qquad (2-15)$$

and is no longer time variable. The intensity is solely a function of $\bar{R}$ and can be any value between

$$I = I_1 + I_2 + 2\sqrt{I_1 I_2}$$

and

$$I = I_1 + I_2 - 2\sqrt{I_1 I_2}.$$

The result will be a standing interference pattern whose bright and dark fringe intensities are given by these equations.

These results are directly applicable to Young's interference experiment.[1-3] In this experiment, the radiation from a monochromatic source is incident on an opaque screen with two pinholes (see Figure 2). The interaction of the radiation passing through these pinholes is observed on a screen located some distance from the pinhole.

For a linearly polarized source, the fields from pinholes P_1 and P_2 will be polarized in the same direction. Thus, only the magnitudes are significant and the fields may be considered as scalar quantities. The complex fields at points P_1 and P_2 in Figure 2 can be represented by

$$E(\bar{R}_1,t) \quad \text{and} \quad E(\bar{R}_2,t),$$

respectively. At P on the observation screen, the resulting field is given by

$$E(\bar{R},t) = K_1 E(\bar{R}_1,t-t_1) + K_2 E(\bar{R}_2,t-t_2),$$

where K_1 and K_2 are complex constants which depend on the pinhole size and the geometry. The times $t_1 = s_1/c$ and $t_2 = s_2/c$ are the propagation times for the radiation in going from P_1 to P and P_2 to P, respectively.

The intensity at P is given by

$$I(\bar{R}) = \tfrac{1}{2}\sqrt{\epsilon/\mu}\ E(\bar{R},t)E^*(\bar{R},t)$$

$$= \tfrac{1}{2}\sqrt{\epsilon/\mu}\ [K_1 K_1^* E(\bar{R}_1,t-t_1)E^*(\bar{R}_1,t-t_1) + K_2 K_2^* E(\bar{R}_2,t-t_2)E^*(\bar{R}_2,t-t_2)$$

$$+ 2Re\{K_1 K_2^* E(\bar{R}_1,t-t_1)E^*(\bar{R}_2,t-t_2)\}]$$

$$= I_1(\bar{R}) + I_2(\bar{R}) + \sqrt{\epsilon/\mu}\ Re\{K_1 K_2^* E(\bar{R}_1,t-t_1)E^*(\bar{R}_2,t-t_2)\}. \qquad (2\text{-}16)$$

Now, for the geometry in Figure 2, $K_1 = K_2 = K$ and

$$E(\bar{R}_1,t) = E(\bar{R}_2,t) = Ae^{j\omega t},$$

so that

$$E(\bar{R}_1,t-t_1) = KAe^{j[\omega t-ks_1]}.$$

and

$$E(\bar{R}_2, t-t_2) = KAe^{j[\omega t - ks_2]},$$

where $k = \omega/c$. Putting these into equation 2-16, we get

$$I(\bar{R}) = I_1(\bar{R}) + I_2(\bar{R}) + Re\{\sqrt{\epsilon/\mu}\,|K|^2 A^2 e^{jk(s_2-s_1)}\}$$

$$= I_1(\bar{R}) + I_2(\bar{R}) + 2\sqrt{I_1(\bar{R})I_2(\bar{R})}\,\cos k(s_2-s_1). \qquad (2\text{-}17)$$

Equations 2-17 and 2-15 correspond exactly with

$$(\bar{k}_2-\bar{k}_1)\cdot\bar{R} = k(s_2-s_1).$$

We can see that depending on s_2-s_1, we will get bright or dark interference fringes.

A quantity related to the fringe contrast can be defined. The fringe visibility, first introduced by Michelson, is defined as

$$\nu = \frac{I_{max} - I_{min}}{I_{max} + I_{min}},$$

where I_{max} and I_{min} are the intensities of adjacent bright and dark fringes, in the vicinity of point P. For the interference pattern given by equation 2-17, ν becomes

$$\nu = \frac{2\sqrt{I_1(\bar{R})I_2(\bar{R})}}{I_1(\bar{R}) + I_2(\bar{R})} . \qquad (2\text{-}18)$$

As we shall later see, this is the maximum visibility we can expect.

The Interference of Non-monochromatic Radiation

As we have seen, two beams of monochromatic radiation will always interfere as long as they are not mutually orthogonally polarized. When more than one frequency is present in the radiation, the conditions for interference are more severe. These conditions are determined primarily by the spectral width of the radiation, and the correlation between the fluctuations in amplitude and phase of the interfering waves.

The position of the bright and dark fringes in an interference experiment are frequency dependent as can be seen from equation 2-17. Therefore, when the radiation is composed of many frequencies, the bright fringes produced by one frequency component may coincide with the dark fringes produced by another. The visibility of the fringes may, therefore, be seriously reduced.

Consider the superposition of two linearly polarized quasi-monochromatic waves whose complex representations are

$$\bar{E}_1(\bar{R},t) = \bar{A}_1(\bar{R},t)e^{j\bar{\omega}_1 t}$$

and

$$\bar{E}_2(\bar{R},t) = \bar{A}_2(\bar{R},t)e^{j\bar{\omega}_2 t},$$

where $\bar{A}_1$ and $\bar{A}_2$ are the complex envelopes and $\bar{\omega}_1$ and $\bar{\omega}_2$ are the radian center frequencies of $\bar{E}_1$ and $\bar{E}_2$, respectively. The total field is

$$\bar{E}(\bar{R},t) = \bar{E}_1(\bar{R},t) + \bar{E}_2(\bar{R},t).$$

For quasi-monochromatic fields the magnetic field is approximately orthogonally polarized to the electric field so equation 2-13 can be used to compute the intensity if the fields are nearly normal to the observer. It is given by

$$I(\bar{R},t) = \tfrac{1}{2}\sqrt{\epsilon/\mu}\ (\bar{E}_1+\bar{E}_2)\cdot(\bar{E}_1^*+\bar{E}_2^*)$$

$$= \tfrac{1}{2}\sqrt{\epsilon/\mu}\ [\bar{E}_1\cdot\bar{E}_1^* + \bar{E}_2\cdot\bar{E}_2^* + 2\mathrm{Re}\{\bar{E}_1\cdot\bar{E}_2^*\}$$

$$= I_1(\bar{R},t) + I_2(\bar{R},t) + \sqrt{\epsilon/\mu}\ \mathrm{Re}\{\bar{E}_1(\bar{R},t)\cdot\bar{E}_2^*(\bar{R},t)\}, \qquad (2\text{-}19)$$

where I_1 and I_2 are the intensities at point $\bar{R}$ due to $\bar{E}_1$ and $\bar{E}_2$, individually. Looking just at the last term, we can simplify

$$\sqrt{\epsilon/\mu}\ \mathrm{Re}\{\bar{E}_1\cdot\bar{E}_2^*\} = \sqrt{\epsilon/\mu}\ \mathrm{Re}\{e^{j(\bar{\omega}_1-\bar{\omega}_2)t}\bar{A}_1(\bar{R},t)\cdot\bar{A}_2^*(\bar{R},t)\}$$

$$= \sqrt{\epsilon/\mu}\ \bar{A}_1(\bar{R},t)\cdot\bar{A}_2(\bar{R},t)\cos[(\bar{\omega}_1-\bar{\omega}_2)t + (\bar{k}_2(\bar{R},t)-\bar{k}_1(\bar{R},t))\cdot\bar{R}].$$

When $\bar{E}_1$ and $\bar{E}_2$ are polarized in the same direction, this is maximized to

$$\sqrt{\epsilon/\mu}\ A_1(\bar{R},t)A_2(\bar{R},t)\cos[(\bar{\omega}_1-\bar{\omega}_2)t + (\bar{k}_2(\bar{R},t)-\bar{k}_1(\bar{R},t))\cdot\bar{R}]$$

$$= 2\sqrt{I_1(\bar{R},t)I_2(\bar{R},t)}\ \cos[(\bar{\omega}_1-\bar{\omega}_2)t + (\bar{k}_2(\bar{R},t) - \bar{k}_1(\bar{R},t))\cdot\bar{R}].$$

This is a time varying term of radian frequency $\bar{\omega}_1-\bar{\omega}_2$ whose amplitude and phase fluctuates with time.

Unlike the monochromatic case, the complex magnitude of this oscillating term is time varying. It is given by

$$A_1(\bar{R},t)A_2^*(\bar{R},t).$$

In general A_1 and A_2 will both contain some fluctuations in value about an average magnitude and phase. If E_1 and E_2 are generated separately, these fluctuations will not be correlated.

In order for there to be an average stationary pattern in $A_1A_2^*$ over some region, as there was in the monochromatic case, its fluctuations at two points $\bar{R}_1$ and $\bar{R}_2$ within this region must be correlated. This means the fluctuations in A_1 at $\bar{R}_1$ and $\bar{R}_2$ must be correlated to some extent and likewise for A_2 at $\bar{R}_1$ and $\bar{R}_2$. In other words, the two fields must be nearly perfectly coherent within this region. If the fields were not coherent, the intensity fluctuations from point-to-point would not be correlated.

Next let us consider Young's interference experiment using a non-monochromatic source. In this case, the intensity at the observation point P is given by

$$I(\bar{R},t) = I_1(\bar{R},t) + I_2(\bar{R},t) + \sqrt{\epsilon/\mu}\ \text{Re}\{K_1 K_2^* E(R_1,t-t_1)E^*(\bar{R}_2,t-t_2)\},$$

where

$$E(\bar{R}_1,t-t_1) = A(\bar{R}_1,t-t_1)e^{j\bar{\omega}t}$$

$$= A(\bar{R}_1,t-t_1)e^{j[\bar{\omega}t-\bar{k}(\bar{R}_1,t)\cdot(\bar{R}-\bar{R}_1)]}$$

$$= A(\bar{R}_1,t-t_1)e^{j[\bar{\omega}t-ks_1-\alpha(\bar{R}_1,t)]}$$

and

$$E(\bar{R}_2,t-t_2) = A(\bar{R}_2,t-t_2)e^{j\bar{\omega}t}$$

$$= A(\bar{R}_2,t-t_2)e^{j[\bar{\omega}t-\bar{k}(\bar{R}_2,t)\cdot(\bar{R}-\bar{R}_2)]}$$

$$= A(\bar{R}_2,t-t_2)e^{j[\bar{\omega}t-ks_2-\alpha(\bar{R}_2,t)]},$$

where

$$\alpha(\bar{R}_i,t) = \bar{k}(\bar{R}_i,t)\cdot(\bar{R}-\bar{R}_i) - ks_i \quad \text{for i=1,2,}$$

and k is an average wave vector. The expected value of the intensity
is given by

$$E[I(\bar{R},t)] = E[E_1(\bar{R},t)] + E[I_2(\bar{R},t)]$$

$$+ \sqrt{\epsilon/\mu} \ Re\{K_1 K_2^* E[E(\bar{R}_1,t-t_1)E^*(\bar{R}_2,t-t_2)]\},$$

which from equation 2-1 is

$$E[I(\bar{R},t)] = E[I_1(\bar{R},t)] + E[I_2(\bar{R},t)]$$

$$+ \sqrt{\epsilon/\mu} \ Re\{K_1 K_2^* \Gamma_e(\bar{R}_1,\bar{R}_2,t-t_1,t-t_2)\}.$$

For the case of a stationary field, this is

$$E[I(\bar{R})] = E[I_1(\bar{R})] + E[I_2(\bar{R})]$$

$$+ \sqrt{\epsilon/\mu} \ Re\{K_1 K_2^* \Gamma_e(\bar{R}_1,\bar{R}_2,\tau)\},$$

which using equation 2-2 is

$$E(I(\bar{R})] = E[I_1(\bar{R})] + E[I_2(\bar{R})]$$

$$+ \sqrt{\epsilon/\mu} \ Re\{K_1 K_2^* \sqrt{\Gamma_e(\bar{R}_1,\bar{R}_1,0)\Gamma_e(\bar{R}_2,\bar{R}_2,0)} \ \gamma_e(\bar{R}_1,\bar{R}_2,\tau)\}.$$

Now for the geometry in Figure 2, $K_1 = K_2$ and

$$K_1 K_2^* \sqrt{\Gamma_e(\bar{R}_1,\bar{R}_1,0)\Gamma_e(\bar{R}_2,\bar{R}_2,0)} = \sqrt{|K_1|^2\Gamma_e(\bar{R}_1,\bar{R}_1,0)|K_2|^2\Gamma_e(\bar{R}_2,\bar{R}_2,0)}$$

$$= 2\sqrt{E[I_1(\bar{R})]E[I_2(\bar{R})]} \qquad (2\text{-}20)$$

$$E[I(\bar{R})] = E[I_1(\bar{R})] + E[I_2(\bar{R})] + 2\sqrt{E[I_1(\bar{R})]E[I_2(\bar{R})]}\ Re\{\gamma_e(\bar{R}_1,\bar{R}_2,\tau)\}. \quad (2\text{-}21)$$

Using the results of equation 2-20, we can rewrite equation 2-21 as

$$E[I(\bar{R})] = E[I_1(\bar{R})] + E[I_2(\bar{R})]$$

$$+ 2\sqrt{E[I_1(\bar{R})]E[I_2(\bar{R})]}\ |\gamma_e(\bar{R}_1,\bar{R}_2,\tau)|\cos[k(s_2-s_1)-\alpha'(\bar{R}_1,\bar{R}_2,\tau)],$$

where

$$\alpha'(\bar{R}_1,\bar{R}_2,\tau) = \alpha(\bar{R}_2,t-t_2) - \alpha(\bar{R}_1,t-t_1).$$

The maximum and minimum intensities around $\bar{R}$ are

$$I_{max} = E[I_1(\bar{R})] + E[I_2(\bar{R})] + 2\sqrt{E[I_1(\bar{R})]E[I_2(\bar{R})]}\ |\gamma_e(\bar{R}_1,\bar{R}_2,\tau)|$$

and

$$I_{min} = E[I_1(\bar{R})] + E[I_2(\bar{R})] - 2\sqrt{E[I_1(\bar{R})]E[I_2(\bar{R})]}\ |\gamma_e(\bar{R}_1,\bar{R}_2,\tau)|, \qquad (2\text{-}22)$$

so the fringe visibility is

$$\nu = \frac{2\sqrt{E[I_1(\bar{R})]E[I_2(\bar{R})]}}{E[I_1(\bar{R})] + E[I_2(\bar{R})]} \left| \gamma_e(\bar{R}_1,\bar{R}_2,\tau) \right|.$$

This corresponds to equation 2-18 for the monochromatic case but with

the added factor of $\left| \gamma_e(\bar{R}_1,\bar{R}_2,\tau) \right|$. If the field is non-monochromatic,

the field variations at $\bar{R}_1$ and $\bar{R}_2$ will not be perfectly correlated thus

causing a reduction in fringe contrast or visibility from the mono-

chromatic case. If the field variations are not correlated, then no

average interference pattern will result. Young's interference experi-

ment can therefore be used to measure the coherence of a particular

field.

Principles of Optical Heterodyning

In this section, a discussion of the theory of optical hetero-

dyning is presented along with the development of the equations

describing its operation. In addition, heterodyning will be compared

to ordinary optical photodetection and the relative merits of each are

discussed.

A basic heterodyne system shown in block diagram in Figure 3

consists of a signal field on which a local oscillator field is super-

imposed usually by a beam splitter, both being made incident on a

photoelectric detector surface. Under appropriate conditions discussed

later, the fields interact with the photosurface to produce a signal of

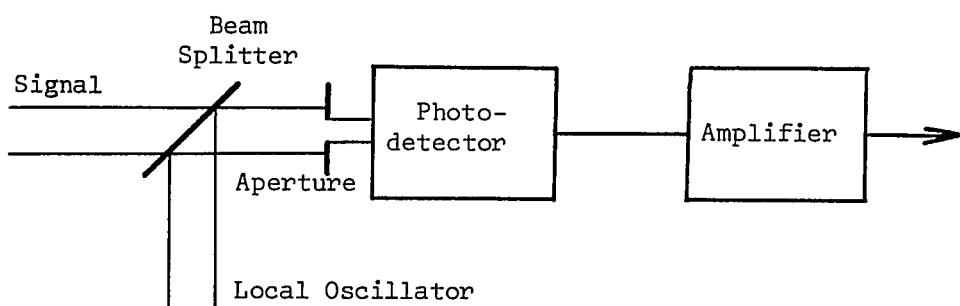intermediate frequency in the photodetector output. This intermediate

Figure 3. A Basic Optical Heterodyne System

intermediate frequency is equal to the difference in frequency between the local oscillator and signal fields.

There are several different optical configurations used for optical heterodyning. Three of the most common ones are shown in Figure 4. The first employs just a beam splitter and aperture before photodetection, the second, a lens to focus the radiation after super-position but before photodetection, and the third, focussing before superposition and photodetection. The last two have the advantage of being easier to align optically, but all three have been shown to be equivalent.[5,6] For analysis purposes, however, the configuration of Figure 4a is the simplest and will be used here.

The incident electric field $\bar{E}$ at a point $\bar{R}$ on the photosurface is given by

$$\bar{E}(\bar{R},t) = \bar{E}_L(\bar{R},t) + \bar{E}_s(\bar{R},t),$$

where $\bar{E}_L(\bar{R},t)$ and $\bar{E}_s(\bar{R},t)$ are the local oscillator field and signal field at $\bar{R}$, respectively. If $\bar{E}_L$ and $\bar{E}_s$ are quasi-monochromatic and near normal to the photosurface, the intensity at $\bar{R}$ as defined by equation 2-13 is

$$I(\bar{R},t) = \tfrac{1}{2}\sqrt{\epsilon/\mu}\ \bar{E}_L(\bar{R},t) \cdot \bar{E}_L^*(\bar{R},t) + \tfrac{1}{2}\sqrt{\epsilon/\mu}\ \bar{E}_s(\bar{R},t) \cdot \bar{E}_s^*(\bar{R},t)$$

$$+ \sqrt{\epsilon/\mu}\ \mathrm{Re}\{\bar{E}_L(\bar{R},t) \cdot \bar{E}_s^*(\bar{R},t)\}$$
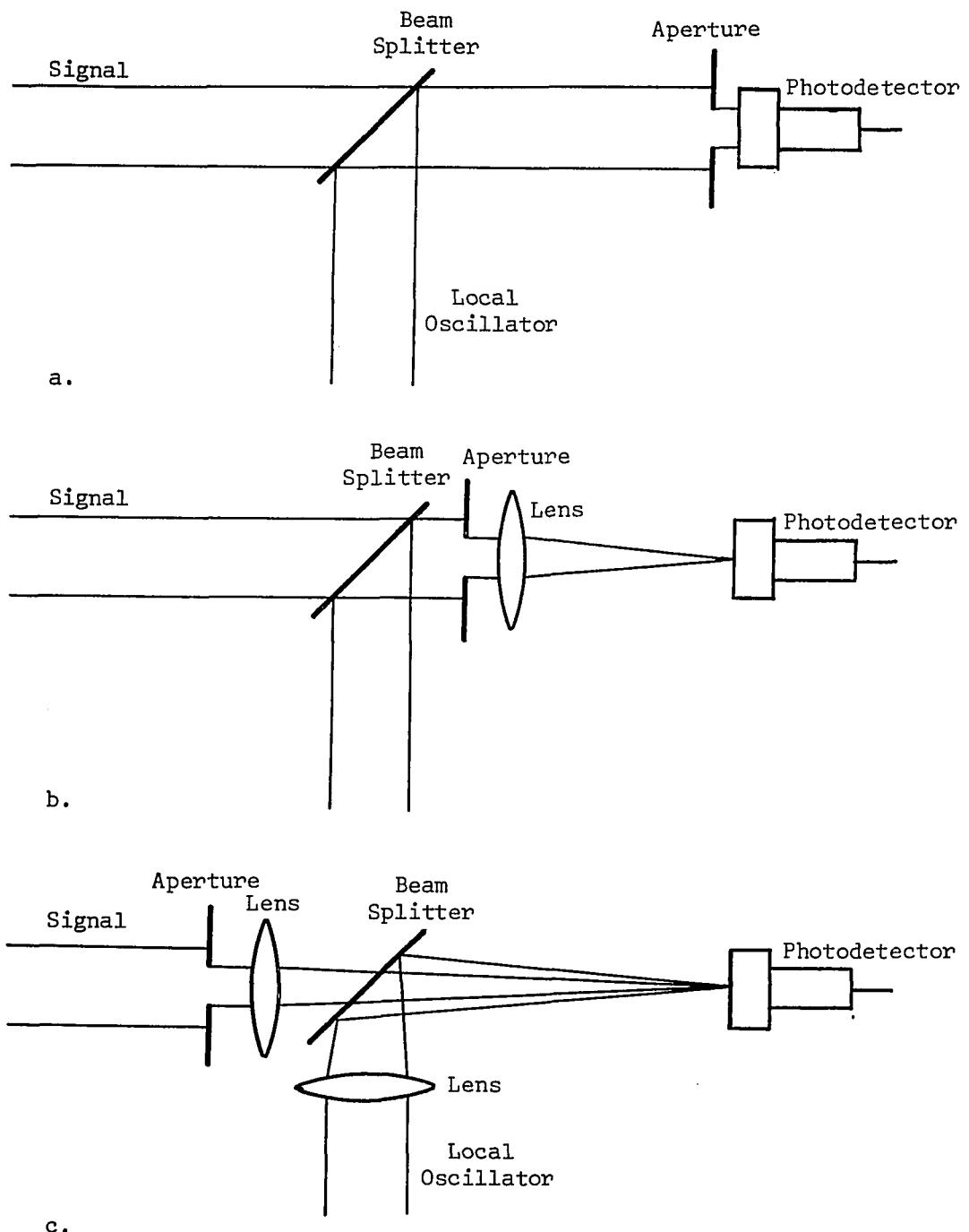
Figure 4. Three Optical Configurations for Optical Heterodyning

$$= I_L(\bar{R},t) + I_s(\bar{R},t) + \sqrt{\epsilon/\mu} \; Re\{\bar{E}_L(\bar{R},t) \cdot \bar{E}_s(\bar{R},t)\}.$$

For quasi-monochromatic fields

$$\bar{E}_L(\bar{R},t) = \bar{A}_L(\bar{R},t)e^{j\bar{\omega}_L t}$$

and

$$\bar{E}_s(\bar{R},t) = \bar{A}_s(\bar{R},t)e^{j\bar{\omega}_s t},$$

where A_L and A_s, $\bar{\omega}_L$ and $\bar{\omega}_s$ are the complex envelopes and radian center frequencies of the local oscillator and signal fields. Putting equation 24 into 23 gives us

$$I(\bar{R},t) = I_L(\bar{R},t) + I_s(\bar{R},t) + \sqrt{\epsilon/\mu} \; Re\{e^{j\omega_D t}\bar{A}_L(\bar{R},t) \cdot \bar{A}_s^*(\bar{R},t)\}, \quad (2\text{-}23)$$

where $\bar{\omega}_D = \bar{\omega}_L - \bar{\omega}_s$. This corresponds to equation 2-19 derived in the last section describing the interference between $\bar{E}_L$ and $\bar{E}_s$. The first two terms, as we have seen, are the constant components of the total intensity due to the local oscillator and signal fields individually, while the last is the fluctuating component varying at frequency $\bar{\omega}_D = \bar{\omega}_L - \bar{\omega}_s$, the difference frequency due to interference.

The photodetector, although basically a quantum device providing a current output proportional to the incident photon flux, can be considered from a classical viewpoint. The output current has been shown

to be proportional to the average intensity of the fields incident on its photosensitive surface.[7] That is

$$i(t) = \frac{qe}{hf} \int_S I(\bar{R},t)dA, \qquad (2-24)$$

where $I(\bar{R},t) = \sqrt{\epsilon/\mu} \; \langle\bar{E}(\bar{R},t)\cdot\bar{E}(\bar{R},t)\rangle_T$ is the intensity at $\bar{R}$ on the photosurface S, and T is the response time of the photodetector (usually less than 10^{-8} sec.). For analysis purposes, S is taken to be that portion of the photosurface that is exposed to incident radiation as limited by the receiving aperture. The constant q is the quantum efficiency of the photosurface (electrons/incident proton), e is the magnitude of the electronic charge, h is Planck's constant and f is the frequency of the field. The average over T eliminates any optical frequency variations in $i(t)$. Now we have

$$i(t) = \frac{qe}{hf} \sqrt{\epsilon/\mu} \int_S \langle\bar{E}(\bar{R},t)\cdot\bar{E}(\bar{R},t)\rangle_T dA$$

$$\cong \frac{qe}{2hf} \sqrt{\epsilon/\mu} \int_S \bar{E}(\bar{R},t)\cdot\bar{E}^*(\bar{R},t)dA.$$

Putting equation 2-23 into 2-24, we get

$$i(t) = \frac{qe}{2hf} \sqrt{\epsilon/\mu} \int_S \bar{E}_L(\bar{R},t)\cdot\bar{E}_L^*(\bar{R},t)dA$$

$$+ \frac{qe}{2hf} \sqrt{\epsilon/\mu} \int_S \bar{E}_s(\bar{R},t)\cdot\bar{E}_s^*(\bar{R},t)dA$$

$$+ \frac{qe}{hf} \sqrt{\epsilon/\mu} \; Re\{e^{j\bar{\omega}_D t} \int_S \bar{A}_L(\bar{R},t) \cdot \bar{A}_S^*(\bar{R},t) dA\}$$

$$= i_{DC_L} + i_{DC_S} + i_s(t). \tag{2-25}$$

The first two terms are DC or low frequency components of the photo-current due to the field intensities of the signal and local oscillator individually. The last term is the heterodyne signal current of the difference frequency $\bar{\omega}_D$. Note that any amplitude or phase modulation in the signal field will result in proportional changes in $\bar{A}_L \cdot \bar{A}_S^*$ and hence in i_s. The heterodyne detection system is, therefore best suited for processing of signals containing amplitude, phase or frequency modulation. The amplitude, phase, or frequency modulation of the signal is preserved in the conversion of the signal down to the lower difference frequency.

The integral in the last term of equation 2-25 gives the complex amplitude of the heterodyne signal. The integrand gives the complex amplitude of fluctuating intensity of the interfering waves. We see that for interference to take place, the fields must overlap ($\bar{E}_L \neq 0$ and $\bar{E}_S \neq 0$ at all $\bar{R}$ over S) and not be mutually orthogonally polarized. For maximum interference effect, the signal and local oscillator beams must be coaxial[8] and if they are linearly polarized, they should be polarized in the same direction.

For a maximum value of the integral and hence a maximum hetero-dyne signal, the integrand must, in addition to satisfying the above

requirements, be of constant phase for all $\bar{R}$ on S. This requires a

constant phase difference between $A_L(\bar{R},t)$ and $A_S(\bar{R},t)$ for all $\bar{R}$ on S,

a condition satisfied only when the fluctuations of $A_L A_S^*$ are correlated

over S and when the wavefronts of the signal and local oscillator

fields have identical shape and are perfectly aligned. This requires

the fields to be nearly coherent over S and to have the same direction

of propagation.

This last requirement is equivalent to that of having the inten-

sity fluctuations produced by the interfering wave to all be in phase.

If the wavefronts were distorted or tilted with respect to each other,

the resulting intensity fluctuations at different points on S will not

be in phase and in some cases not be correlated and, hence, may cancel,

a condition that clearly will not yield a maximum heterodyne signal.

In summary, therefore, there are four requirements for efficient

heterodyning. The signal and local oscillator fields must

   (1) be identically polarized,

   (2) overlap on the photosurface,

   (3) have the same direction of propagation sometimes

        referred to as angular alignment, and

   (4) be nearly perfectly coherent, i.e. approximately mono-

        chromatic.

These four requirements are not easily satisfied and are sometimes so

difficult as to make heterodyne detection of doubtful advantage.

As a standard for comparing all heterodyne systems, let us

consider the simple ideal case of uniform plane, linearly polarized,

monochromatic signal and local oscillator fields superimposed and normally incident on the photosurface so that all four requirements are ideally satisfied. The incident field is given by

$$E(\bar{R},t) = A_L e^{j\omega_L t} + A_s e^{j\omega_s t},$$

where A_L and A_s are the amplitudes of the local oscillator and signal carrier fields and are real (taking the photosurface as a phase reference). The resulting intensity on S is

$$I(\bar{R},t) = I_L + I_s + \sqrt{\epsilon/\mu}\ A_L A_s \cos\omega_D t,$$

where $\omega_D = \omega_L - \omega_s$ and $I_L = A_L^2/2$ and $I_s = A_s^2/2$. The intensity fluctuations at all points on S are in phase. The photocurrent is

$$i(t) = \frac{qe}{hf} I_L A + \frac{qe}{hf} I_s A + \frac{qe}{hf} \sqrt{\epsilon/\mu}\ A_L A_s A\cos\omega_D t = i_{DC_L} + i_{DC_s} + i_s(t),$$

where A is the photosurface area. The carrier signal power delivered to a unit resistance after amplification is

$$S_h = \langle G^2 i_s^2(t)\rangle = \frac{q^2 e^2 \epsilon}{2h^2 f^2 \mu} G^2 A_L^2 A_s^2 A^2 = 2G^2 \frac{q^2 e^2}{h^2 f^2} I_L I_s A^2, \qquad (2\text{-}26)$$

where G is the gain of the following amplifier. The RMS shot noise current is given after amplification by[14]

$$i_{n_{rms}} = <G^2 i_n^2(t)>^{\frac{1}{2}} = G\sqrt{2eB(i_{DC_L} + i_{DC_s})} \ ,$$

where B is the equivalent rectangular bandwidth of the amplifier. The shot noise power is therefore given by

$$N_h = 2G^2 eB(i_{DC_L} + i_{DC_s}) = \frac{2qe^2 BG^2}{hf}(I_L + I_s)A. \qquad (2\text{-}27)$$

The carrier signal-to-shot noise ratio (SNR), then, is

$$SNR_h = \frac{S_h}{N_h} = \frac{qe}{hfB}\frac{I_L I_s A}{I_L + I_s} \ .$$

As the local oscillator intensity is increased

$$N_h \longrightarrow \frac{2qe^2 BG^2}{hf} I_L A$$

and

$$SNR_h \longrightarrow \frac{qe}{hfB} I_s A. \qquad (2\text{-}28)$$

This results in a signal-to-noise ratio dependent on the signal power only, not on local oscillator power. I_L can therefore be increased to the point that the shot noise produced by it completely predominates over any other source of noise generated in the detection process. The signal-to-noise ratio is unaffected because the signal power increases at the same rate with I_L as the noise.

To examine the performance of a heterodyne system in comparison to other detection systems, let us consider a direct detection such as the one shown in Figure 5. In this system, the signal field $\bar{E}_s(\bar{R},t)$ is incident on a photodetector. The photocurrent is given by

$$i_s(t) = \frac{qe}{2hf} \sqrt{\epsilon/\mu} \int_S \bar{E}_s(\bar{R},t) \cdot \bar{E}_s^*(\bar{R},t) dA.$$

Any intensity modulation of the signal field will, therefore, result in proportional changes in i_s. The direct detection system is, thus, best suited for detection of intensity modulated signals. Since there is no local oscillator, there are no alignment requirements in a direct detection system.

Examine the ideal case of a uniform plane, linearly polarized signal carrier normally incident on the photosurface. The incident field is given by

$$E_s(\bar{R},t) = A_s e^{j\omega_s t}$$

where A_s is amplitude of the signal field and is real. The signal output is

$$i_s = \frac{qe}{2hf} \sqrt{\epsilon/\mu} A_s^2 A = \frac{qe}{hf} I_s A.$$
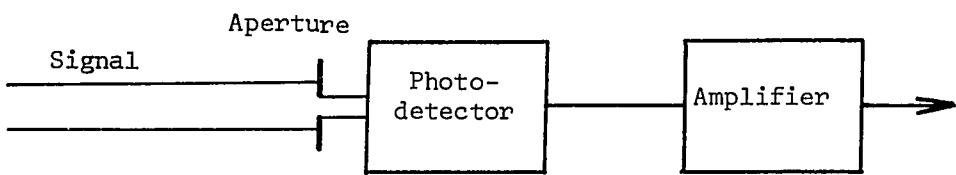
The carrier signal power, thus, is given by

Figure 5. A Basic Direct Detection System

$$S_d = \langle G^2 i_s^2(t) \rangle = \frac{q^2 e^2 G^2}{h^2 f^2} I_s^2 A^2. \qquad (2\text{-}29)$$

The signal shot noise power is given by

$$N_d = 2G^2 eBi_{DC} = \frac{2qe^2 BG^2}{hf} I_s A, \qquad (2\text{-}30)$$

where again B is the bandwidth of the photodetection process or the signal amplifier that follows. The ideal signal-to-noise ratio is

$$SNR_d = \frac{S_d}{N_d} = \frac{qe}{2hfB} I_s A. \qquad (2\text{-}31)$$

Comparing this with equation 2-28 we note a twofold improvement in signal-to-noise ratio for the heterodyne case, an advantage for hetero-dyning but not a distinct one. In comparing equation 2-29 to 2-26 we have

$$\frac{S_h}{S_d} = 2 \frac{I_L}{I_s},$$

a conversion gain in the heterodyne process not exhibited by direct detection that increases with I_L. The shot noise also increases with I_L, however, since from equations 2-27 and 2-30, we have

$$\frac{N_h}{N_d} = \frac{I_L + I_s}{I_s} \rightarrow \frac{I_L}{I_s} \quad \text{for} \quad I_L \gg I_s,$$

but only at half the rate of the signal power, hence the twofold
improvement in signal-to-noise ratio.

The real advantage of heterodyning is more obvious, however,
when one considers the effects of other sources of noise. In practice,
the noise for the direct detection case is usually much greater than
the signal shot noise due to noise created by background light, photo-
detector dark current, and most important, thermal effects. The
signal-to-noise ratio, in this case, will be much less than that given
in equation 2-31. Such reductions even for ideal signals are typical
in many direct detection systems and can limit the usefulness for cer-
tain applications.

In a heterodyne system, I_L can be made large enough for the
local oscillator shot noise to predominate over these other noise
sources. Because of the conversion gain in signal that accompanies
a large I_L, the signal-to-noise ratio will still be given by equation
2-28 and, therefore, will not be affected by these other noise sources.

Heterodyne Efficiency

Heterodyne detection, as we have just seen, is generally more
advantageous than direct detection provided it is efficient, that is,
when its performance is comparable to that theoretically possible under
ideal conditions. This is possible only with the exact fulfillment
of the four requirements. Should any or all of these requirements not
be exactly fulfilled, a reduction in efficiency and a subsequent
reduction in signal-to-noise ratio from the ideal case will result.
This reduction is customarily measured by a parameter η_h usually called
the heterodyne efficiency. It is usually given by

$$\eta_h = \frac{\langle i_s^2(t)\rangle_{actual}}{\langle i_s^2(t)\rangle_{ideal}}, \tag{2-32}$$

that is, the ratio of the signal power obtainable under actual operating conditions to the signal power obtainable under ideal conditions. Values near one indicate high efficiency heterodyning (near ideal operation); values near zero indicate low efficiency heterodyning.

The obtainable SNR ratio is given in terms of the ideal SNR by

$$SNR_{actual} = \eta_h SNR_{ideal}.$$

Therefore, for realization of near ideal signal-to-noise ratios, the heterodyne detector must operate efficiently.

The effects of polarization, overlap, and propagation direction misalignments on heterodyne operation have been studied extensively.[8,12,13] The general conclusions are that these alignment requirements are very strict and sometimes cannot be met. The effects of the reductions in signal or local oscillator field coherence, however, have received little attention. This is the performance limiting factor in many systems.

CHAPTER III

THE DERIVATION OF THE HETERODYNE

EFFICIENCY AND SNR EQUATIONS

The equations describing ideal operation of a heterodyne detection system are given in the preceding chapter. In this chapter, the equations for the efficiency and signal-to-noise ratio are derived for a non-ideal system where the amplitude and phase variations of the signal and local oscillator fields are not perfectly correlated. This will be shown to be mathematically related to the degree of coherence of each field.

Consider a heterodyne system where the signal and local oscillator fields are polarized linearly in the same direction. The signal current is given from equation 2-25 by

$$i_s(t) = \frac{qe}{hf} \sqrt{\epsilon/\mu} \, \text{Re}\{\int_S E_L(\bar{R},t)E_s^*(\bar{R},t)dA\},$$

where

$$E_L(\bar{R},t) = A_L(\bar{R},t)e^{j\omega_L t}$$

and

$$E_s(\bar{R},t) = A_s(\bar{R},t)e^{j\omega_s t}, \tag{3-1}$$

so that the average power delivered by the photodetector to a unit resistance is given by

$$\langle i_s^2(t) \rangle = \left\langle \left[\frac{qe}{hf} \sqrt{\epsilon/\mu} \, \mathrm{Re}\{ \int_S E_L(\bar{R},t) E_s^*(\bar{R},t) dA \} \right]^2 \right\rangle .$$

The squared integral can be written as an iterated integral;

$$i_s^2(t) = \left\langle \frac{q^2 e^2 \epsilon}{h^2 f^2 \mu} \, \mathrm{Re}\{ \int_{S_1} E_L(\bar{R}_1,t) E_s^*(\bar{R}_1,t) dA_1 \} \right.$$

$$\left. \cdot \, \mathrm{Re}\{ \int_{S_2} E_L(\bar{R}_2,t) E_s^*(\bar{R}_2,t) dA_2 \} \right\rangle$$

$$= \left\langle \frac{q^2 e^2 \epsilon}{h^2 f^2 \mu} \int_{S_1} \mathrm{Re}\{ E_L(\bar{R}_1,t) E_s^*(\bar{R}_1,t) \} dA_1 \right.$$

$$\left. \cdot \int_{S_2} \mathrm{Re}\{ E_L(\bar{R}_2,t) E_s^*(\bar{R}_2,t) \} dA_2 \right\rangle$$

$$= \left\langle \frac{q^2 e^2 \epsilon}{h^2 f^2 \mu} \int_{S_1} \int_{S_2} \mathrm{Re}\{ E_L(\bar{R}_1,t) E_s^*(\bar{R}_1,t) \} \right.$$

$$\left. \cdot \, \mathrm{Re}\{ E_L(\bar{R}_2,t) E_s^*(\bar{R}_2,t) \} dA_1 dA_2 \right\rangle ,$$

where $S_1 = S_2 = S$.

The time average is given by the integral

$$\langle i_s^2(t) \rangle = \lim_{T \to \infty} \frac{1}{2T} \int_{-T}^{T} i_s^2(t) dt.$$

Only the integrand is a function of time so the order of integration may be interchanged to give

$$i_s^2(t) = \frac{q^2 e^2 \epsilon}{h^2 f^2 \mu} \int_{S_1} \int_{S_2} <\text{Re}\{E_L(\bar{R}_1,t)E_s^*(\bar{R}_1,t)\}$$

$$\cdot \text{Re}\{E_L(\bar{R}_2,t)E_s^*(\bar{R}_2,t)\}>dA_1 dA_2.$$

Let us consider just the integrand for the moment.

$$<\text{Re}\{E_L(\bar{R}_1,t)E_s^*(\bar{R}_1,t)\}\text{Re}\{E_L(\bar{R}_2,t)E_s^*(\bar{R}_2,t)\}>$$

$$= <\tfrac{1}{2}(E_L(\bar{R}_1,t)E_s^*(\bar{R}_1,t) + E_L^*(\bar{R}_1,t)E_s(\bar{R}_1,t))$$

$$\cdot \tfrac{1}{2}(E_L(\bar{R}_2,t)E_s^*(R_2,t) + E_L^*(\bar{R}_2,t)E_s(\bar{R}_2,t))>$$

$$= \tfrac{1}{4}[<E_L(\bar{R}_1,t)E_L^*(\bar{R}_2,t)E_s^*(\bar{R}_1,t)E_s(\bar{R}_2,t)>$$

$$+ <E_L^*(\bar{R}_1,t)E_L(\bar{R}_2,t)E_s(\bar{R}_1,t)E_s^*(\bar{R}_2,t)>$$

$$+ <E_L(\bar{R}_1,t)E_L(\bar{R}_2,t)E_s^*(\bar{R}_1,t)E_s^*(\bar{R}_2,t)>$$

$$+ <E_L^*(\bar{R}_1,t)E_L^*(\bar{R}_2,t)E_s(\bar{R}_1,t)E_s(\bar{R}_2,t)>].$$

By substituting equations 3-1 into this, we see that before the time average is performed, the first two terms are of low frequency variation while the last two are of $2\bar{\omega}_D$ variation. The time average, therefore, eliminates the last two terms and

$$\langle \mathrm{Re}\{E_L(\bar{R}_1,t)E_s^*(\bar{R}_1,t)\}\mathrm{Re}\{E_L(\bar{R}_2,t)E_s(\bar{R}_2,t)\}\rangle$$

$$= \tfrac{1}{4}[\langle E_L(\bar{R}_1,t)E_L^*(\bar{R}_2,t)E_s^*(\bar{R}_1,t)E_s(\bar{R}_2,t)\rangle$$

$$+ \langle E_L^*(\bar{R}_1,t)E_L(\bar{R}_2,t)E_s(\bar{R}_1,t)E_s^*(\bar{R}_2,t)\rangle]$$

$$= \tfrac{1}{2}\,\mathrm{Re}\{\langle E_L(\bar{R}_1,t)E_L^*(\bar{R}_2,t)E_s^*(\bar{R}_1,t)E_s(\bar{R}_2,t)\rangle\}.$$

In many practical systems, the field processes can be assumed to be ergodic.[2] Making this assumption here, we have

$$\tfrac{1}{2}\,\mathrm{Re}\{\langle E_L(\bar{R}_1,t)E_L^*(\bar{R}_2,t)E_s^*(\bar{R}_1,t)E_s(\bar{R}_2,t)\rangle\}$$

$$= \tfrac{1}{2}\,\mathrm{Re}\{E[E_L(\bar{R}_1,t)E_L^*(\bar{R}_2,t)E_s^*(\bar{R}_1,t)E_s(\bar{R}_2,t)]\}.$$

In addition, if the signal and local oscillator fields are statistically independent, as they would be if generated separately, this equation becomes

$$\tfrac{1}{2}\,\mathrm{Re}\{E[E_L(\bar{R}_1,t)E_L^*(\bar{R}_2,t)]E[E_s^*(\bar{R}_1,t)E_s(\bar{R}_2,t)]\}$$

$$= \tfrac{1}{2}\,\mathrm{Re}\{\langle E_L(\bar{R}_1,t)E_L^*(\bar{R}_2,t)\rangle\langle E_s^*(\bar{R}_1,t)E_s(\bar{R}_2,t)\rangle\}.$$

Comparing the time average in this last term to those of equation 2-3, we see that

$$\langle E_L(\bar{R}_1,t)E_L^*(\bar{R}_2,t)\rangle = \Gamma_{L_t}(\bar{R}_1,\bar{R}_2,0) = \Gamma_{L_e}(\bar{R}_1,\bar{R}_2,0)$$

$$= \Gamma_L(\bar{R}_1,\bar{R}_2)$$

and

$$\langle E_s^*(\bar{R}_1,t)E_s(\bar{R}_2,t)\rangle = \Gamma_{s_t}^*(\bar{R}_1,\bar{R}_2,0) = \Gamma_{s_e}^*(\bar{R}_1,\bar{R}_2,0)$$

$$= \Gamma_s^*(\bar{R}_1,\bar{R}_2),$$

the mutual coherence functions for the local oscillator and signal field. The t and e subscripts are dropped since the averages are equivalent under the ergodic assumptions and the τ variable is dropped since it is always zero. The expression for the average signal power, therefore, is

$$\langle i_s^2(t)\rangle = \frac{q^2e^2\epsilon}{2h^2f^2\mu} \int_{S_1} \int_{S_2} \text{Re}\{\Gamma_L(\bar{R}_1,\bar{R}_2)\Gamma_s^*(\bar{R}_1,\bar{R}_2)\}dA_1 dA_2.$$

The mutual coherence functions, in terms of the degree of coherence functions are given from equations 2-2 and 2-13 by

$$\Gamma_L(\bar{R}_1,\bar{R}_2) = [\Gamma_L(\bar{R}_1,\bar{R}_1)\Gamma_L(\bar{R}_2,\bar{R}_2)]^{\frac{1}{2}}\gamma_L(\bar{R}_1,\bar{R}_2)$$

$$= 2\sqrt{\mu/\epsilon}\,[I_L(\bar{R}_1)I_L(\bar{R}_2)]^{\frac{1}{2}}\gamma_L(\bar{R}_1,\bar{R}_2)$$

and

$$\Gamma_s(\bar{R}_1,\bar{R}_2) = [\Gamma_s(\bar{R}_1,\bar{R}_1)\Gamma_s(\bar{R}_2,\bar{R}_2)]^{\frac{1}{2}}\gamma_s(\bar{R}_1,\bar{R}_2)$$

$$= 2\sqrt{\mu/\epsilon}\,[I_s(\bar{R}_1)I_s(\bar{R}_2)]^{\frac{1}{2}}\gamma_s(\bar{R}_1,\bar{R}_2),$$

so

$$<i_s(t)> = \frac{2q^2e^2}{h^2f^2}\int_{S_1}\int_{S_2}[I_L(\bar{R}_1)I_L(\bar{R}_2)I_s(\bar{R}_1)I_s(\bar{R}_2)]^{\frac{1}{2}}$$

$$\cdot\,Re\{\gamma_L(\bar{R}_1,\bar{R}_2)\gamma_s^*(\bar{R}_1,\bar{R}_2)\}dA_1dA_2. \qquad (3\text{-}2)$$

The signal power is thus related to the respective degree of coherence
of the signal and local oscillator fields through the above integral.

In the ideal case, the signal and local oscillator must be per-
fectly coherent. In addition, if the signal and local oscillator are
perfectly aligned and normal to the photosurface.

$$\gamma_L(\bar{R}_1,\bar{R}_2) = \gamma_s(\bar{R}_1,\bar{R}_2) = 1 \quad \text{for } \bar{R}_1,\bar{R}_2 \text{ on S.}$$

This is because E_L and E_s are perfectly monochromatic and $\bar{R}_1$ and $\bar{R}_2$
lies along an equiphase front. The signal power for this case is

$$<i_s(t)>_{ideal} = \frac{2q^2e^2}{h^2f^2}\int_{S_1}\int_{S_2}[I_L(\bar{R}_1)I_L(\bar{R}_2)I_s(\bar{R}_1)I_s(\bar{R}_2)]^{\frac{1}{2}}dA_1dA_2.$$

The heterodyne efficiency, therefore, is given from equation 2-32 by

$$\eta_h = \frac{<i_s^2(t)>_{actual}}{<i_s^2(t)>_{ideal}}$$

$$= \frac{\int_{S_1}\int_{S_2}[I_L(\bar{R}_1)I_L(\bar{R}_2)I_s(\bar{R}_1)I_s(\bar{R}_2)]^{\frac{1}{2}}Re\{\gamma_L(\bar{R}_1,\bar{R}_2)\gamma_s^*(\bar{R}_1,\bar{R}_2)\}dA_1dA_2}{\int_{S_1}\int_{S_2}[I_L(\bar{R}_1)I_L(\bar{R}_2)I_s(\bar{R}_1)I_s(\bar{R}_2)]^{\frac{1}{2}}dA_1dA_2} \quad . \quad (3-3)$$

The numerator and denominator are identical except for the coherence functions whose maximum values are unity. The heterodyne efficiency for the perfect coherence case is, as might be expected, equal to one. Since

$$[I_L(\bar{R}_1)I_L(\bar{R}_2)I_s(\bar{R}_1)I_s(\bar{R}_2)]^{\frac{1}{2}}$$

is always positive and $0\leq|\gamma_L|\leq1$ and $0\leq|\gamma_s|\leq1$, reduction in either the signal field coherence or the local oscillator coherence result in a decrease in efficiency.

The SNR for this case assuming local oscillator shot noise limited operation is given by

$$SNR = \frac{<i_s^2(t)>}{<i_n^2(t)>} = \frac{qe}{hfB}$$

$$\cdot \frac{\int_{S_1}\int_{S_2}[I_L(\bar{R}_1)I_L(\bar{R}_2)I_s(\bar{R}_1)I_s(\bar{R}_2)]^{\frac{1}{2}}Re\{\gamma_L(\bar{R}_1,\bar{R}_2)\gamma_s^*(\bar{R}_1,\bar{R}_2)\}dA_1dA_2}{\int_S I_L(\bar{R})dA} \quad .$$

$$(3-4)$$

Both the heterodyne efficiency and signal-to-noise ratio of a hetero-
dyne system can, thus, be determined as functions of the signal and
local oscillator field coherence functions, γ_L and γ_s, at the photo-
surface, the intensity distribution, I_L and I_s, of the local oscillator
and signal field, and the photosurface size and shape S. We see that
with everything else fixed, a reduction in the coherence of either the
signal or local oscillator will cause a reduction in η_h and SNR.

In summary, the efficiency and SNR of any heterodyne detection
system are given by equation 3-3 and 3-4. The only conditions placed
on the system are:

1. The system is ergodic in the mean and correlation.

2. The local oscillator and signal are statistically independent.
These are not severe restrictions and apply to many practical and useful
heterodyne systems. Although the effects of imperfect overlap and
angular alignment are not included in this study, their effects can be
studied from these equations. These equations can, therefore, be very
useful in a thorough analysis of most heterodyne systems regardless of
their structure.

CHAPTER IV

THE ANALYTICAL STUDY

Thus far, only the most general type of heterodyne system has been considered. In this chapter, the general equations that have been developed are applied to three specific systems to evaluate their performance as heterodyne systems. The systems are (1) a communications link through a turbulent atmosphere, (2) a laser Doppler surface motion measuring system, and (3) a laser Doppler fluid flow measuring system. The basic approach, for each system, is to (1) calculate the signal field coherence function based on a statistical description of the system, and (2) calculate the heterodyne efficiency and signal-to-noise ratio from equation 3-3 and 3-4 for different receiving apertures, different local oscillator intensity functions, and different degrees of local oscillator coherence. The main objective is to determine conditions at the receiver for efficient operation and maximum SNR. The effects of changing signal parameters are not considered here.

An Optical Communications Link

The development of the laser has established a great new interest in coherent light as a carrier for information in communications systems. Not only does this provide wider bandwidth and greater information capacity in a highly colimated beam, but also the possibility of the use of coherent detection techniques and the resulting improved

noise immunity. Ironically, for earthbound communication links, the coherence of such a signal can be seriously reduced by random atmospheric effects, limiting the usefulness of this type of optical communication system.

The random atmospheric effects are primarily of the form of random variations in the index of refraction from point-to-point caused by atmospheric turbulence. These variations produce, in turn, random fluctuations in amplitude and phase in an optical signal propagating through the atmosphere. This is illustrated in Figure 6. The subsequent reduction in signal coherence can severely reduce the effectiveness of the optical heterodyne receiver as a coherent detector.

The performance of an optical heterodyne communications system as it is affected by atmospheric turbulence has been investigated by many authors in different ways. Gardner studied power loss in heterodyne signal due to turbulence compared to no turbulence for various size circular receiver apertures.[6] Fried studied the signal-to-noise ratio as a function of the turbulence intensity and receiver aperture diameter.[5] Rosner investigates the IF signal power for various receiver aperture diameters.[15] In this thesis, the heterodyne system will be re-examined in terms of heterodyne efficiency and signal-to-noise ratio as defined in equations 3-3 and 3-4.

Derivation of the Coherence Function

In deriving the degree of coherence function for the signal field, the second order statistics of the amplitude and phase fluctuations must be known. These depend on the statistics of the refractive
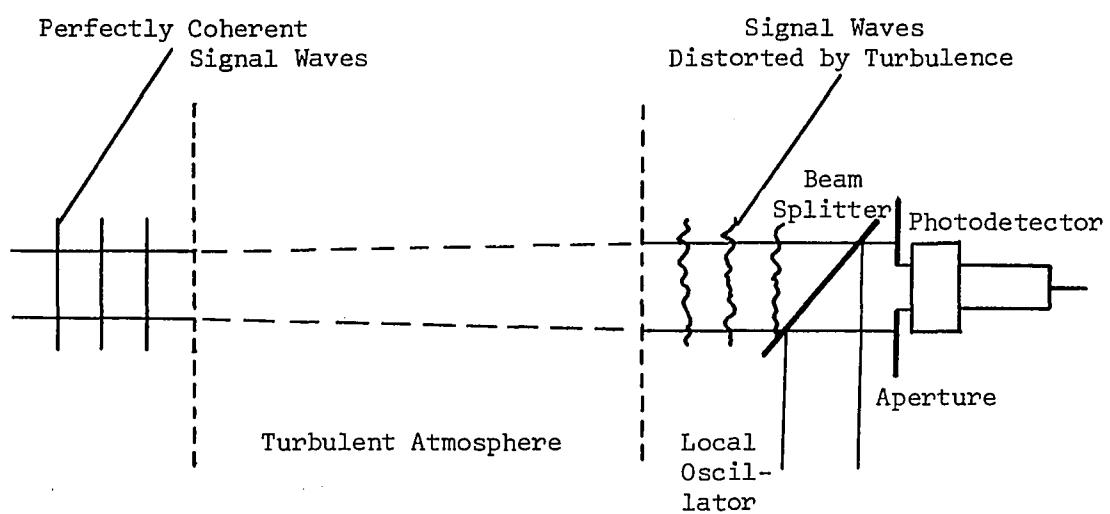
Figure 6. Optical Heterodyne Communications Link
Through a Turbulent Atmosphere

index fluctuations. These statistics have been the subject of investigations by many authors, most notably, Kolmogoroff[16] and Tatarski.[17] They have found that the most convenient way to describe these fluctuations is with a structure function given by

$$D_n(|\bar{R}_2 - \bar{R}_1|) = E[(\Delta n(\bar{R}_2) - \Delta n(\bar{R}_1))^2],$$

where Δn is the variation in index of refraction from the average, i.e., $\Delta n = n - E[n]$. The structure function in contrast to the correlation function, is stationary over a certain period of time (usually an hour or two) and largely unaffected by changes in the variance of Δn from point-to-point. Kolmogoroff has shown that the structure function for separations $|\bar{R}_2 - \bar{R}_1|$ up to a few meters is given by

$$D_n(|\bar{R}_2 - \bar{R}_1|) = c_n^2 |\bar{R}_2 - \bar{R}_1|^{2/3},$$

where c_n^2 is known as the structure constant and depends primarily on the variance of the refractive index fluctuation. It is usually determined experimentally.[5]

The corresponding variations in amplitude and phase of an optical wave are also described by a structure function. This is given by Tartarski[17] as

$$D(|\bar{R}_2 - \bar{R}_1|) = D_1(|\bar{R}_2 - \bar{R}_1|) + D_\phi(|\bar{R}_2 - \bar{R}_1|)$$
$$= \mathcal{D}|\bar{R}_2 - \bar{R}_1|^{5/3}, \qquad\qquad (4\text{-}1)$$

where $\mathcal{D}$ is a constant determined by the path of propagation, turbulence along the path, and wavelength of the optical wave. It is given for paths just above ground level by

$$\mathcal{D} = 2.91\left(\frac{2\pi}{\lambda}\right)^2 Lc_n^2,$$

where λ is the wavelength of the light, L is the communication path length and c_n^2 is the structure constant. In a typical example of $\lambda = 0.63$ μm (He-Ne laser wavelength), L = 1 km, and $c_n^2 = 10^{-15}$ (mid-day turbulence), $\mathcal{D} = 291$. D_1 and D_ϕ are the log-amplitude and phase structure functions and are given by

$$D_1(|\bar{R}_2-\bar{R}_1|) = E[(\ln(A(\bar{R}_2)/E[A^2(\bar{R}_2)]^{\frac{1}{2}} - \ln(A(\bar{R}_1)/E[A^2(\bar{R}_1)]^{\frac{1}{2}})^2]$$

$$= E[(1(\bar{R}_2) - 1(\bar{R}_1))^2]$$

and

$$D_\phi(|\bar{R}_2-\bar{R}_1|) = E[(\phi(\bar{R}_2)-\phi(\bar{R}_1))^2],$$

where

$$1(\bar{R}) = \ln(A(\bar{R})/E[A^2(\bar{R})]^{\frac{1}{2}}).$$

These functions are also stationary for a period of about an hour or two, homogeneous, and isotropic. In addition, the log-amplitude and phase variations are Gaussian in nature.[5,17] With these results,

the ensemble degree of coherence function can be derived in terms of this structure function.

Let us assume that the structure function is ergodic. This assumption is not always justifiable because the constant $\mathcal{D}$ in equation 4-1 varies with the intensity of the turbulence which, in turn, varies with time of day. Over a short time, however, the structure function as stated above, is stationary, and one might expect to see all possible configurations of refractive index variation along the propagation path. Under these conditions, the ergodic assumption is reasonable.

The degree of coherence of a linearly polarized signal carrier field is given from equation 2-2 by

$$\gamma_s(\bar{R}_1,\bar{R}_2) = \frac{E[E_s(\bar{R}_1,t)E_s^*(\bar{R}_2,t)]}{[E[E_s(\bar{R}_1,t)E_s^*(\bar{R}_1,t)]E[E_s(\bar{R}_2,t)E_s^*(\bar{R}_2,t)]]^{\frac{1}{2}}} \; ,$$

where

$$E_s(\bar{R},t) = A_s(\bar{R},t)e^{j\bar{\omega}_s t} \; ,$$

and

$$A_s(\bar{R},t) = A_s(\bar{R},t)e^{j\phi(\bar{R},t)}$$

in this case. This may be rewritten, dropping the t, as

$$\gamma_s(\bar{R}_1, \bar{R}_2) = \frac{E[A_s(\bar{R}_1)A_s^*(\bar{R}_2)]}{E[A_s^2(\bar{R}_1)]^{\frac{1}{2}}E[A_s^2(\bar{R}_1)]^{\frac{1}{2}}}$$

$$= E\left[\frac{A_s(\bar{R}_1)}{E[A_s^2(\bar{R}_1)]^{\frac{1}{2}}} \cdot \frac{A_s(\bar{R}_2)}{E[A_s^2(\bar{R}_2)]^{\frac{1}{2}}} e^{j(\phi(\bar{R}_1)-\phi(\bar{R}_2))}\right]$$

$$= E[e^{[(1(\bar{R}_1)+1(\bar{R}_2)) + j(\phi(\bar{R}_1)-\phi(\bar{R}_2))]}].$$

Fried shows, using the property[5]

$$E[e^{(a\alpha+b\beta)}] = e^{[a^2/2\, E[(\alpha-E[\alpha])^2] + b^2/2\, E[(\beta-E[\beta])^2]}$$

$$+ aE[\alpha] + bE[\beta]]$$

of independent Gaussian random variables α and β with constants a and b and in addition using the fact

$$E[(1(\bar{R}) - E[1(\bar{R})])^2] + E[1(\bar{R})] = 0$$

and assuming $1(\bar{R}_1) + 1(\bar{R}_2)$ and $\phi(\bar{R}_1) - \phi(\bar{R}_2)$ are independent, that

$$E[e^{[(1(\bar{R}_1)+1(\bar{R}_2)) + j(\phi(\bar{R}_1)-\phi(\bar{R}_2))]}]$$

$$= e^{-\frac{1}{2}[E[(1(\bar{R}_2)-1(\bar{R}_1))^2] + E[(\phi(\bar{R}_2)-\phi(\bar{R}_1))^2]}}.$$

The degree of coherence is, therefore, equal to

$$\gamma_s(\bar{R}_1,\bar{R}_2) = e^{-\frac{1}{2}E[(1(\bar{R}_2)-1(\bar{R}_1))^2] - \frac{1}{2}E[(\phi(\bar{R}_2)-\phi(\bar{R}_1))^2]}$$

$$= e^{-\frac{1}{2}D_1(|\bar{R}_2-\bar{R}_1|) - \frac{1}{2}D_\phi(|\bar{R}_2-\bar{R}_1|)}$$

$$= e^{-\frac{1}{2}D(|\bar{R}_2-\bar{R}_1|)}.$$

The degree of coherence of the carrier signal field from this and equation 4-1 is

$$\gamma_s(\bar{R}_1,\bar{R}_2) = e^{-\mathcal{D}/2 |\bar{R}_2-R_1|^{5/3}}. \tag{4-2}$$

For two fixed points $\bar{R}_1$ and $\bar{R}_2$, an increase in turbulence will result in a decrease in the field coherence at points $\bar{R}_1$ and $\bar{R}_2$. For the example used earlier where $\mathcal{D} = 291$, the degree of coherence will drop to $1/e$ when the separation is $|\bar{R}_2-\bar{R}_1| = 3.3$ cm.

Calculation of Heterodyne Efficiency and SNR

With the coherence function of equation 4-2, the heterodyne efficiency and signal-to-noise ratio can be calculated for various choices of I_L, the local oscillator distribution on S; various degrees of coherence of the local oscillator beam; and various sizes and shapes of receiver aperture. There are many possible combinations that can be studied. Only the following cases involving receiver parameters are discussed: (1) constant I_s on S and Gaussian I_L of different diameters as a function of different circular aperture diameters for a perfectly coherent local oscillator, (2) constant I_s and Gaussian I_L

at one specific circular aperture diameter for a "nearly" perfect local oscillator coherence, and (3) constant I_s and rectangular I_L of one specific beam radius for a perfectly coherent and a "nearly perfectly coherent local oscillator.

The coordinate system used for the calculation at the photosurface is shown in Figure 7. The degree of coherence in terms of points (y_1'', z_1'') and (y_2'', z_2'') on the photosurface from equation 4-2 is

$$\gamma_s(y_1'', z_1'', y_2'', z_2'') = e^{-\mathcal{D}/2([(y_1''-y_2'')^2+(z_1''-z_2'')^2]^{\frac{1}{2}})^{5/3}}$$

$$= e^{-\mathcal{D}/2[(y_1''-y_2'')^2+(z_1''-z_2'')^2]^{5/6}} .$$

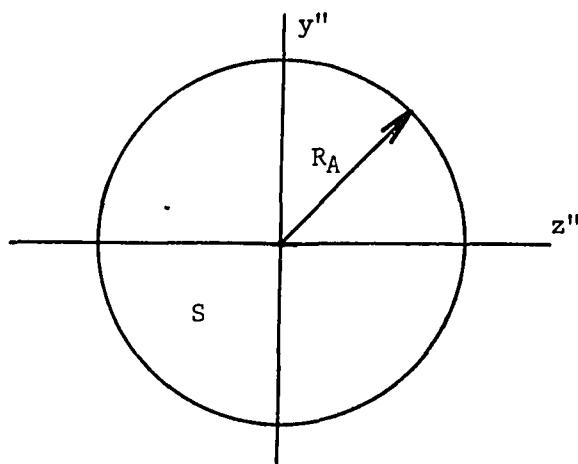Normalizing by letting

$$Y = \frac{y''}{(2/\mathcal{D})^{3/5}} \quad \text{and} \quad Z = \frac{z''}{(2/\mathcal{D})^{3/5}} ,$$

we have

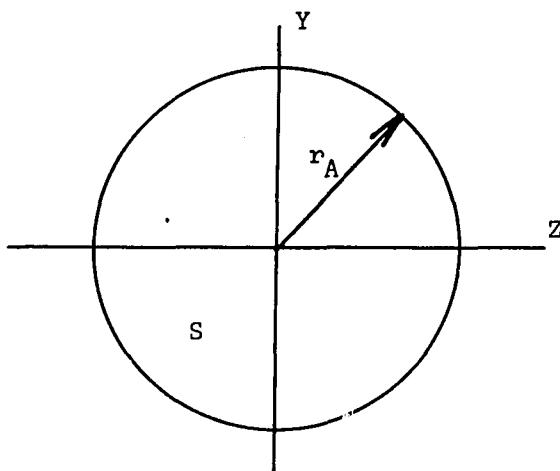$$dy'' = (2/\mathcal{D})^{3/5} dY \quad \text{and} \quad dz = (2/\mathcal{D})^{3/5} dZ$$

and

$$\gamma_s(y_1'', z_1'', y_2'', z_2'') = e^{-[(Y_1-Y_2)^2+(Z_1-Z_2)^2]^{5/6}} ,$$

a. Actual Coordinate System

b. Normalized Coordinate System

Figure 7. Coordinate System at the Photodetector

The exact form of the functions used in the calculation are

$$\gamma_s(y_1'',z_1'',y_2'',z_2'') = e^{-[(Y_1-Y_2)^2+(Z_1-Z_2)^2]^{5/6}},$$

$$I_L(y'',z'') = e^{-2(Y^2+Z^2)/A^2} \qquad \text{for a Gaussian distribution,}$$

$$I_L(y'',z'') = \begin{cases} 1 & \text{for } Y^2+Z^2 < A^2 \\ 0 & \text{for } Y^2+Z^2 \geq A^2 \end{cases} \qquad \text{for a rectangular distribution,}$$

$$I_s(y'',z'') = 1,$$

$$\gamma_L(y_1'',z_1'',y_2'',z_2'') = 1 \qquad \text{for perfect local oscillator coherence,}$$

and

$$\gamma_L(y_1'',z_1'',y_2'',z_2'') = e^{-[(Y_1-Y_2)^2+(Z_1-Z_2)^2]/(3.1A)^2}$$

for "nearly" perfect coherence, where A is the normalized beam radius. The "nearly" perfect local oscillator coherence function is for a source whose field variations at the center of the beam are 90 per cent coherent with those at the beam radius. Most lasers produce radiation whose coherence is within these limits.

The equations used for calculation of the heterodyne efficiency and SNR are:

1. For the signal power

$$P_S = \int_{-r_A}^{r_A} \int_{-\sqrt{r_A^2 - Y_2^2}}^{\sqrt{r_A^2 - Y_2^2}} \int_{-r_A}^{r_A} \int_{-\sqrt{r_A^2 - Y_1^2}}^{\sqrt{r_A^2 - Y_1^2}} [I_L(y_1'', z_1'') I_L(y_2'', z_2'')]^{\frac{1}{2}}$$

$$\cdot \gamma_L(y_1'', z_1'', y_2'', z_2'') \gamma_s(y_1'', z_1'', y_2'', z_2'') dZ_1 dY_1 dZ_2 dY_2. \qquad (4\text{-}3)$$

2. For the ideal signal power

$$P_I = \int_{-r_A}^{r_A} \int_{-\sqrt{r_A^2 - Y_2^2}}^{\sqrt{r_A^2 - Y_2^2}} \int_{-r_A}^{r_A} \int_{-\sqrt{r_A^2 - Y_1^2}}^{\sqrt{r_A^2 - Y_1^2}} [I_L(y_1'', z_1'') I_L(y_2'', z_2'')]^{\frac{1}{2}}$$

$$dZ_1 dY_1 dZ_2 dY_2. \qquad (4\text{-}4)$$

3. For the noise power

$$P_N = \int_{-r_A}^{r_A} \int_{-\sqrt{r_A^2 - Y^2}}^{\sqrt{r_A^2 - Y^2}} I_L(y'', z'') dZ dY, \qquad (4\text{-}5)$$

where r_A is the normalized circular aperture radius. The heterodyne efficiency and SNR are given in terms of P_S, P_I, and P_N by

$$\eta_h = \frac{P_S}{P_I} \quad \text{and} \quad \text{SNR} = \frac{qeI_s}{hfB} (2/\mathcal{D})^{6/5} \frac{P_S}{P_N}.$$

The equations are too complex for analytical evaluation and were, therefore, evaluated using integral approximation techniques on a digital computer. Sample programs used are presented in Appendix I.

Now let us look at the effects of changing various receiver parameters on n_h and SNR. In Figure 8, the actual signal power P_S, ideal signal power P_I, and shot noise power P_N are plotted in arbitrary units versus r_A for A = 1 and perfect local oscillator coherence. We see that increasing r_A increases all three up to a point where almost all of the local oscillator power is used. We see too that the ideal signal power rises faster than the actual signal power so the efficiency decreases. The actual signal power increases faster than the noise power so the SNR increases.

Figures 9 and 10 show plots of heterodyne efficiency and SNR versus r_A and r_A/A, respectively, for perfect local oscillator coherence. The SNR plotted is the ratio P_S/P_N in Figure 9 and $(P_S/P_N)/(P_S/P_N)_{max}$ in Figure 10. Looking first at Figure 10, we see that for smaller local oscillator beam radi, the heterodyning is more efficient for a constant r_A/A. Nearly perfect operation can be achieved with A = 0.1. A maximum SNR is achieved for $r_A/A \stackrel{\sim}{=} 2$. We can obtain the most efficient operation, therefore, by making A small and adjusting r_A so that $r_A/A \stackrel{\sim}{=} 2$. Figure 9, however, shows that operation in this manner yields poor SNR as compared to larger local oscillator beam radii. Here, better SNR but poorer efficiency results for larger A's. Therefore, good efficiency and good SNR cannot be simultaneously obtained.
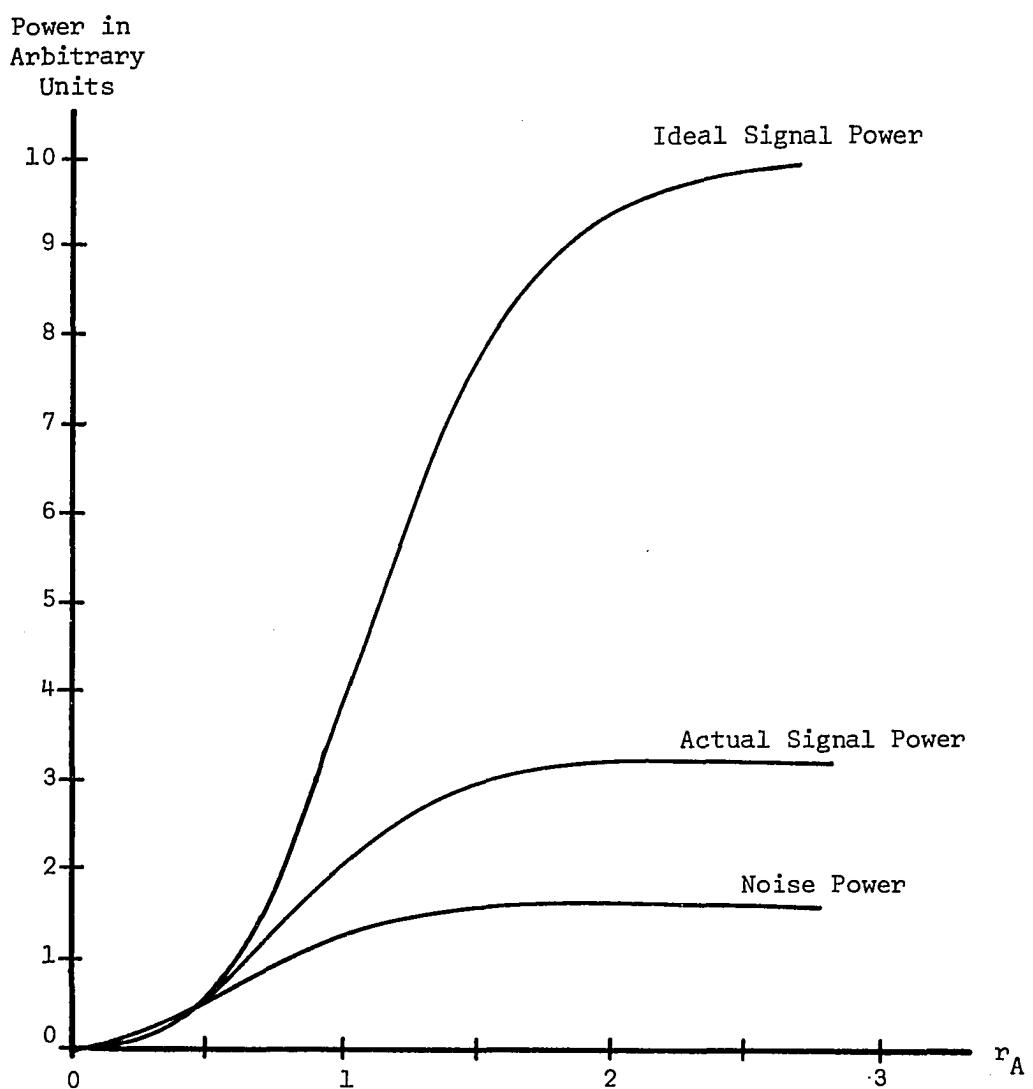
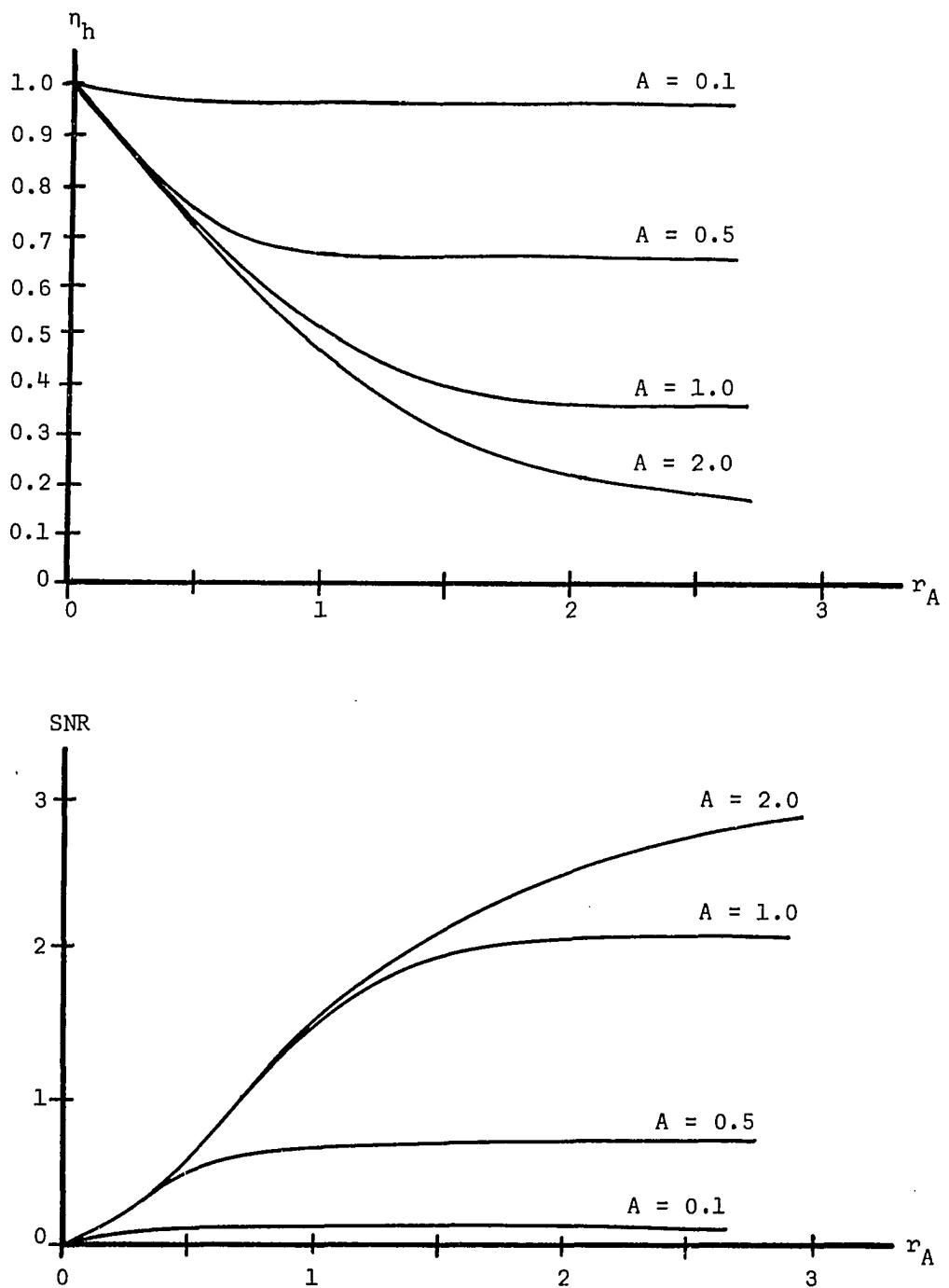Figure 8. A Plot of P_S, P_I, and P_N for A = 1

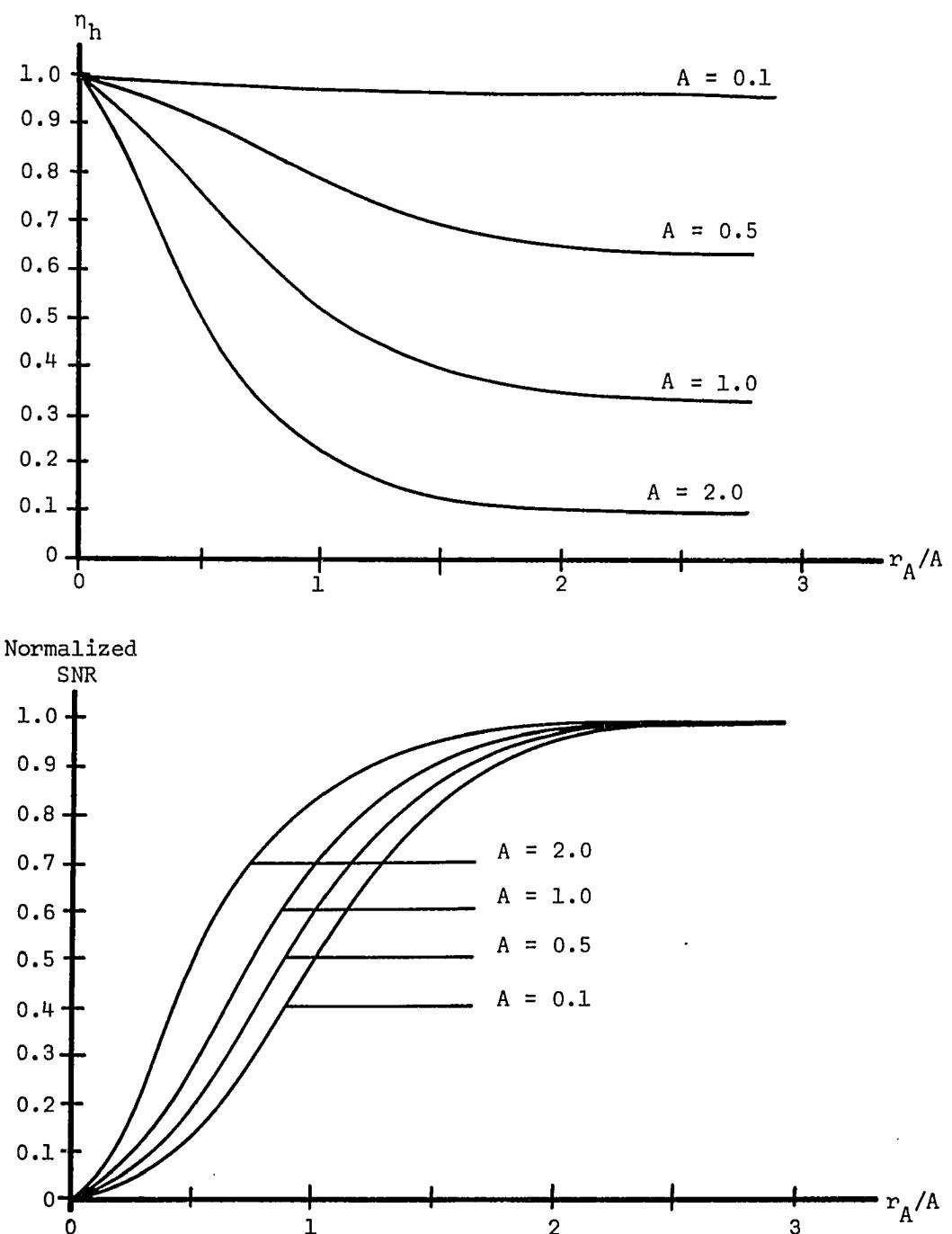Figure 9. Plots of η_h and SNR Versus r_A for Various Values of A

Figure 10.   Plots of η_h and Normalized SNR
Versus r_A/A for Various Values of A

Figure 11 shows the comparison of heterodyne efficiency for a perfect coherent and a "nearly" perfect coherent local oscillator field. We see that small reductions in local oscillator coherence produce no significant reduction in heterodyne efficiency.

Figure 12 shows the comparison of heterodyne efficiency for a rectangular local oscillator intensity of radius A = 1 to a Gaussian intensity function of the same radius for perfect local oscillator coherence. We see that there is no significant difference between the curves for r_A less than A.

Figure 13 shows the comparison of heterodyne efficiency for a rectangular I_L with A = 1 for a perfectly coherent and a "nearly" perfectly coherent local oscillator field. The results show that there is no substantial difference in sensitivity to local oscillator coherence than for the Gaussian I_L case.

In summary, we see that the local oscillator beam size is the most important parameter in determining the system efficiency and SNR. Slight reductions in local oscillator coherence and small changes in oscillator beam shape do not significantly change the system operation. We see, too, that for maximum SNR, the local oscillator beam radius must be made as large as possible, whereas, for maximum efficiency, it should be made as small as possible.

A Laser Doppler Surface Motion Measuring System

Heterodyne detection has been extensively applied in various types of measurement systems, primarily in velocity measuring systems. Optical heterodyne detection of coherent light scattered from a moving
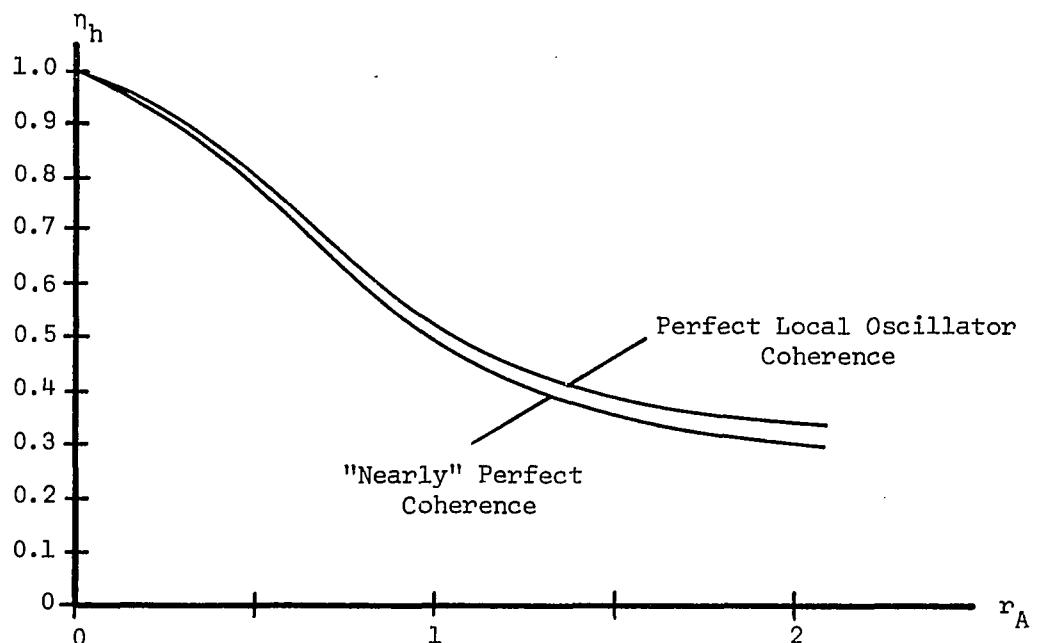
Figure 11. A Plot of η_h Versus r_A for A = 1 for Perfect
and "Nearly" Perfect Local Oscillator
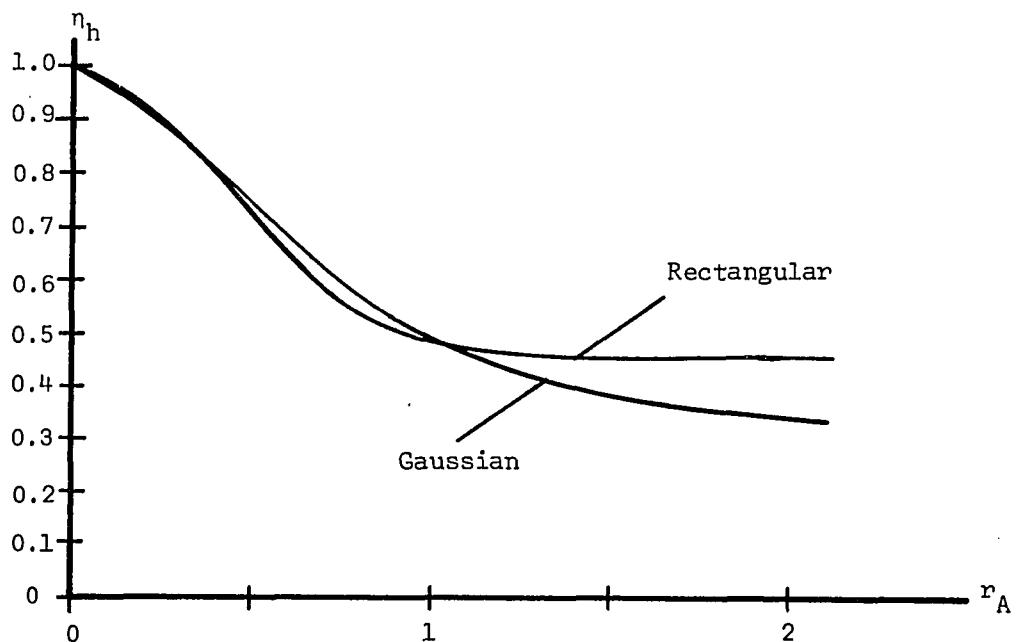Coherence, Gaussian Intensity Distribution

Figure 12. A Plot of η_h Versus r_A for Gaussian and
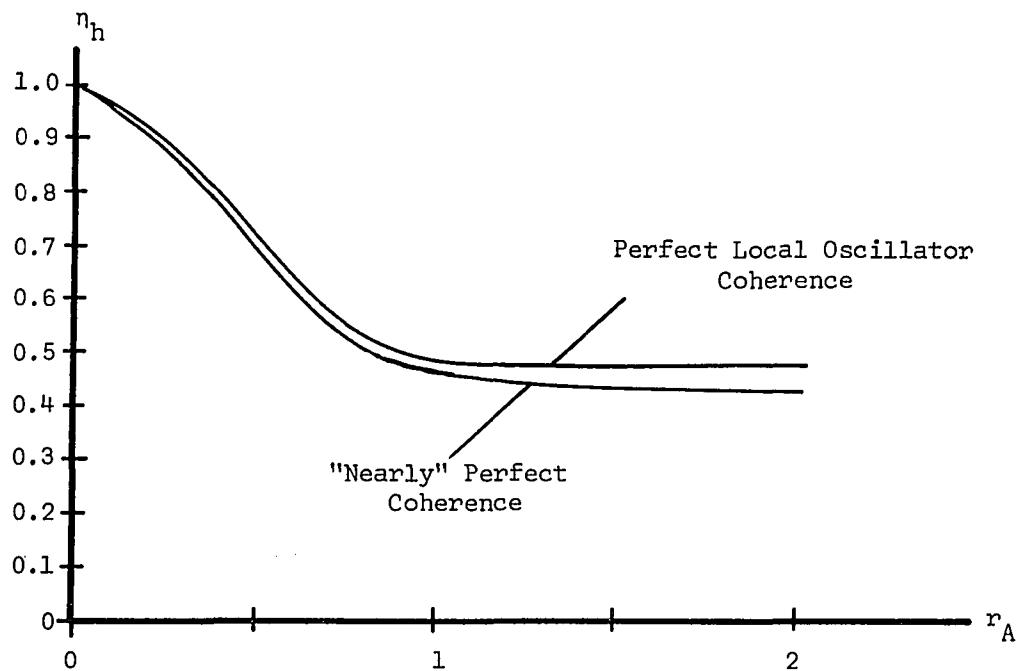Rectangular Intensity Distribution, A = 1

Figure 13. A Plot of η_h Versus r_A for A = 1 for Perfect
and "Nearly" Perfect Local Oscillator
Coherence, Rectangular Intensity Distribution

object provides a very accurate and sensitive method for measuring its velocity. One specific example is the use of optical heterodyning to measure the velocity of a rough surface. Two such applications have been reported.[18,19] Another specific system called a laser Doppler surface velocimeter (LDSV) is investigated here.

The system to be investigated is illustrated in Figure 14. In this arrangement, a beam from a continuous wave laser is focused on a rough surface. A portion of the incident beam is split off for use as a local oscillator. The portion of the light scattered at an angle θ by the surface constitutes the signal. The optical components are aligned so both beams travel equal path lengths in reaching the photo-detector, and are refocused coincident there. Because of the Doppler effect, the heterodyne signal output will be of frequency[20]

$$f_D = \frac{\omega_D}{2\pi} = \frac{1}{2\pi} (\bar{k}_s - \bar{k}_0) \cdot \bar{v},$$

where $\bar{k}_s$ and $\bar{k}_0$ are the wave vectors of the scattered and incident light and $\bar{v}$ is the velocity at the surface at the focal point. In terms of the angles involved

$$f_D = \frac{k_o v}{\pi} \sin \frac{\theta}{2} \cos(\psi + \frac{\theta}{2})$$

$$= \frac{2v}{\lambda_0} \sin \frac{\theta}{2} \cos(\psi + \frac{\theta}{2}),$$

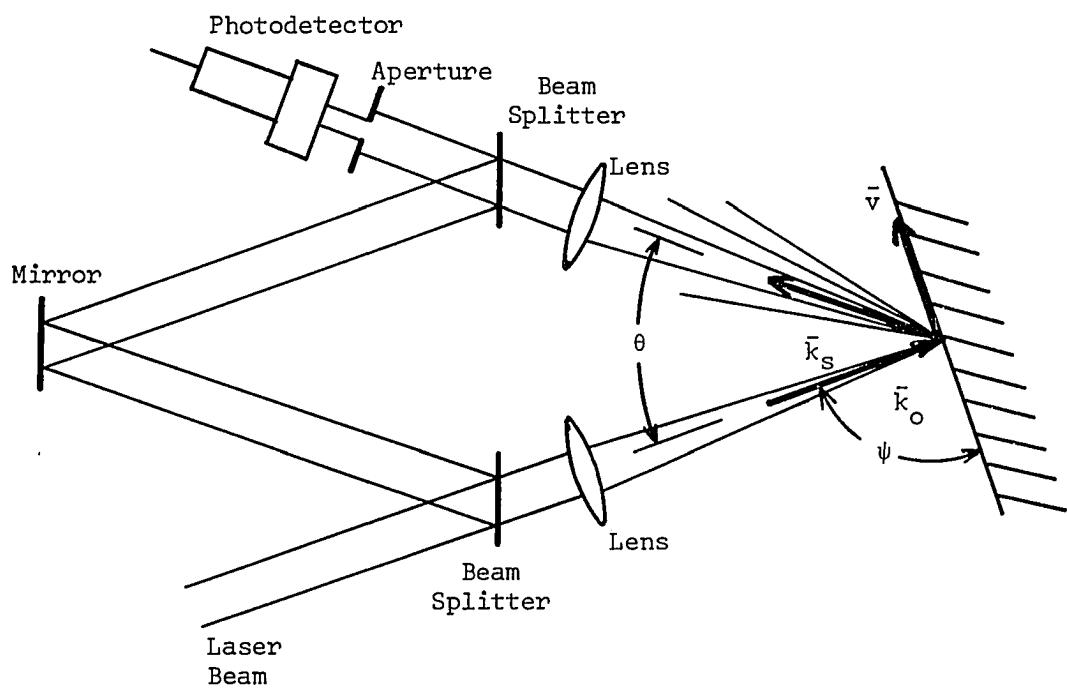where λ_0 is the wavelength of the incident radiation and $k_s \cong k_o$

Figure 14. A Laser Doppler Surface Velocimeter

(valid for non-relativistic velocities). By measuring f_D, θ, and ψ, we can determine the velocity v of the surface.

Since the signal beam is composed of light scattered from a moving random rough surface, the signal field will fluctuate randomly. These fluctuations will not be perfectly correlated over the photo-surface, therefore, a reduction in signal field coherence results. To calculate this, the system must first be mathematically modeled.

Mathematical Model for the System

In modeling the laser Doppler surface motion measuring system, mathematically, the following assumptions are initially made:

1. The rough surface is modeled by a two-dimensional densely packed monodispersed distribution of spherical particles. These particles are distributed at random in a Poisson way so that the probability of finding N particles in a square area A is given by.

$$P(N,A) = \frac{(MA)^N}{N!} e^{-MA},$$

where M denotes the average number of particles per unit area. All particles have the same velocity.

2. The incident radiation is approximated by a Gaussian beam. The field in the focal region for such a beam is given by[21]

$$E(r,x) = \frac{E_o w_o}{w} e^{-[r^2/w^2 + j(kx-\Phi-kr^2/2R)]},$$

where propagation is along the x axis, $r^2 = y^2 + z^2$, k is the

propagation constant, w is the beam radius defined by

$$w = w_o[1 + (\lambda x/\pi w_o^2)^2]^{\frac{1}{2}}$$

and w_o is the beam radius at the focal point, Φ is given by

$$\Phi = \tan^{-1}(\lambda x/\pi w_o^2),$$

and R is the radius of curvature of the wavefronts and is given by

$$R = x[1 + (\pi w_o^2/\lambda x)^2].$$

Figure 15 shows constant intensity contours and wavefront curvatures. Away from the focal area the beam radius diverges at an angle of

$$\Theta = \frac{\lambda}{\pi w_o}$$

from the propagation axis. Within a few beam radii of the focal point,

$$R \rightarrow \infty, \quad w \tilde{=} w_o, \quad \text{and} \quad \Phi \tilde{=} 0,$$

so the field is given by the approximate form

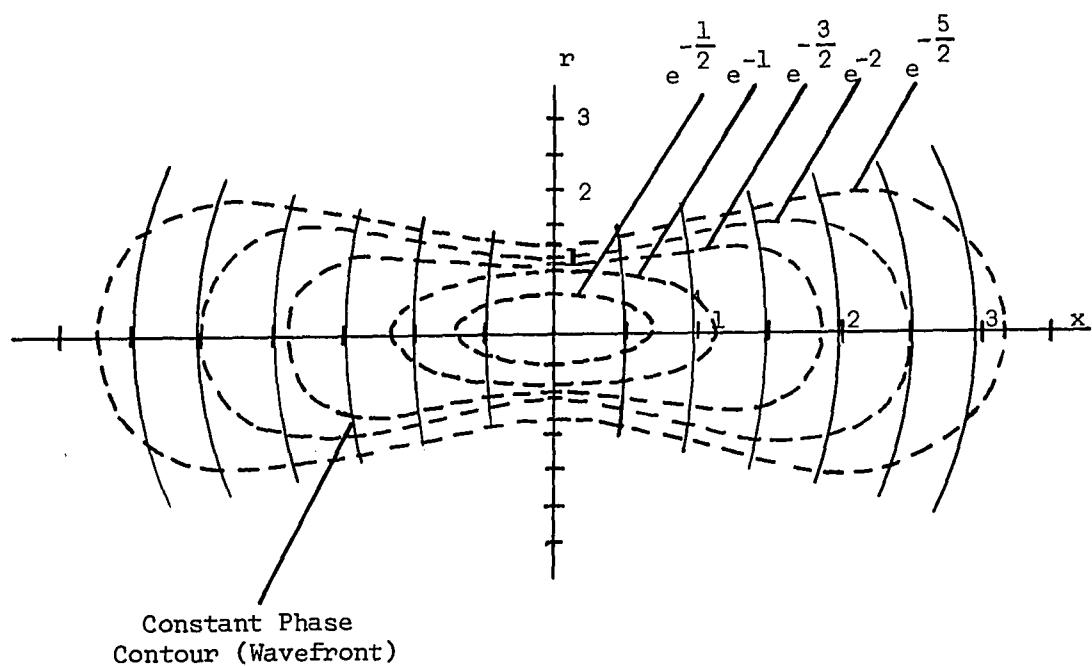$$E(r,x) = E_o e^{-r^2/w_o^2} e^{-jkx} \tag{4-7}$$

Figure 15. Constant Intensity and Phase Contours for an Ideal Gaussian Beam

3. The scattered wave from each particle is assumed to be spherical so that each particle can be considered as a point scatterer. The intensity of the scattered wave is essentially constant over the receiving aperture. The velocity of the particles is slow enough so that a quasi-static approach may be taken where the particle is considered stationary in calculating the scattered wave. No multiple scattering is considered.

4. The photosurface is considered to be spherical with center at the focal point. The transformation of the plane photosurface at the focal point of the collecting lens back through the lens yields such a surface. For further simplification, the expression of a scattered spherical wave on this spherical photosurface is approximated by the expression of a scattered plane wave on a plane surface. The error for typical dimensions of the scattering region (w_o = 100 μm) and the receiving aperture at a distance of 40 cm (R_A = 1 mm) is less than one-tenth of a wavelength, a negligible amount.

5. The average quantities are assumed to be stationary and ergodic. This assumption is discussed in Appendix II. In addition, the signal and local oscillator are assumed to be independent and linearly polarized so equations 3-3 and 3-4 may be used to evaluate the system performance. Actually, the signal and local oscillator variations are coupled to some extent because they are derived from the same beam in most systems. The coherence of this beam is such that this effect is negligible, however. There will be a cross polarization component of the signal beam due to scattering but only

the parallel component will heterodyne with the linearly polarized local oscillator.

Figure 16 illustrates the coordinate systems to be used. The photosurface is in the x,y,z coordinate system, y" and z" represent a point on it. The rough surface is in the y_p, z_p plane and the incident radiation is most conveniently described in the x', y', z' coordinate system being incident in the -x' direction.

The incident radiation is given from equation 4-7 by

$$E_{inc}(x',y',z') = E_o e^{-y'^2+z'^2/w_o^2} e^{jk_L x'}.$$

The scattered wave at a point x,y,z from the kth particle is given by

$$E_{s_k}(x,y,z) = mE_{inc}(x_k',y_k',z_k')e^{-jk_L d_k(x,y,z)}.$$

The quantity m is a scattering coefficient given by

$$m = E_s/E_o$$

and d_k is the distance from x,y,z, to the kth scattering particle. The total scattered field is given by

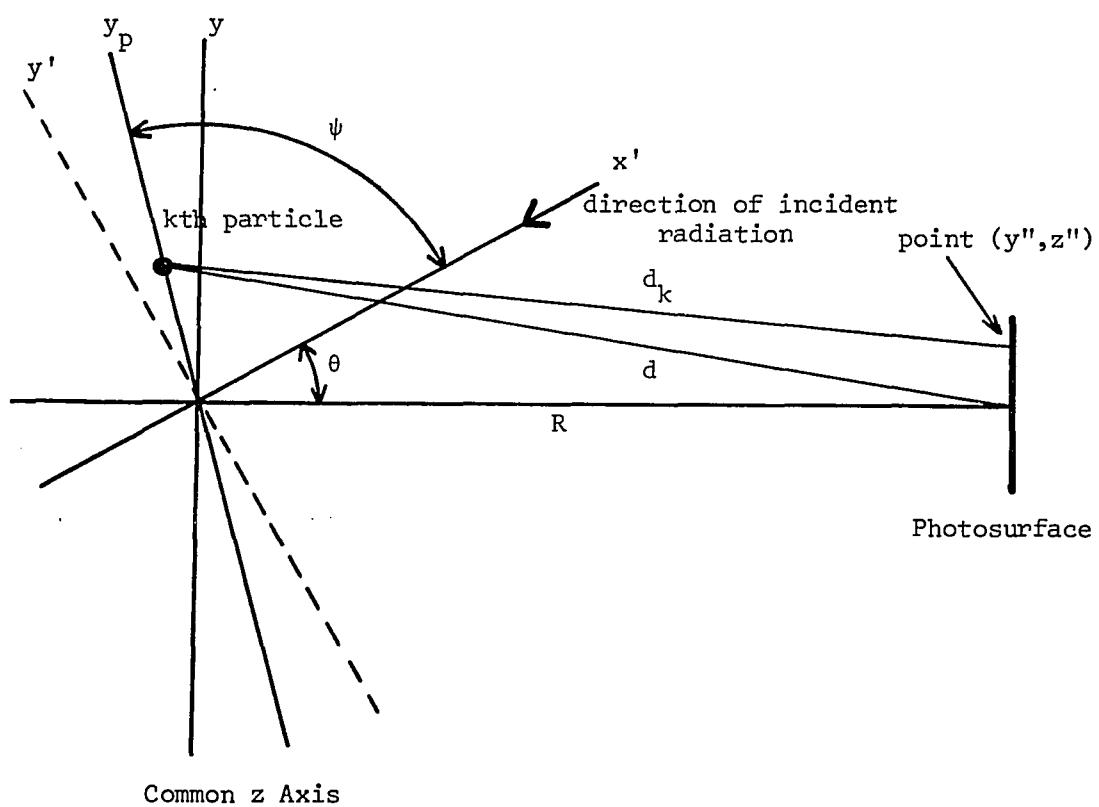$$E_s(x,y,z) = \sum_{k}^{\substack{all \\ particles}} E_{s_k}(x,y,z).$$

Figure 16. The Coordinate System for the LDSV Calculations

The ensemble mutual coherence in the scattered radiation at two points on the photosurface is given by

$$\Gamma_s(y_1'',z_1'',y_2'',z_2'') = E[E_s(y_1'',z_1'')E_s^*(y_2'',z_2'')]$$

$$= E\left[\sum_i \sum_j E_{s_i}(y_1'',z_1'')E_{s_j}^*(y_2'',z_2'')\right].$$

This average has been derived in Appendix II and is equal to

$$\Gamma_s(y_1'',z_1'',y_2'',z_2'') = M \int_{-\infty}^{\infty} \int_{-\infty}^{\infty} E_{s_k}(y_1'',z_1'')E_{s_k}^*(y_2'',z_2'')dy_{p_k} dz_{p_k},$$

where M is the average number of particles per unit area. Looking just at the integrand, we have

$$E_{s_k}(y_1'',z_1'')E_{s_k}^*(y_2'',z_2'')$$

$$= m^2 E_{inc} E_{inc}^* e^{-jk_L d_k(y_1'',z_1'')} e^{jk_L d_k(y_2'',z_2'')}$$

$$= E_s^2 e^{-2(y_k'^2+z_k'^2/w_o^2)} e^{jk_L(d_k(y_2'',z_2'')-d_k(y_1'',z_1''))}.$$

Using the plane-wave approximation for the scattered wave, we have for the phase term

$$d_k(y_2'',z_2'') - d_k(y_1'',z_1'') \cong \left[d - \frac{y_2''y_k}{d} - \frac{z_2''z_k}{d}\right] - \left[d - \frac{y_1''y_k}{d} - \frac{z_1''z_k}{d}\right]$$

$$= (y_1''-y_2'')\frac{y_k}{d} + (z_1''-z_2'')\frac{z_k}{d},$$

which using the coordinate transformation to y_p, z_p system is

$$\cong (y_1''-y_2'') \frac{\sin(\theta+\psi)}{R} y_{p_k} + (z_1''-z_2'') \frac{z_{p_k}}{R} ,$$

where $d \cong R$ at points on the surface where E_{inc} has significant amplitude. The integrand now becomes

$$E_{s_k}(y_1'',z_1'')E_{s_k}^*(y_2'',z_2'') = E_3^2 e^{-2(y_{p_k}^2 \sin^2\psi + z_{p_k}^2 /w_o^2)}$$

$$\cdot e^{j k_L y_{p_k} \sin(\phi+\psi)/R (y_1''-y_2'')} e^{j k_L z_{p_k}/R (z_1''-z_2'')} .$$

Therefore,

$$\Gamma_s(y_1'',z_1'',y_2'',z_2'') = ME_s^2 \int_{-\infty}^{\infty} e^{-2z_{p_k}^2 /w_o^2} e^{j k_L z_{p_k}/R (z_1''-z_2'')} dz_{p_k}$$

$$\cdot \int_{-\infty}^{\infty} e^{-2y_{p_k}^2 \sin^2\psi/w_o^2} e^{j k_1 y_{p_k} \sin(\theta+\psi)/R (y_1''-y_2'')} dy_{p_k}$$

$$= ME_3^2 \left[\frac{\sqrt{\pi} w_o}{\sqrt{2}} e^{-\pi^2 w_o^2/2R^2\lambda^2 (z_1''-z_2'')^2} \right]$$

$$\cdot \left[\frac{\sqrt{\pi} w_o}{\sqrt{2} \sin\psi} e^{-\pi^2 w_o^2/2R^2\lambda^2 \sin^2(\theta+\psi)/\sin^2\psi \cdot (y_1''-y_2'')^2} \right] .$$

Identifying

$$\Theta = \frac{\lambda}{\pi w_o}$$

the angular divergence of a Gaussian beam of focal radius w_o and

normalizing by letting

$$Y = \frac{y''}{R\Theta} \qquad \text{and} \qquad Z = \frac{z''}{R\Theta} \text{ ,}$$

we have

$$\Gamma_s(y_1'',z_1'',y_2'',z_2'') = \frac{ME_s^2 \pi w_o^2}{2\sin\psi} e^{-\frac{1}{2}[(Y_1-Y_2)^2 \sin^2(\theta+\psi)/\sin^2\psi + (Z_1-Z_2)^2]} \text{ .}$$

Now

$$\Gamma_s(y_1'',z_1'',y_1'',z_1'') = \Gamma_s(y_2'',z_2'',y_2'',z_2'') = \frac{ME_s^2 \pi w_o^2}{2\sin\psi} \text{ ,}$$

so

$$\gamma_s(y_1'',z_1'',y_2'',z_2'') = e^{-\frac{1}{2}[(Y_1-Y_2)^2 \sin^2(\theta+\psi)/\sin^2\psi + (Z_1-Z_2)^2]} \text{ .} \qquad (4\text{-}8)$$

Making w_o smaller at the rough surface as expected increases the region

of coherence at the photosurface. This region of coherence is elliptic

in shape, however, due to the $\sin^2(\theta+\psi)/\sin^2\psi$ factor in γ_s above.

Calculation of Heterodyne Efficiency and SNR

The heterodyne efficiency and SNR are calculated from equations 3-3 and 3-4 for the following important cases: (1) constant I_s and Gaussian I_L of different diameters as a function of different circular aperture diameters for a perfectly coherent local oscillator, (2) constant I_s and Gaussian I_L of one specific diameter at different circular aperture diameters for "nearly" perfect local oscillator coherence, (3) constant I_s and Gaussian I_L of one specific diameter for various elliptic apertures that matches the eccentricity of the coherence region for perfect and "nearly" perfect local oscillator coherence, and (4) constant I_s and rectangular I_L at various circular aperture diameters for perfect and "nearly" perfect local oscillator coherence. The coordinate system shown in Figure 7 is again used for calculation except for this case,

$$Y = \frac{y''}{R\Theta}\,, \quad Z = \frac{z''}{R\Theta}\,, \quad dy'' = R\Theta dY, \quad \text{and} \quad dz'' = R\Theta dZ,$$

so that

$$\gamma_s(y_1'',z_1'',y_2'',z_2'') = e^{-\frac{1}{2}[(Y_1-Y_2)^2 \sin^2(\theta+\psi)/\sin^2\psi + (Z_1-Z_2)^2]}, \quad (4\text{-}9)$$

$$I_L(y'',z'') = e^{-2(Y^2+Z^2)/A^2} \quad \text{for a Gaussian distribution}, \quad (4\text{-}10)$$

$$I_L(y'',z'') = \begin{cases} 1 & \text{for } Y^2+Z^2<A^2 \\ 0 & \text{for } Y^2+Z^2\geq A^2 \end{cases} \quad \text{for a rectangular distribution},$$

$$I_S(y'',z'') = 1,$$

$$\gamma_L(y_1'',z_1'',y_2'',z_2'') = 1 \quad \text{for perfect local oscillator coherence,}$$

and

$$\gamma_L(y_1'',z_1'',y_2'',z_2'') = e^{-[(Y_1-Y_2)^2+(Z_1-Z_2)^2]/(3.1A)^2} \tag{4-11}$$

for "nearly" perfect coherence.

The equations for the heterodyne efficiency and SNR are

$$\eta_h = \frac{P_S}{P_I} \tag{4-12}$$

and

$$SNR = \frac{qe}{hfB} \frac{E_s^2 \pi w_o^2 R^2 \Theta^2}{2\sin\psi} \frac{P_S}{P_N} , \tag{4-13}$$

where P_S, P_I and P_N are given by equations 4-3, 4-4, 4-5 and r_A in those equations is the normalized circular aperture radius. For the case of the elliptic aperture, the upper and lower limit in the Z integration of the equations are

$$\sqrt{r_A^2-Y^2} \, \frac{\sin(\theta+\psi)}{\sin\psi} \quad \text{and} \quad -\sqrt{r_A^2-Y^2} \, \frac{\sin(\theta+\psi)}{\sin\psi} \, .$$

Since these equations are again too complex for analytical evaluation, a digital computer was used. Sample programs are presented in Appendix

I. The values of θ and ψ were taken as 30° and 90°, respectively.
The results are presented in Figures 17 through 22.

Figures 17 and 18 show plots of heterodyne efficiency and SNR
versus r_A and r_A/A, respectively, for perfect local oscillator
coherence. The SNR plotted in Figure 17 is P_S/P_N, and in Figure 18,
is $(P_S/P_N)/(P_S/P_N)_{max}$. Looking first at the plots in Figure 18,
we see that for smaller local oscillator beam radii, the heterodyning
is more efficient for constant r_A/A. We see, too, that maximum SNR
for each case is obtained by making $r_A/A \cong 2$. From Figure 17, however,
we see that operating in this manner yields poor SNR as compared to
larger local oscillator radii. Therefore, good efficiency and good
SNR cannot be obtained simultaneously.

Figure 19 shows the comparison of heterodyne efficiency for
perfect and "nearly" perfect local oscillator coherence. We see that
slight reductions in the local oscillator coherence have no significant
effect on heterodyne efficiency.

Figure 20 shows the comparison of circular versus elliptic aper-
ture for perfect local oscillator coherence. There is very little
difference between the two curves.

Figure 21 shows this comparison for rectangular versus Gaussian
local oscillator intensity distribution. We see essentially no sig-
nificant difference for r_A less than A.

Figure 22 shows this comparison for rectangular I_L with A = 1
for perfect and "nearly" perfect local oscillator coherence. Slight
reductions in the local oscillator coherence have no significant effect
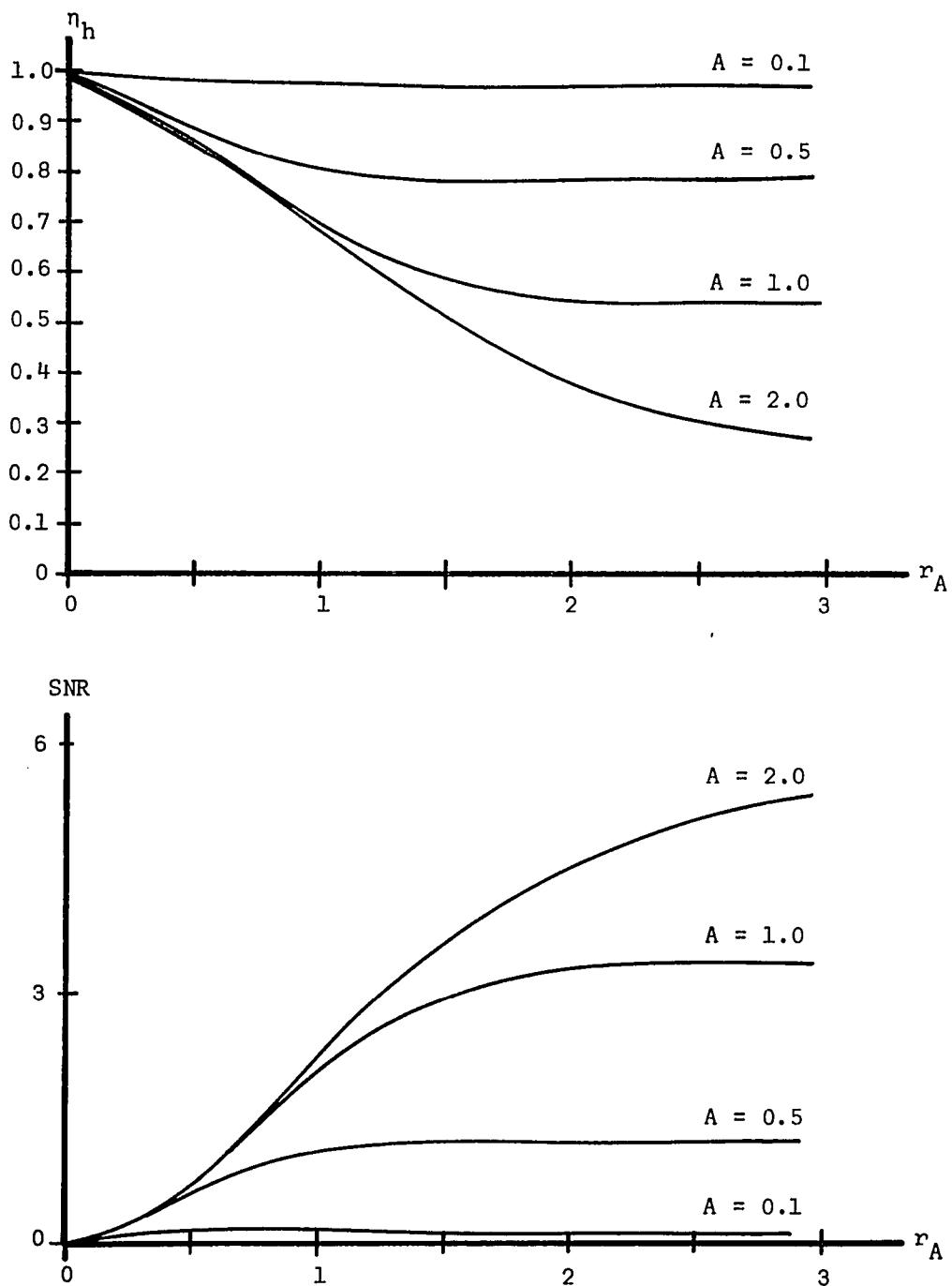on the efficiency.

Figure 17.   Plots of η_h and SNR Versus r_A for Various
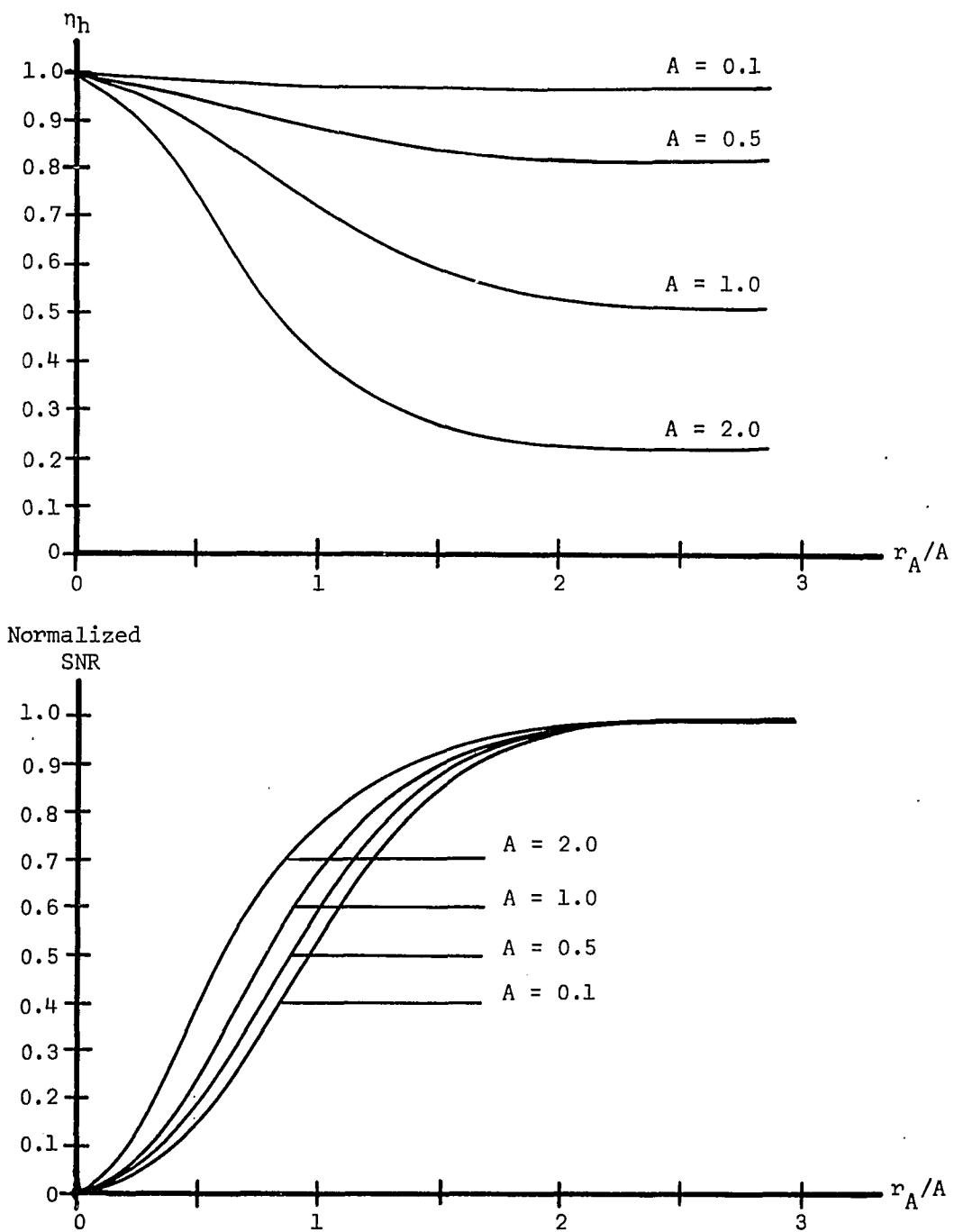Values of A, Gaussian Intensity Distribution

Figure 18. Plots of η_h and Normalized SNR Versus r_A/A
for Various Values of A, Gaussian I_L
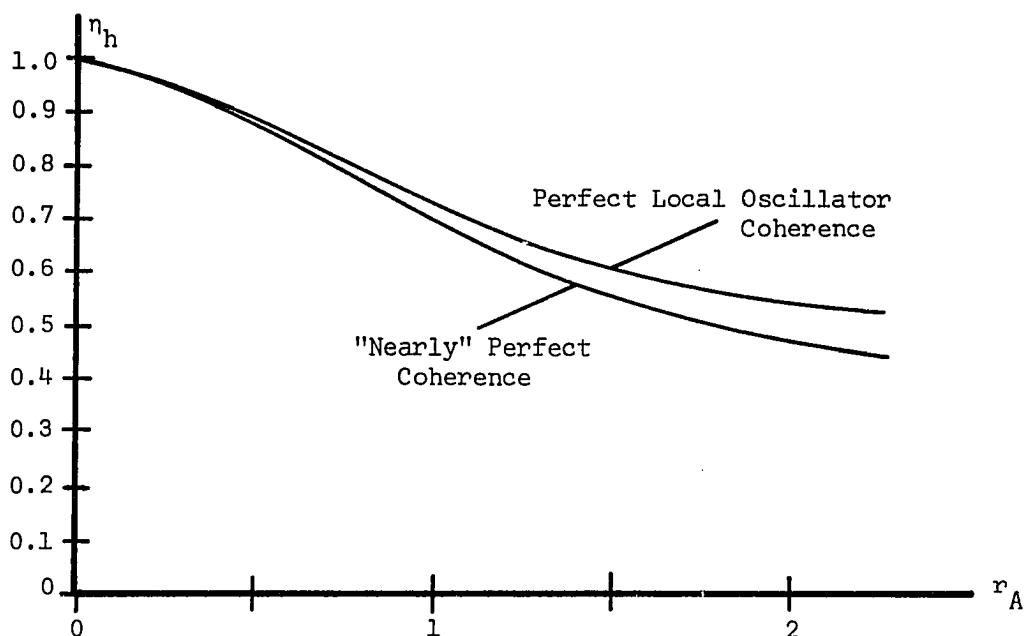
Figure 19. A Plot of η_h Versus r_A for A = 1 for Perfect and "Nearly" Perfect Local Oscillator Coherence, Gaussian I_L

Figure 20. A Plot of η_h Versus r_A for A = 1 for a Circular and an Elliptic Aperture, Gaussian I_L

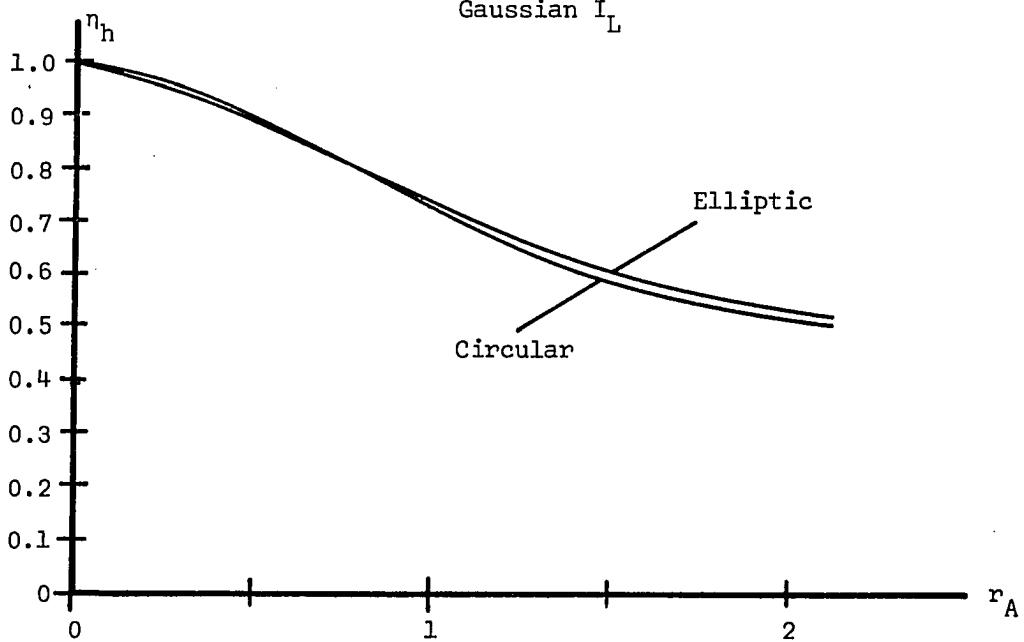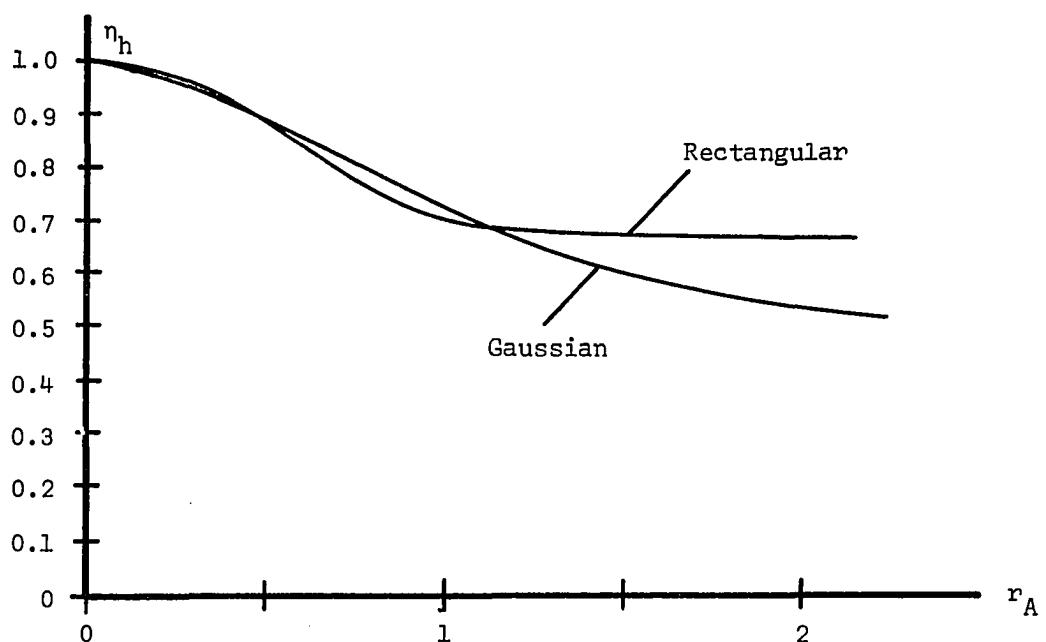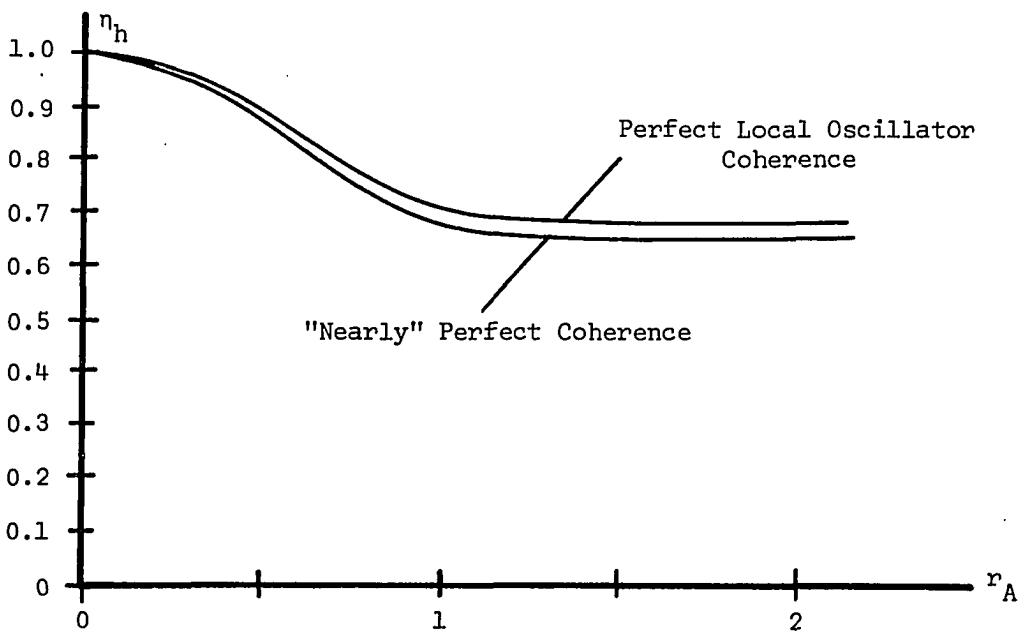Figure 21. A Plot of η_h Versus r_A for Gaussian and Rectangular I_L, $A = 1$

Figure 22. A Plot of η_h Versus r_A for Perfect and "Nearly" Perfect Local Oscillator Coherence, Rectangular I_L with $A = 1$

Comparison of these results to those for the communications link shows that the operation of both systems is very similar. The conclusions that can be made here are identical to those made in the communication system.

A Laser Doppler Fluid Flow Measuring System

Another example of the use of optical heterodyning in velocity measurement systems is the laser Doppler flowmeter (LDF). Since its initial development by Yeh and Cummins[22] and Foreman,[20,23,24] it has been extensively analyzed from a system design[25] and a signal spectrum[26] point of view and used for many different types of measurements including laminar and turbulent flow[27] and flow development.[28,29] One great advantage of using the LDF in such measurements is that it does not perturb the flow in any way.

A typical system is shown in Figure 23. In this arrangement, a beam from a continuous wave laser is focused inside a flow chamber at a point P at which the velocity measurement is desired. The unscattered light passing through serves as a local oscillator while the portion scattered at the angle θ by small contaminant particles placed in the flow is the signal. The optical components (Lenses L_1 and L_2, Mirrors M_1 and M_2, and the beam splitter) are aligned so both travel equal path lengths and are refocused coincident at the photodetector. The equal path requirement is necessary when a multi-mode laser is used so that no reduction in output signal will result.[30] The heterodyne signal output because of the Doppler effect will be of frequency
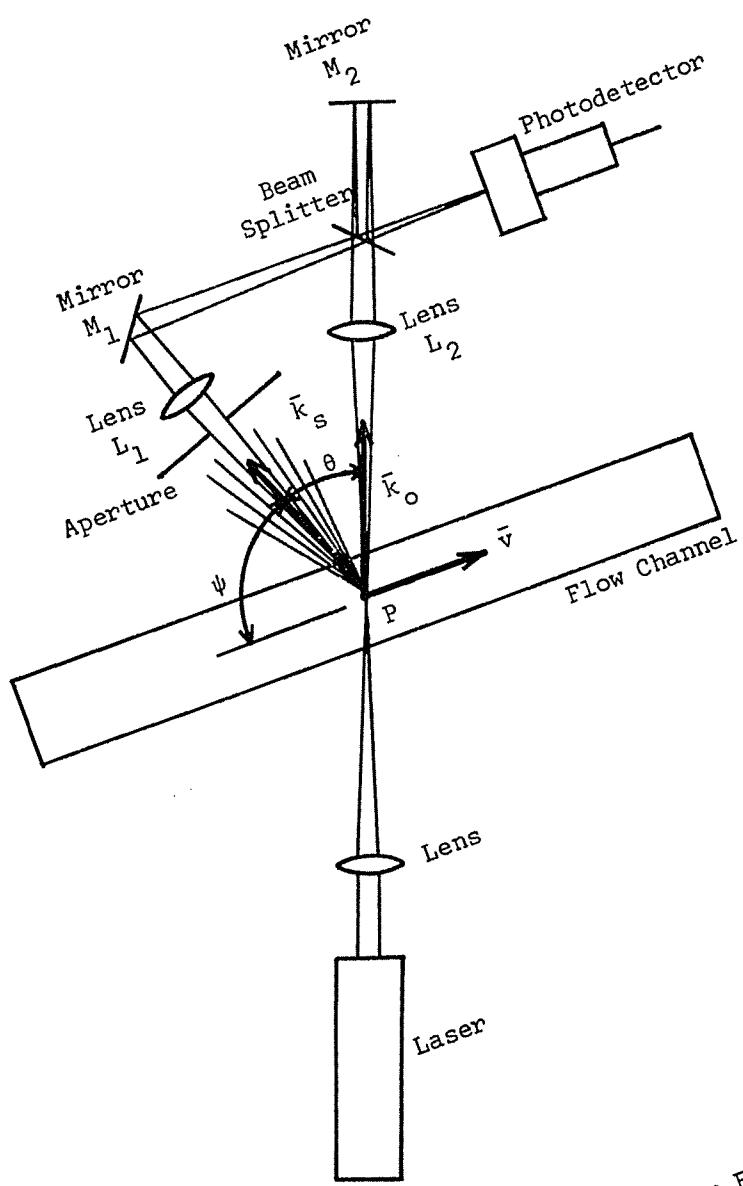
Figure 23. A Laser Doppler Flowmeter

$$f_D = \frac{\omega_D}{2\pi} = \frac{1}{2\pi} (\bar{k}_s - \bar{k}_o) \cdot \bar{v}$$

for the geometry in Figure 23. The component of velocity in the direction of $\bar{k}_s - \bar{k}_o$ can be determined by measuring f_D.

Since the signal field is composed of light scattered from a random distribution of moving particles, its coherence will not be perfect over the photosurface. To calculate the coherence function, the system must first be mathematically modeled.

Mathematical Model for the System

In modeling the LDF system mathematically, the following assumptions are initially made:

1. The contaminant scattering particles are assumed to be distributed at random in a Poisson way so that the probability of finding N particles in a volume V is given by

$$P(N;V) = \frac{(MV)^N}{N!} e^{-MV},$$

where M is the average number of particles per unit volume. They are also assumed to be monodispersed, spherical, and of uniform velocity. Studies have shown that light scattered from a polydispersed distribution of irregularly sized particles has many of the properties of light scattered from a polydispersed distribution of spherical particles.[31] It is shown in Appendix III that if a particle's size is independent of its position, then a polydispersion does not alter the form of the correlation function of the field of a monodispersion.

In addition, other studies have shown that the Brownian motion of the particles have negligible effect on the output spectrum[31] so the particles may be regarded as being of fixed relationship to each other as they pass through the focal region. The flow is thus considered to be laminar.

2. The incident radiation is approximated by a Gaussian beam as in the last example. The field in the focal region is, therefore, given by equation 4-6.

3. The scattered wave from each particle is assumed to be spherical as in the last example. The quasi-static approach will again be taken.

4. The photosurface is considered to be spherical as in the last example. In addition, the expression for the scattered spherical wave on the spherical photosurface is approximated by the expression of a plane wave on a plane photosurface as before. This approximation results in an error of less than two-tenths of a wavelength for points inside of the $1/e^2$ intensity contour of the incident radiation for a beam radius of 50 μm where the photosurface is 40 cm from the scattering region is of diameter 4 mm.

5. The average quantities are assumed to be stationary and ergodic. This assumption is discussed in Appendix II. In addition, the signal and local oscillator are assumed to be independent and linearly polarized as in the last example.

Figure 24 illustrates the coordinate systems to be used. The photosurface is in the x,y,z coordinate system, y" and z" represent a
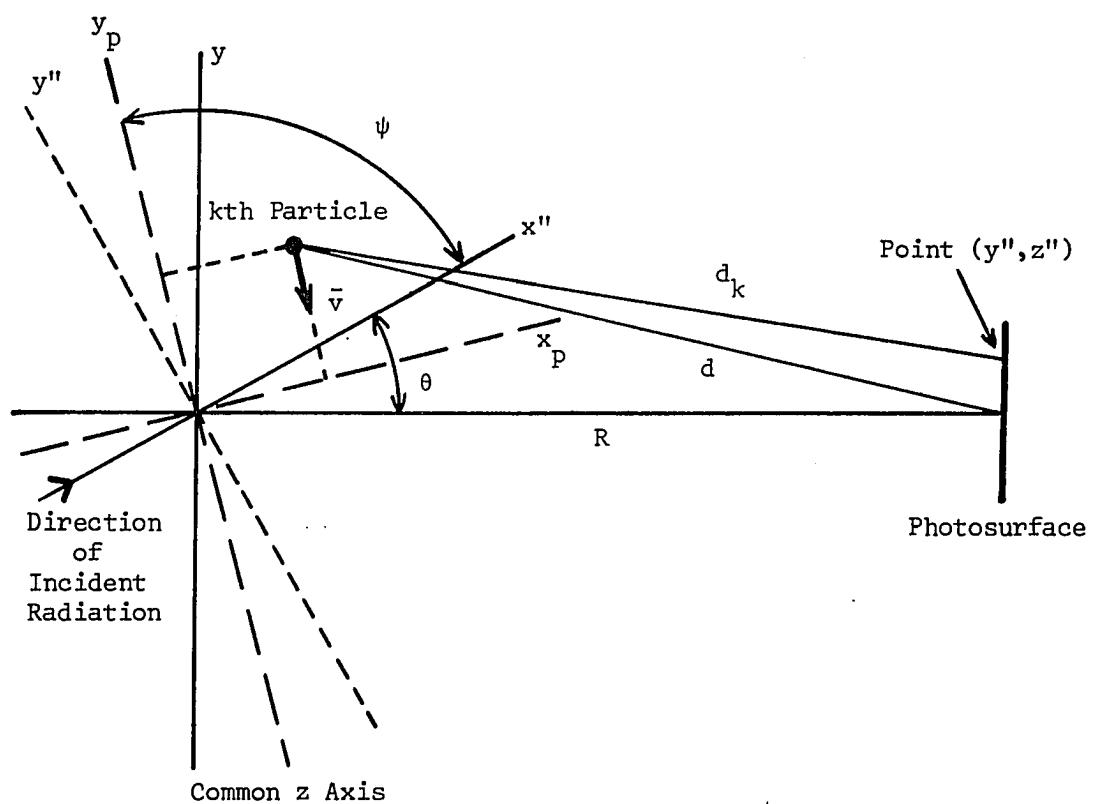
Figure 24. The Coordinate System for the LDF Calculations

point on it. The scattering particles are in the x_p, y_p, z_p system moving in the y_p direction. The incident radiation is described in the x',y',z' coordinate system being incident in the x' direction.

The incident radiation is given from 4-6 by

$$E_{inc}(x',y',z') = E_o \frac{w_o}{w} e^{-(y'^2 + z'^2/w^2)} e^{j\phi(x',y',z')}.$$

The scattered wave at a point (x,y,z) from the kth particle is given by

$$E_{s_k}(x,y,z) = mE_{inc}(x_k',y_k',z_k') e^{-jk_L d_k(x,y,z)}.$$

The constant m is a scattering coefficient given by

$$m = E_s/E_o$$

and d_k is the distance from x,y,z to the kth scattering particle. The total scattered field is given by

$$E_s(x,y,z) = \sum_{k}^{\substack{all \\ particles}} E_{s_k}(x,y,z).$$

The ensemble mutual coherence function for the scattered field on the photosurface is

$$\Gamma_s(y_1'',z_1'',y_2'',z_2'') = E[E_s(y_1'',z_1'')E_s^*(y_2'',z_2'')]$$

$$= E[\sum_i \sum_j E_{s_i}(y_1'',z_1'')E_{s_j}^*(y_2'',z_2'')].$$

This average has been computed in Appendix II and is equal to

$$\Gamma_s(y_1'',z_1'',y_2'',z_2'') = M \int_{-\infty}^{\infty} \int_{-\infty}^{\infty} \int_{-\infty}^{\infty} E_{s_k}(y_1'',z_1'') E_{s_k}^*(y_2'',z_2'') dx_{p_k} dy_{p_k} dz_{p_k},$$

where M is the average number of particles per unit volume. Looking just at the integrand, we have

$$E_{s_k}(y_1'',z_1'') E_{s_k}^*(y_2'',z_2'') = m^2 E_{inc} E_{inc}^* e^{jk_L[d_k(y_2'',z_2'')-d_k(y_1'',z_1'')]}$$

$$= E_s^2 \frac{e^{-2\left[\frac{{y_k'}^2 + {z_k'}^2}{w_o^2(1+\Theta^2(x_k'/w_o)^2)}\right]}}{1 + \Theta^2(x_k'/w_o)^2} e^{jk_L[d_k(y_2'',z_2'')-d_k(y_1'',z_1'')]},$$

where

$$\Theta = \frac{\lambda}{\pi w_o}.$$

The phase term using the plane wave approximation for the scattered wave is

$$d_k(y_2'',z_2'') - d_k(y_1'',z_1'') \cong \left[d - \frac{y_2''y_k}{d} - \frac{z_2''z_k}{d}\right] - \left[d - \frac{y_1''y_k}{d} - \frac{z_1''z_k}{d}\right]$$

$$= (y_1''-y_2'') \frac{y_k}{d} + (z_1''-z_2'') \frac{z_k}{d},$$

which approximating d by R is

$$\cong (y_1''-y_2'') \frac{y_k}{R} + (z_1''-z_2'') \frac{z_k}{R} .$$

This introduces an error of about ten wavelengths for points y_k and z_k at the $1/e^2$ intensity contours of the incident radiation. The error is much less at greater intensities.

Performing the integration analytically with respect to x_{pk}, y_{pk}, z_{pk} is difficult if not impossible. Transformation from x_{pk}, y_{pk}, z_{pk} to x_k', y_k', z_k' is made without affecting the value of the integral.[33] For this transformation

$$\Gamma_s(y_1'',z_1'',y_2'',z_2'') = ME_s^2 \int_{-\infty}^{\infty} \frac{e^{j \frac{k_L \sin\theta(y_1''-y_2'')}{R} x_k'}}{1 + \theta^2(x_k'/w_o)^2}$$

$$\cdot \int_{-\infty}^{\infty} e^{\frac{-2y_k'^2}{w_o^2[1+\theta^2(x_k'/w_o)^2]}} e^{j \frac{k_L \cos(y_1''-y_2'')}{R} y_k'} dy_k'$$

$$\cdot \int_{-\infty}^{\infty} e^{\frac{-2z_k'^2}{w_o^2[1+\theta^2(x_k'/w_o)^2]}} e^{j \frac{k_L(z_1''-z_2'')}{R} z_k'} dz_k' \, dx_k',$$

where coordinate transformation is made from the x_k, y_k, z_k to x_k', y_k', z_k' in the phase term. Letting

$$x_w = \frac{x_k'}{w_o}, \quad y_w = \frac{y_k'}{w_o}, \quad \text{and} \quad z_w = \frac{z_k'}{w_o},$$

and

$$Y = \frac{y''}{R\Theta} \quad \text{and} \quad Z = \frac{z''}{R\Theta},$$

we have for the integrals

$$\Gamma_s(y_1'',z_1'',y_2'',z_2'') = ME_s^2 w_o^3 \int_{-\infty}^{\infty} \frac{e^{j2(Y_1-Y_2)\sin\theta x_w}}{1 + \Theta^2 x_w^2}$$

$$\cdot \int_{-\infty}^{\infty} e^{-2y_w^2/1+\Theta^2 x_w^2} e^{j2(Y_1-Y_2)\cos\theta y_w} dy_w$$

$$\cdot \int_{-\infty}^{\infty} e^{-2z_w^2/1+\Theta^2 x_w^2} e^{j2(Z_1-Z_2)z_w} dz_w dx_w$$

$$= ME_s^2 w_o^3 \int_{-\infty}^{\infty} \frac{e^{j2(Y_1-Y_2)\sin\theta x_w}}{1 + \Theta^2 x_w^2}$$

$$\cdot \sqrt{\pi/2} \, [1 + \Theta^2 x_w^2]^{\frac{1}{2}} e^{-\frac{1}{2}(1+\Theta^2 x_w^2)(Y_1-Y_2)^2\cos^2\theta}$$

$$\cdot \sqrt{\pi/2} \, [1+\Theta^2 x_w^2]^{\frac{1}{2}} e^{-\frac{1}{2}(1+\Theta^2 x_w^2)(Z_1-Z_2)^2}$$

$$= \frac{ME_s^2 \pi w_o^3}{2} e^{-\frac{1}{2}[(Y_1-Y_2)^2\cos^2\theta+(Z_1-Z_2)^2]}$$

$$\cdot \int_{-\infty}^{\infty} e^{-\Theta^2 x_w^2/2 \, [(Y_1-Y_2)^2\cos^2\theta+(Z_1-Z_2)^2]} e^{j2(Y_1-Y_2)\sin\theta x_w} dx_w.$$

If a slit of width 2W' is placed so as to restrict the scattered radiation reaching the photodetector to come from

$$-\frac{W'}{w_o} < x_w < \frac{W'}{w_o},$$

the integral becomes

$$\int_{-W}^{W} e^{-\theta^2 x_w^2/2\ [(Y_1-Y_2)^2\cos^2\theta+(Z_1-Z_2)^2]}\ e^{j2(Y_1-Y_2)\sin\theta x_w}\ dx_w,$$

where $W = W'/w_o$, which for $\theta^2 \ll 1$, is approximately

$$\int_{-W}^{W} e^{j2(Y_1-Y_2)\sin\theta x_w}\ dx_w = \int_{-W}^{W} \cos[2(Y_1-Y_2)\sin\theta x_w]dx_w$$

$$= 2W\ \frac{\sin[2W\sin\theta(Y_1-Y_2)]}{2W\sin\theta(Y_1-Y_2)}\ .$$

This can be, and often is, done at the flow channel or at the photo-detector by placing a slit so as to block the x_w extent of the image of the scattered radiation. Now we have

$$\Gamma_s(y_1'',z_1'',y_2'',z_2'') = ME_s^2 \pi w_o^3 W$$

$$\cdot\ e^{-\frac{1}{2}[(Y_1-Y_2)^2\cos^2\theta+(Z_1-Z_2)]}\ \frac{\sin[2W\sin\theta(Y_1-Y_2)]}{2W\sin\theta(Y_1-Y_2)}\ .$$

Now, we have

$$\Gamma_s(y_1'',z_1'',y_1'',z_1'') = \Gamma_s(y_2'',z_2'',y_2'',z_2'') = ME_s^2 \pi w_o^3 W,$$

so

$$\gamma_s(y_1'',z_1'',y_2'',z_2'') = e^{-\frac{1}{2}[(Y_1-Y_2)^2\cos^2\theta+(Z_1-Z_2)^2]}$$

$$\cdot \frac{\sin[2W\sin\theta(Y_1-Y_2)]}{2W\sin\theta(Y_1-Y_2)} \cdot \qquad (4\text{-}14)$$

This function is very similar to that of the last example but contains

an extra factor due to the x_p' extent of the scatterers not present in

the last example. Making w_o or W smaller increases the region of

coherence at the photosurface. This region is again elliptic due to

the $\cos^2\theta$ factor in γ_s.

Calculation of Heterodyne Efficiency and SNR

The heterodyne efficiency and SNR are calculated from equations

3-3 and 3-4 for the following cases: (1) constant I_s and Gaussian I_L

of different circular aperture diameters for a perfectly coherent local

oscillator, (2) constant I_s and Gaussian I_L of one specific diameter

at different circular aperture diameters for "nearly" perfect local

oscillator coherence, (3) constant I_s and Gaussian I_L of one specific

diameter for various elliptic apertures that match the eccentricity

of the elliptic coherence region for perfect and "nearly" perfect local

oscillator coherence, and (4) constant I_s and rectangular I_L at various

circular aperture diameters for perfect and "nearly" perfect local

oscillator coherence. The coordinate system shown in Figure 7 is again

used for calculation. For this case

$$Y = \frac{y''}{R\Theta} \quad \text{and} \quad Z = \frac{z''}{R\Theta},$$

$$dy'' = R\Theta dY \quad \text{and} \quad dz'' = R\Theta dZ,$$

so that

$$\gamma_S(y_1'', z_1'', y_2'', z_2'') = e^{-\frac{1}{2}[(Y_1-Y_2)^2\cos^2\theta+(Z_1-Z_2)]^2}$$

$$\cdot \frac{\sin[2W\sin\theta(Y_1-Y_2)]}{2W\sin\theta(Y_1-Y_2)}$$

evaluated for $W = 5$ (slit width projected along x' axis $= 10 \ w_o$).

$$I_L(y'', z'') = e^{-2(Y^2+Z^2)/A^2} \quad \text{for Gaussian distribution,} \quad (4\text{-}15)$$

$$I_L(y'', z'') = \begin{cases} 1 \text{ for } Y^2+Z^2<A^2 \\ 0 \text{ for } Y^2+Z^2 \geq A^2 \end{cases} \quad \text{for rectangular distribution,}$$

$$I_S(y'', z'') = 1,$$

$$\gamma_L(y_1'', z_1'', y_2'', z_2'') = 1 \quad \text{for perfect local oscillator coherence,}$$

and

$$\gamma_L(y_1'',z_1'',y_2'',z_2'') = e^{-[(Y_1-Y_2)^2+(Z_1-Z_2)^2]/(3.1A)^2} \qquad (4\text{-}16)$$

for "nearly" perfect coherence as before.

The equations for the heterodyne efficiency and SNR are

$$\eta_h = \frac{P_S}{P_I} \qquad (4\text{-}17)$$

and

$$SNR = \frac{qe}{hfB} ME_s^2 \pi w_o^3 WR^2\Theta^2 \frac{P_S}{P_N}, \qquad (4\text{-}18)$$

where P_S, P_I, and P_N are given by equations 4-3, 4-4, and 4-5 and r_A is the normalized circular aperture radius. For the elliptic aperture, the upper and lower limits in the Z-integration are

$$\sqrt{r_A^2-Y^2}\ \cos\theta \quad \text{and} \quad -\sqrt{r_A^2-Y^2}\ \cos\theta.$$

The equations are again too complex for analytical evaluation so a digital computer was used. Sample programs are presented in Appendix I. The values of θ and ψ are taken as 30° and 90°, respectively. The results are presented in Figures 25 through 30.

Figures 25 and 26 show plots of heterodyne efficiency and SNR versus r_A and r_A/A, respectively, for perfect local oscillator coherence. The SNR plotted in Figure 25 is P_S/P_N, and in Figure 26 is $(P_S/P_N)/(P_S/P_N)\text{max}$. Looking at Figure 26, we see that for smaller
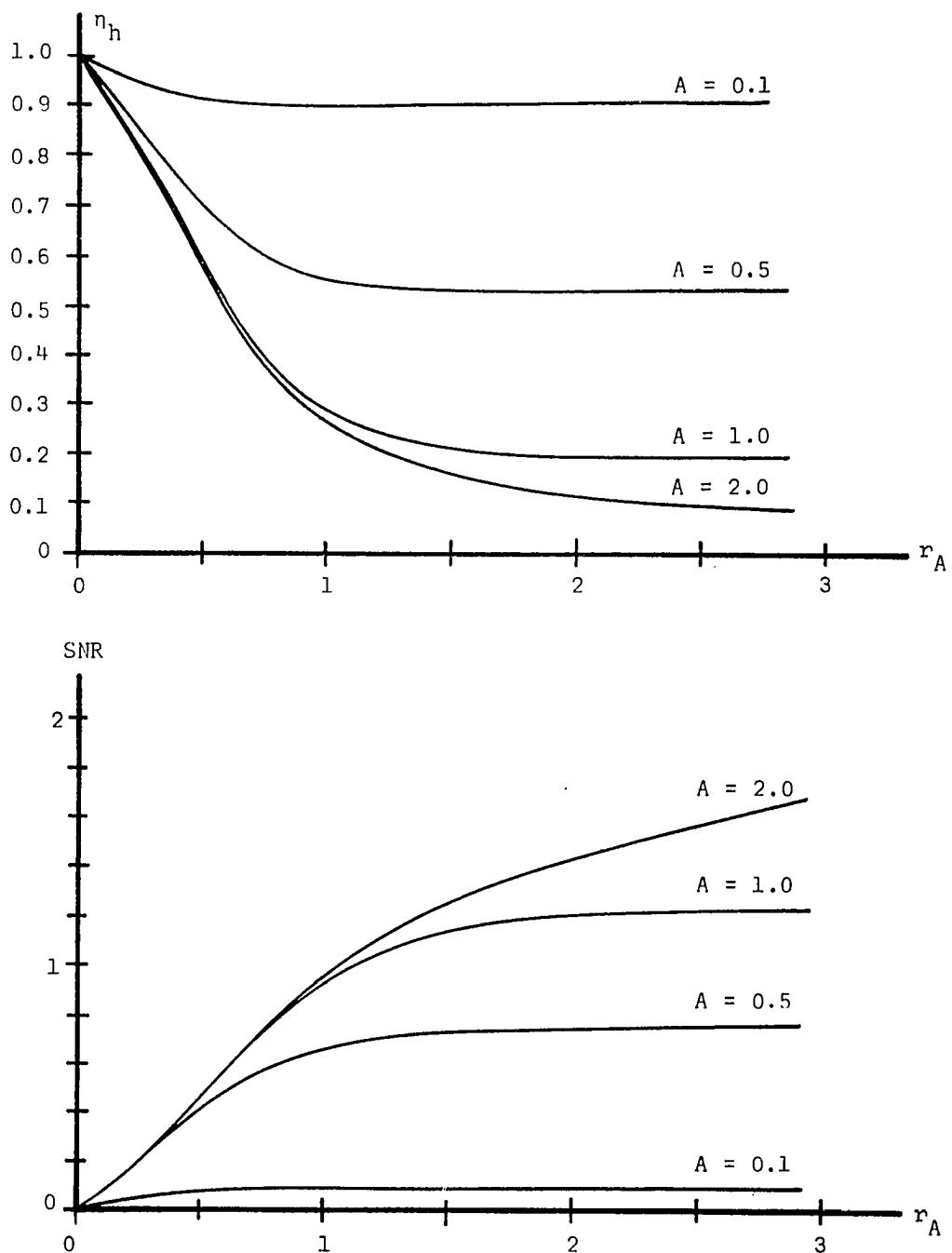
Figure 25. Plots of η_h and SNR Versus r_A for
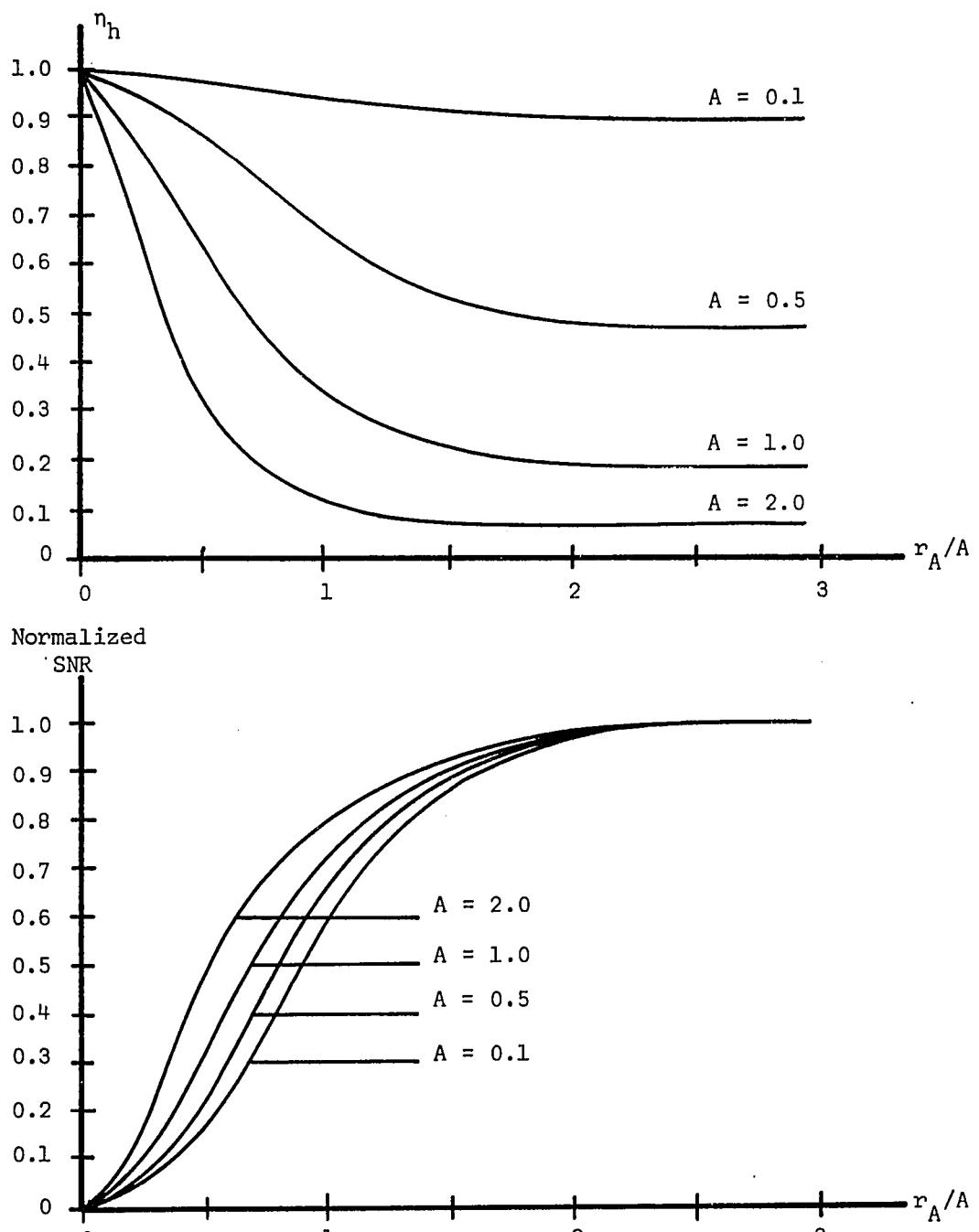Various Values of A, Gaussian I_L

Figure 26. Plots of n_h and Normalized SNR Versus r_A/A for Various Values of A, Gaussian I_L

local oscillator radii A, the heterodyning is more efficient for a
constant r_A/A. From Figure 25, however, wee see that operating in
this manner yields poor SNR as compared to larger A. Good efficiency
and good SNR cannot be obtained simultaneously.

Figure 27 shows the comparison of heterodyne efficiency for
perfect and "nearly" perfect local oscillator coherence. Again we see
that a small reduction in local oscillator coherence has no signifi-
cant effect on heterodyne efficiency.

Figure 28 shows the comparison of circular versus elliptic
aperture for perfect local oscillator coherence. There is only a
very small difference between the two.

Figure 29 shows this comparison for constant versus Gaussian
local oscillator intensity distribution for A = 1. No significant
difference for R less A is apparent.

Figure 30 shows the comparison for constant I_L with A = 1 for
perfect and "nearly" perfect local oscillator coherence. Slight
reductions in the local oscillator coherence have no significant effect
on the heterodyne efficiency.

In comparing these results to those of the other two examples,
we see that for the cases studied, the results are almost identical.
They can be summarized as follows:

1. For efficient operation, the local oscillator diameter
should be made small and the aperture should be about twice its size.
This results in a relative maximum SNR and good efficiency; i.e. nearly
ideal operation.
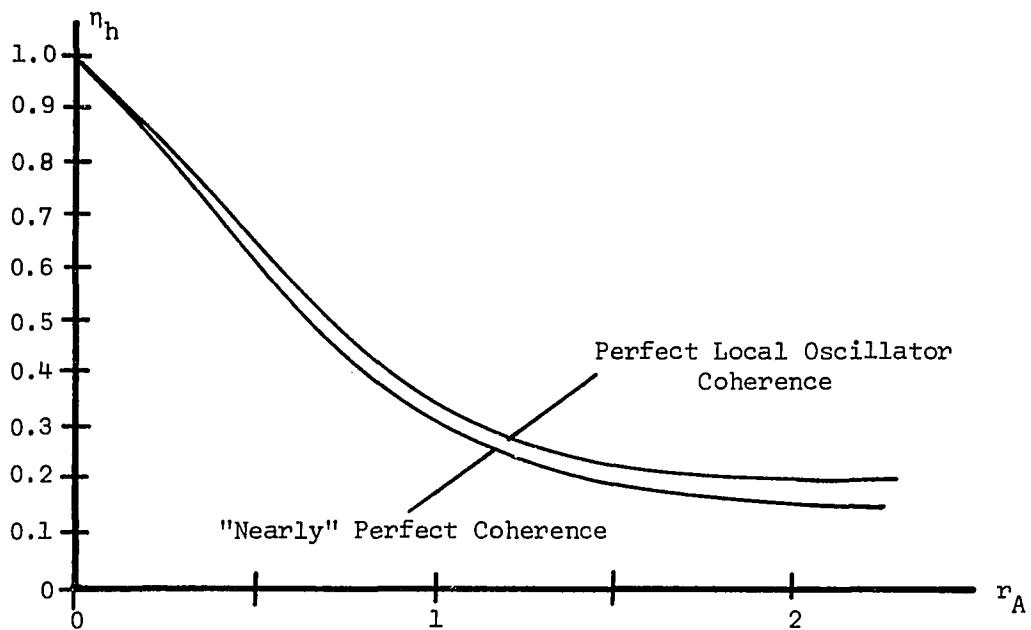
Figure 27. A Plot of η_h Versus r_A for Perfect and "Nearly" Perfect Local Oscillator Coherence, Gaussian I_L with A = 1
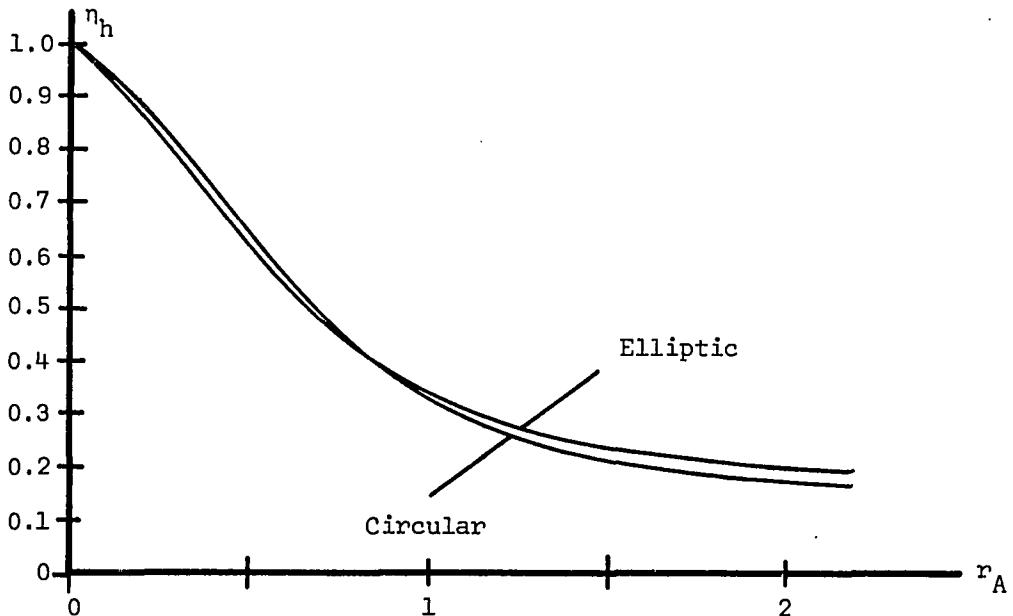
Figure 28. A Plot of η_h Versus r_A for Circular and Elliptic Aperture, Gaussian I_L with A = 1
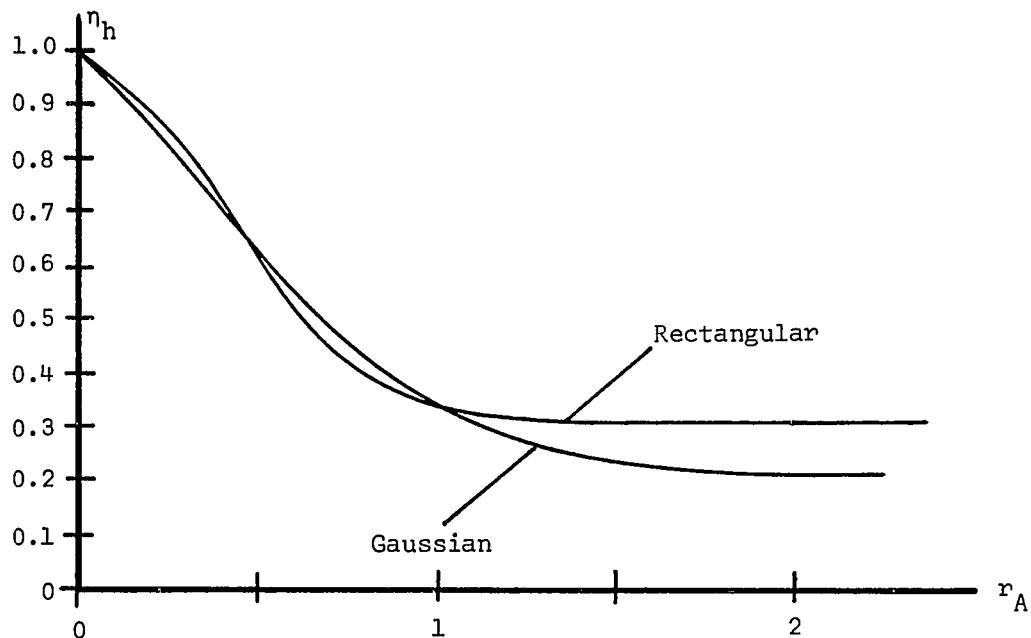
Figure 29. A Plot of η_h Versus r_A for Gaussian and Rectangular I_L, $A = 1$.
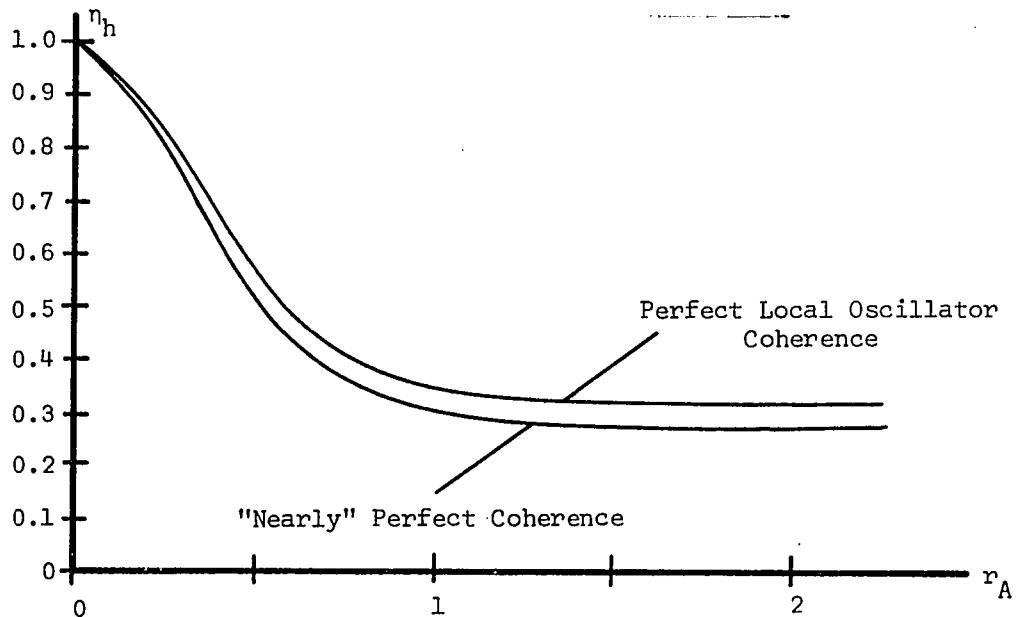
Figure 30. A Plot of η_h Versus r_A for Perfect and "Nearly" Perfect Local Oscillator Coherence, Rectangular I_L with $A = 1$

2. For maximizing the SNR, a large local oscillator diameter is required with the aperture diameter again approximately equal to twice the local oscillator diameter.

3. For a fixed aperture diameter, changes in the shape of the local oscillator intensity distribution function and changes in aperture shape have little effect on heterodyne efficiency.

4. Slight reductions in local oscillator coherence have no significant effect on system performance.

CHAPTER V

THE EXPERIMENTAL STUDY

An experimental investigation of heterodyne efficiency and SNR
for the last two examples in Chapter IV is presented in this chapter.
The work is limited in scope; the main objective is to verify the
applicability of the heterodyne efficiency and SNR equations derived
in Chapter III to these examples. The experimental systems used
duplicate as much as possible the assumptions and conditions placed
on the corresponding analytical study. A few specific cases are
studied experimentally with the heterodyne efficiency and SNR being
measured and compared to theoretically predicted results.

The Experimental Apparatus

The experimental arrangements that were used are shown in
Figure 31 and 32. In each arrangement, the beam from an Optics Tech-
nology Model 230 He-Ne laser was passed through a spatial filter to
an input lens L_3. Lens L_2 was adjusted to vary the input beam
diameter. The beam was focused by L_3 through a beam splitter BS_1 to
the scattering medium located approximately 40 cm from L_3 a rough
surface mounted on a turntable in one case, a rectangular liquid flow
channel in the other. The flow channel used was a rectangular tube
12 inches long and 3/4 inches square in cross section; distilled water
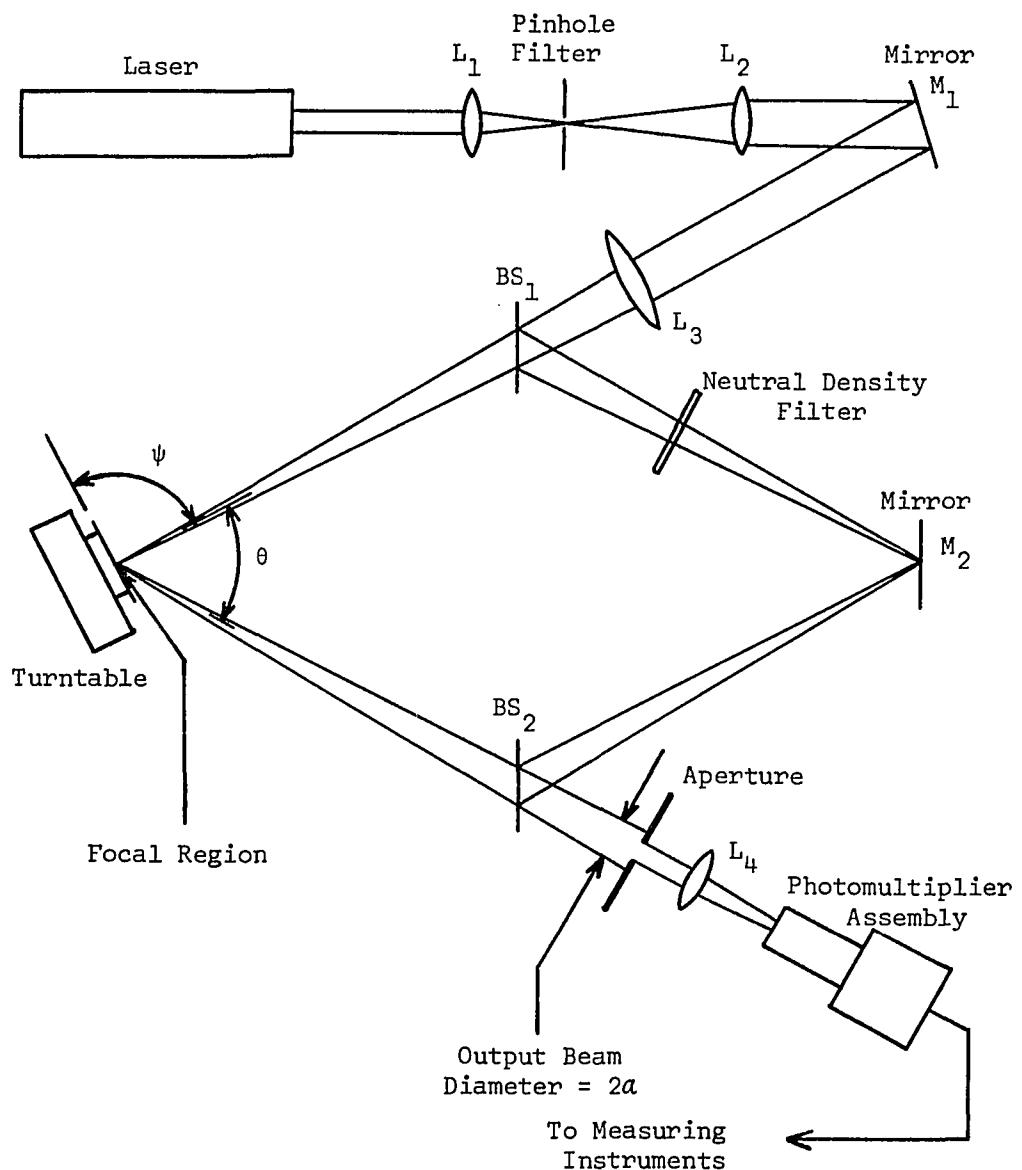was used with contaminant particles added as scattering agents. Small
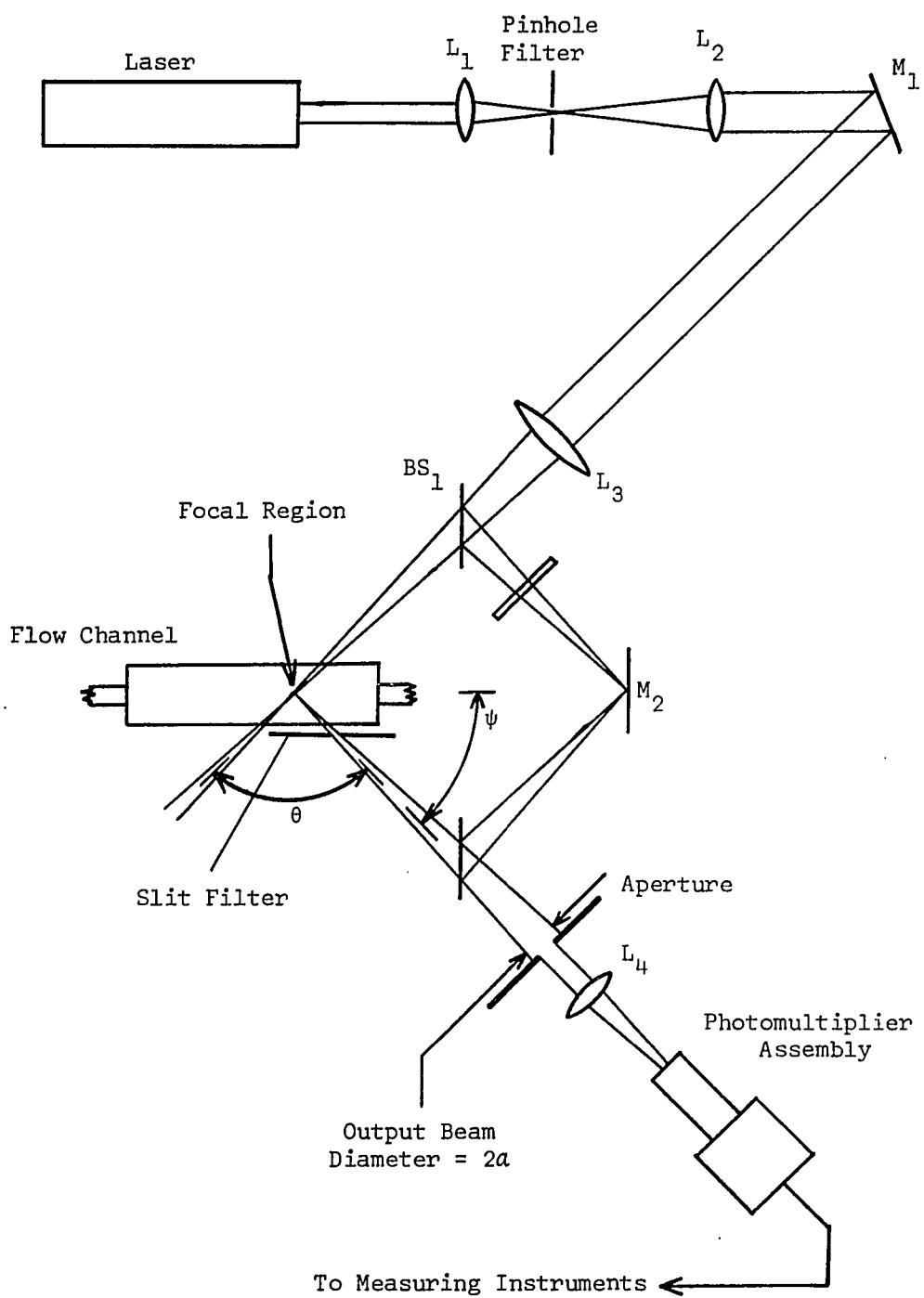
Figure 31. The Experimental LDSV Arrangement

Figure 32. The Experimental LDF Arrangement

kaolinite particles of irregular size and shape varying from one to
two microns in size were used as contaminant particles in one case,
spherical pollen particles of 16 μm in diameter were used in others.
A sheet of 400 mesh silicon carbide paper was used as a rough surface.
This paper contained silicon carbide particles of irregular sizes
and shapes but all smaller than 37 μm across distributed randomly on
the paper. Part of the incident radiation is reflected by BS_1 through
a natural density filter to M_2, then to beam splitter BS_2. This beam
was used as a local oscillator. The radiation scattered at the angle
θ was combined with the local oscillator beam by BS_2, limited by a
circular aperture A located approximately 40 cm from the scattering
medium and refocused by lens L_4 on the RCA 8645 photomultiplier tube.
A pinhole of diameter of 450 μm and an iris diaphragm variable in
diameter from 1 mm to 10 mm were used as apertures. The two path
lengths from BS_1 to BS_2 were made equal. The neutral density filter
serves to keep the reference beam from saturating the photomultiplier.

The output current from the photomultiplier was fed to the
instrumental arrangement shown in Figure 33. The total photomultiplier
tube current is divided into its signal and DC components by a high
pass and low pass filter, respectively. The high pass filter is used
to eliminate any low frequency noise caused by vibration and fluctua-
tions in the laser output. The signal is amplified using a C-Cor 3597
low noise amplifier, passed through a Krohn-Hite 3202 variable band-
pass electronic filter to remove the noise not in the signal band,
and fed to a Hewlitt Packard 3400A true RMS voltmeter. The RMS
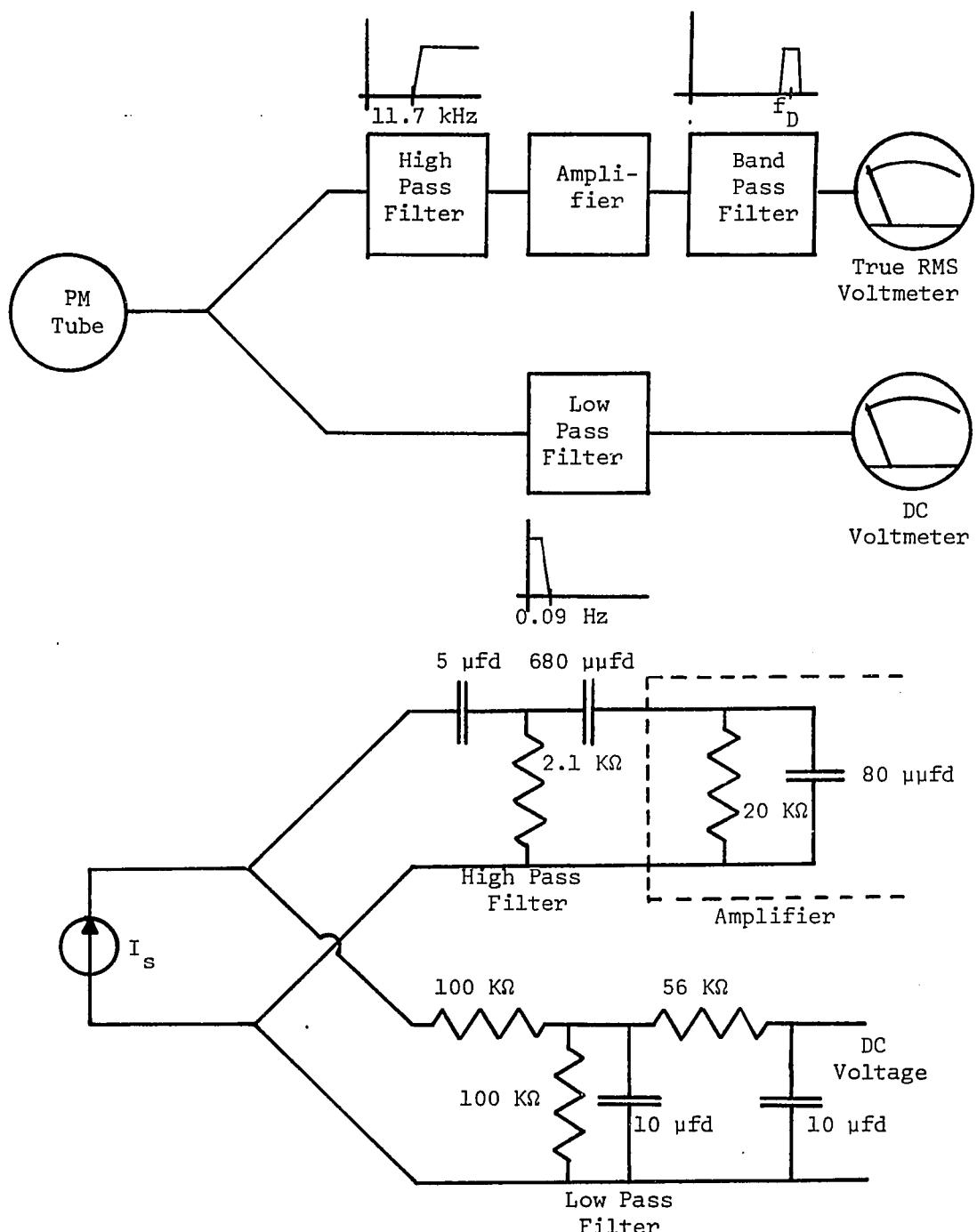
Figure 33.   The Instrumental Arrangement

voltmeter gives readings proportional to the square root of the signal and noise powers. The DC current is passed through a low pass filter and fed to a DC voltmeter. A General Radio Model 1230A voltmeter and a Fluke Model 845AB voltmeter were used for DC voltage measurements. A Tektrenix IL5 Spectrum Analyser was used with a Tektronix 549 Storage Oscilloscope to monitor the signal waveform and its spectrum to aid in adjusting the bandpass filter. The highpass filter provided a 2kΩ load for the signal current, the low pass filter provided a 100 kΩ load for the DC current. The amplifier had a measured voltage gain of 166 and input capacitance of 80 pfd. The transfer functions of the signal and DC paths are plotted versus frequency in Figure 34. In the pass bands, the signal and DC currents are given in terms of the measured voltages by

$$i_{rms} = \frac{v_{rms}}{306 \text{ k}\Omega} \quad \text{and} \quad i_{DC} = \frac{v_{DC}}{100 \text{ k}\Omega} .$$

The noise power was determined from the rms voltage measurements with noise alone present. It is given by

$$\langle i_n^2(t) \rangle = i_{n_{rms}}^2 = \frac{v_{n_{rms}}^2}{(306 \text{ k}\Omega)^2} .$$

The signal power was determined from rms voltage measurements made with signal present along with noise. The signal and noise are statistically independent, therefore, their powers will add. The voltage $v_{s_{rms}}$ is, then, given by

v_{rms}/i_{rms}(dB)

Signal Path

v_{DC}/i_{DC}(dB)

0.01 Hz DC path
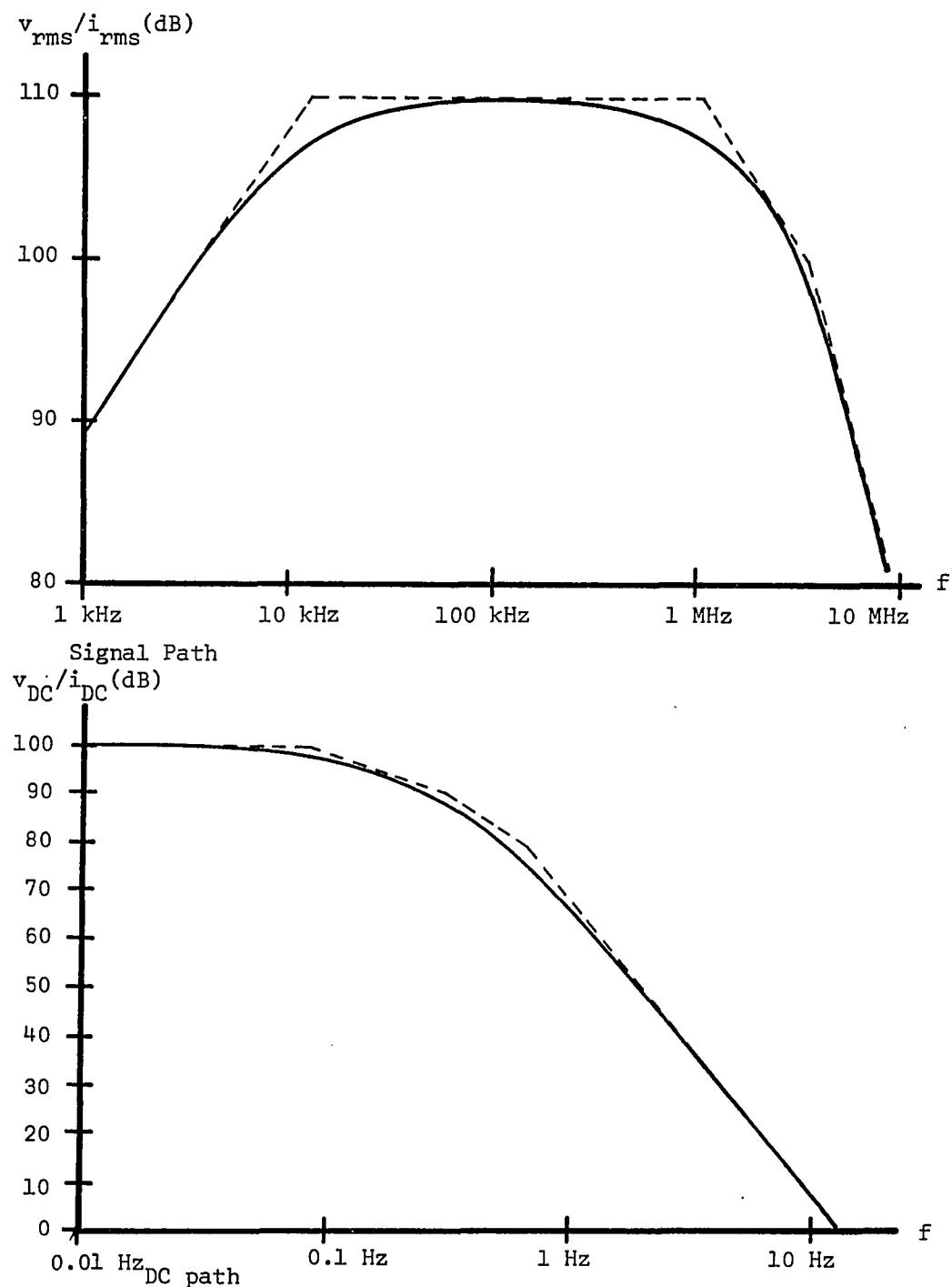
Figure 34.   Plots of the Transfer Functions Versus
             Frequency for the Signal and DC Paths

$$v_{s_{rms}} = \left[v^2_{s+n_{rms}} - v^2_{n_{rms}} \right]^{\frac{1}{2}}, \tag{5-1}$$

where $v_{s+n_{rms}}$ is the signal plus noise voltage and $v_{n_{rms}}$ is the noise alone voltage. The signal-to-noise ratio is, therefore, given by

$$SNR = \frac{<i^2_s(t)>}{<i^2_n(t)>} = \left(\frac{v_{s_{rms}}}{v_{n_{rms}}} \right)^2. \tag{5-2}$$

The ideal signal power was determined from the DC current measurements by

$$<i^2_s(t)>_{ideal} = 2\kappa i_{DC_L} i_{DC_s},$$

where i_{DC_L} and i_{DC_s} are the DC currents due to the local oscillator alone (signal beam obstructed) and signal alone (local oscillator beam obstructed), respectively, and κ is a correction factor that depends on the aperture diameter, local oscillator intensity distribution, and signal intensity distribution. It is given by

$$\kappa = \frac{<i^2_s(t)>_{ideal}}{2i_{DC_L} i_{DC_s}}$$

$$= \frac{2 \frac{q^2 e^2}{h^2 f^2} \int_{S_1} \int_{S_2} [I_L(\bar{R}_1) I_L(\bar{R}_2) I_s(\bar{R}_1) I_s(\bar{R}_2)]^{\frac{1}{2}} dA_1 dA_2}{2 \left(\frac{qe}{hf} \int_S I_L(\bar{R}) dA \right) \left(\frac{qe}{hf} \int_S I_s(\bar{R}) dA \right)}$$

$$= \frac{\left(\int\limits_S [I_L(\bar{R}) I_s(\bar{R})]^{\frac{1}{2}} dA \right)^2}{\int\limits_S I_L(\bar{R}) dA \int\limits_S I_s(\bar{R}) dA} \ . \tag{5-3}$$

The ideal signal power in terms of the DC voltage measurements, then, is

$$\langle i_s^2(t) \rangle_{ideal} = 2\kappa \left(\frac{v_{DC_L}}{100 \text{ k}\Omega} \right) \left(\frac{v_{DC_s}}{100 \text{ k}\Omega} \right),$$

so the heterodyne efficiency is

$$\eta_h = \frac{\langle i_s^2(t) \rangle}{\langle i_s^2(t) \rangle_{ideal}} = \frac{v_{s_{rms}}^2 / (306 \text{ k}\Omega)^2}{2\kappa v_{DC_L} v_{DC_s} / (100 \text{ k}\Omega)^2}$$

$$= \frac{(0.054) v_{s_{rms}}^2}{\kappa v_{DC_L} v_{DC_s}} \ . \tag{5-4}$$

The General Experimental Procedure

The general procedure taken in the experimental study was as follows:

1. Measure the intensity distributions $I_L(\bar{R})$ and $I_s(\bar{R})$ for the local oscillator and signal fields at the receiving aperture to determine if they satisfy the assumptions placed on them in the analytical study.

2. Measure the local oscillator coherence $\gamma_L(\bar{R}_1,\bar{R}_2)$ across the beam.

3. Measure the focal beam size at the point of scattering and the other parameters necessary for the calculation of the signal field coherence $\gamma_s(\bar{R}_1,\bar{R}_2)$.

4. Put these functions in the η_h and SNR equations (equations 3-3 and 3-4) and calculate the theoretical curves for η_h and SNR.

5. Compare these to the measured values of η_h and SNR.

The local oscillator and signal intensity distribution were determined from DC voltage measurements made with different diameter circular apertures. The local oscillator beam, since it was derived from the incident laser TEM_{00} beam, was approximately of Gaussian intensity distribution. For a true Gaussian beam, the output DC voltage variation with aperture radius is plotted in Figure 35. The actual DC voltage measurements were compared to this curve and found to be in close agreement. From this comparison, the local oscillator beam radius, a, was calculated. The scattered beam, on the other hand, is of constant intensity in the ideal case. In this case, the output DC voltage varies as the square of the aperture radius. Again, the actual DC voltage measurements were compared to this ideal case and found to be in very close agreement for the receiving aperture radii used in the experiments.

The local oscillator coherence was measured using Young's interference experiment. The experimental setup that was used is shown in Figure 36. The local oscillator beam was passed through a
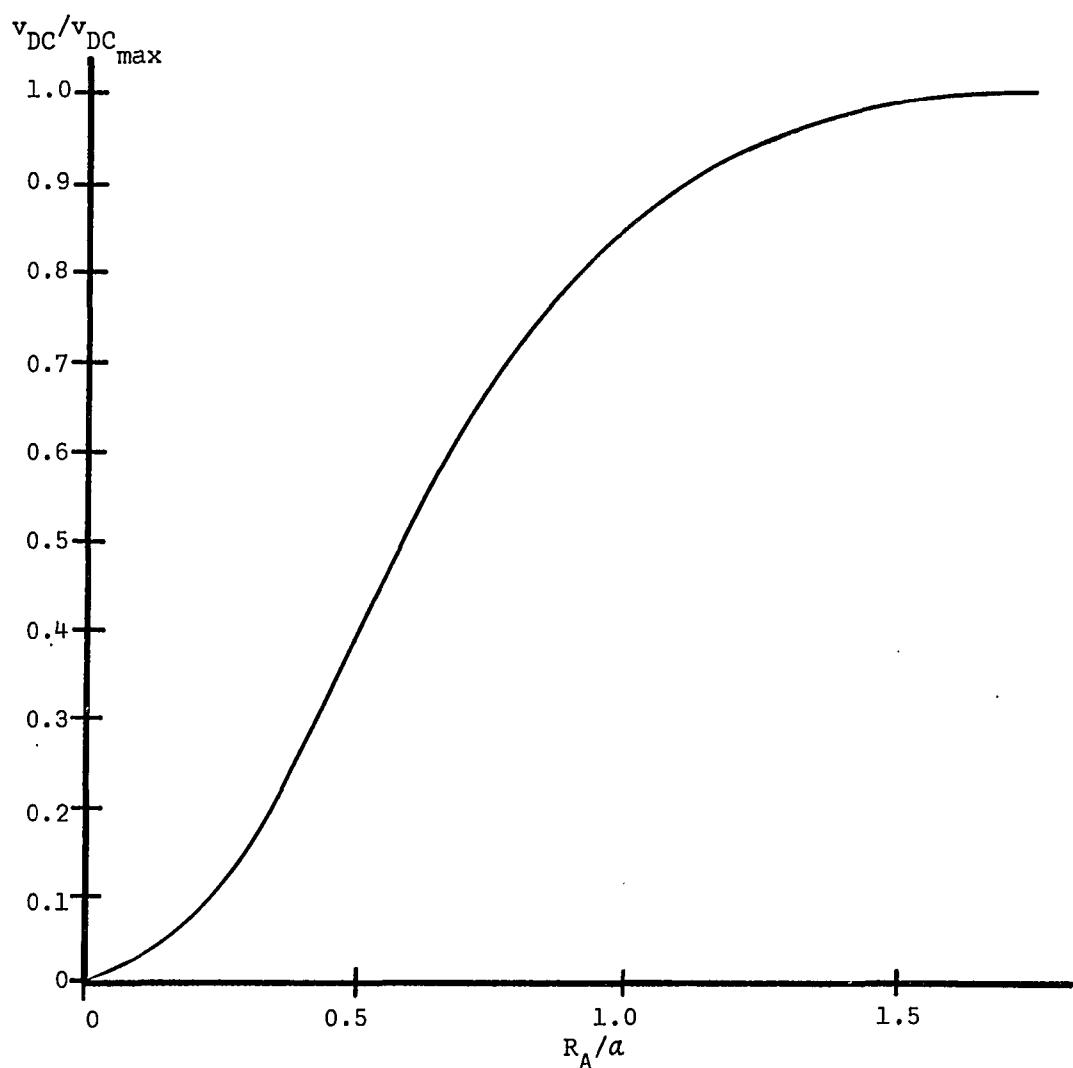
Figure 35. A Plot of $v_{DC}/v_{DC_{max}}$ Versus R_A/a for an Ideal Gaussian Beam
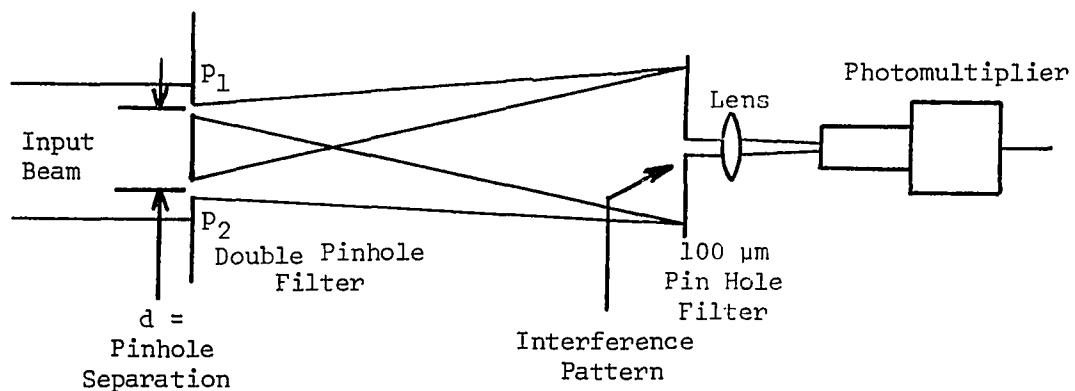
Figure 36. The Experimental Arrangement for
Measuring Local Oscillator Coherence
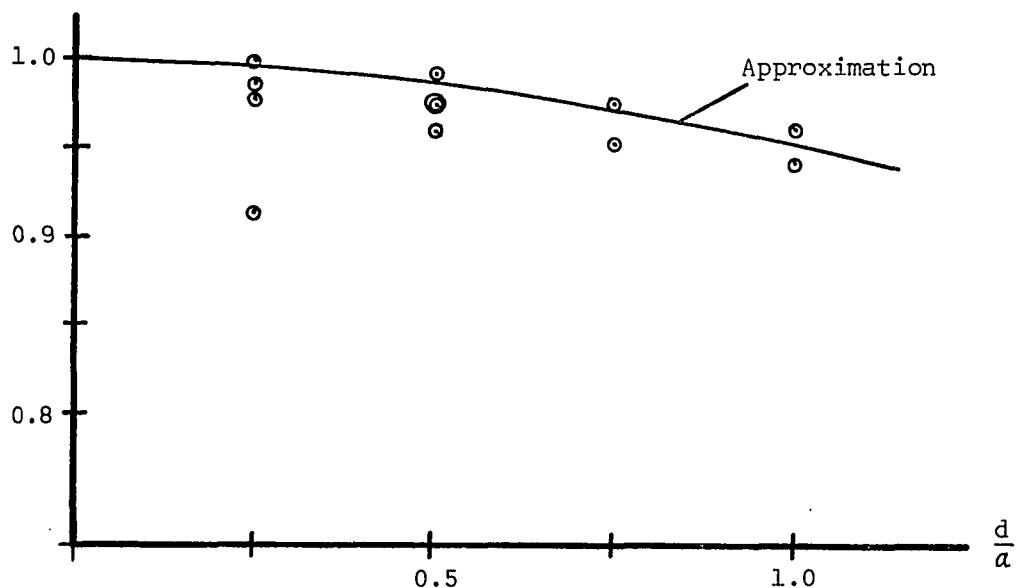
Figure 37. Data from the Coherence Measurements

double pinhole filter and the resulting interference pattern was observed. The maximum and minimum intensities of the pattern from equation 2-22 are

$$I_{max} = I_1 + I_2 + 2\sqrt{I_1 I_2} \; |\gamma_L(\bar{R}_1,\bar{R}_2)|$$

and

$$I_{min} = I_1 + I_2 - 2\sqrt{I_1 I_2} \; |\gamma_L(\bar{R}_1,\bar{R}_2)| \; ,$$

where I_1 and I_2 are the resulting intensities of the radiation from P_1 at $\bar{R}_1$ alone and P_2 at $\bar{R}_2$ alone, respectively. Since the output voltage from the photodetector is proportional to the intensity, we have

$$v_{DC_{max}} = v_{DC_1} + v_{DC_2} + 2\sqrt{v_{DC_1} v_{DC_2}} \; |\gamma_L(\bar{R}_1,\bar{R}_2)|$$

and

$$v_{DC_{min}} = v_{DC_1} + v_{DC_2} - 2\sqrt{v_{DC_1} v_{DC_2}} \; |\gamma_L(\bar{R}_1,\bar{R}_2)| \; .$$

The voltage $v_{DC_{max}}$, $v_{DC_{min}}$, v_{DC_2}, and v_{DC_2} were, therefore, measured for various pinhole separations and $\gamma_L(\bar{R}_1,\bar{R}_2)$ is calculated. The results are shown in Figure 37. A Gaussian curve given by

$$\gamma_L(\bar{R}_1,\bar{R}_2) = e^{-|\bar{R}_2-\bar{R}_1|^2/(4.5a)^2} \quad (5\text{-}5)$$

was used to approximate the local oscillator coherence function where a is the local oscillator beam radius.

The signal coherence function for the LDSV system was calculated using equation 4-8 from measurements of w_o (the incident beam radius at the point of scattering) and R, the distance from the scattering point to the receiving lens. For the LDF, it was calculated using equation 4-14 from measurements of w_o, R and W', the slit width. The incident beam radius was measured in the same way that the local oscillator beam radius was measured. The slit width was determined by the illumination of the slit with a laser beam and the measurement of the distance to the first maximum in the resulting far field diffraction pattern.

The measured values of η_h and SNR are determined from the RMS voltage measurements $v_{s+n_{rms}}$ and $v_{n_{rms}}$ ($v_{s_{rms}}$ is calculated from equation 5-1), the DC voltage measurements, and the correction factor. The local oscillator is approximately Gaussian and the signal is approximately constant so

$$I_L = I_{L_o} e^{-2\,r^2/a^2} \quad \text{and} \quad I_s = I_{s_o},$$

where a is the local oscillator beam radius. Putting these in equation 5-3, the correction factor κ is

$$\kappa = \frac{\left(\int_o^{2\pi} \int_o^{R_A} [I_{L_o} I_{s_o}]^{\frac{1}{2}} e^{-r^2/a^2} \, r dr d\theta \right)^2}{\left(\int_o^{2\pi} \int_o^{R_A} I_{L_o} e^{-2r^2/a^2} r dr d\theta \right) \left(\pi R_A^2 I_{s_o} \right)}$$

$$= \frac{2a^2[1 - e^{-(R_A/a)^2}]^2}{R_A^2[1 - e^{-2(R_A/a)^2}]} = \frac{2[1 - e^{-(R_A/a)^2}]}{(R_A/a)^2[1 + e^{-(R_A/a)^2}]} \; ,$$

where R_A is the receiving aperture radius. This is plotted versus R_A in Figure 38. The correction factor that was used, therefore, depended on the size of the receiving aperture.

Because the radiation from the laser is linearly polarized, the local oscillator radiation will also be linearly polarized. The scattered radiation may, however, have a cross polarization component. Only the component of the scattered beam polarized parallel with the local oscillator will heterodyne. Therefore, only this component of v_{DC_s} should be used in equation 5-4. This is denoted by $v_{DC_{s\parallel}}$ and was determined from measurements, made with a polarizing filter, of the parallel and perpendicular components of v_{DC_s}.

The Laser Doppler Surface Velocimeter

The following four cases were studied:

1. $R = 40$ cm, $\psi = 90°$, $\theta = 39°$, local oscillator beam radius $a = 2.25$ mm $\pm$ 0.1 mm, focal beam radius $w_o = 40$ μm $\pm$ 5 μm, $v_{DC_{s\parallel}} = 0.85 v_{DC_s}$.

2. $R = 40$ cm, $\psi = 90°$, $\theta = 60°$, $a = 2.25$ mm $\pm$ 0.1 mm, $w_o = 40$ μm $\pm$ 5 μm, $v_{DC_{s\parallel}} = 0.75 v_{DC_s}$.

3. $R = 40$ cm, $\psi = 90°$, $\theta = 60°$, $a = 1.25$ mm $\pm$ 0.1 mm, $w_o = 90$ μm $\pm$ 5 μm, $v_{DC_{s\parallel}} = 0.745 \, v_{DC_s}$.
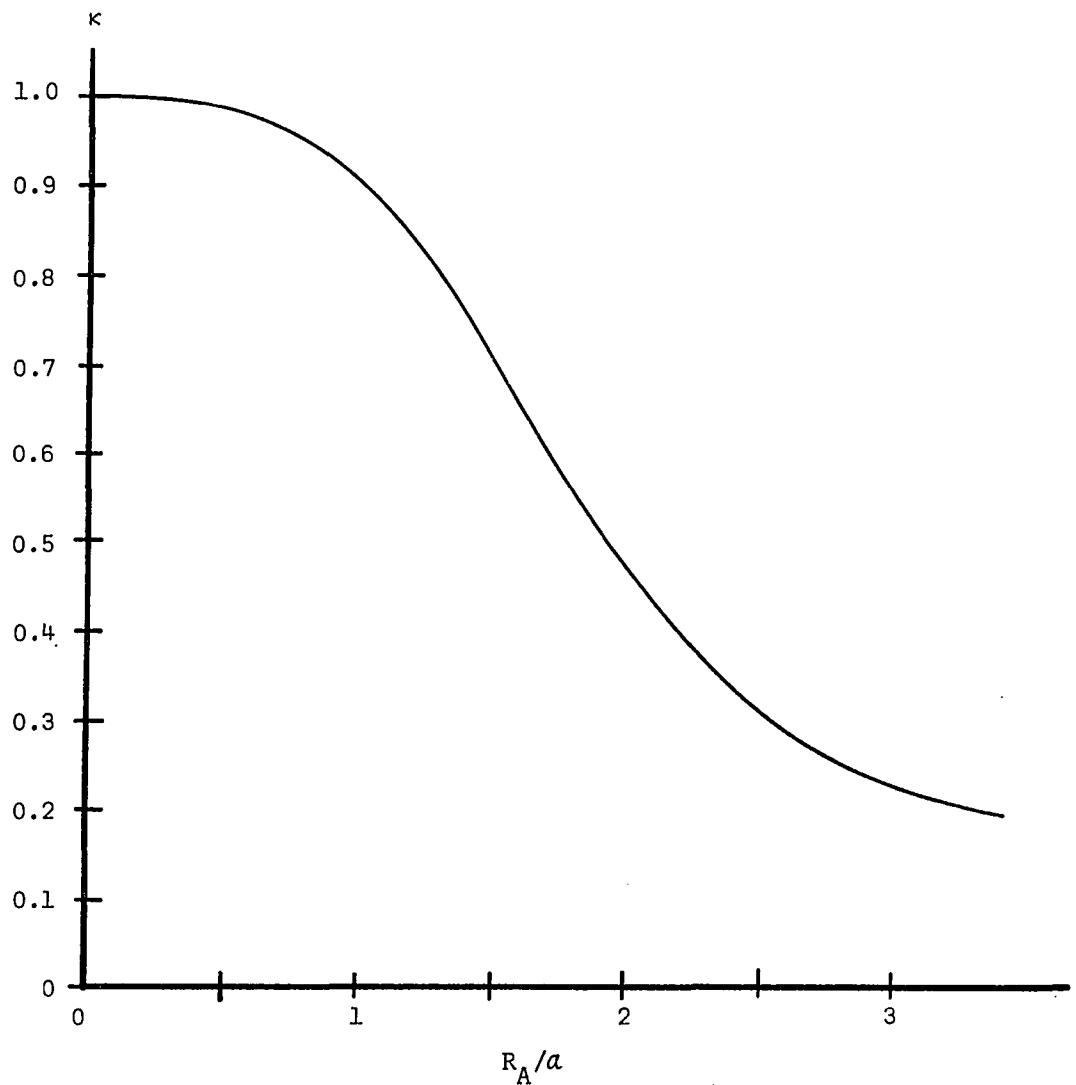
Figure 38. A Plot of κ Versus R_A/a for Gaussian I_L and Constant I_s

4. $R = 40$ cm, $\psi = 90°$, $\theta = 39°$, $a = 1.25$ mm ± 0.1 mm, $w_o = 90$ μm ± 5 μm, $v_{DC_{s\parallel}} = 0.825\ v_{DC_s}$.

The measurements reported here were made from July 22, 1969 through August 27, 1969. Photographs of the experimental arrangement are shown in Figure 39. The signal and noise waveform along with their spectra for a typical case are shown in Figure 40.

The theoretical curves are calculated with the use of the equation developed in Chapter IV, i.e. equations 4-9 through 4-13 with the number 3.1 in equation 4-11 replaced by 4.5 from equation 5-5. The normalized parameters used are as follows for each case:

1.
$$R\Theta = \frac{\lambda R}{\pi w_o} = 2\ \text{mm}$$

so

$$A = \frac{a}{R\Theta} = \frac{2.25\ \text{mm}}{2\ \text{mm}} = 1.125$$

and

$$r_A = \frac{R_A}{R\Theta} = \frac{R_A}{2\ \text{mm}}\ .$$

2. The same as for 1.

3.
$$R\Theta = 0.88\ \text{mm}$$

$$A = \frac{1.25\ \text{mm}}{0.88\ \text{mm}} = 1.43$$

and
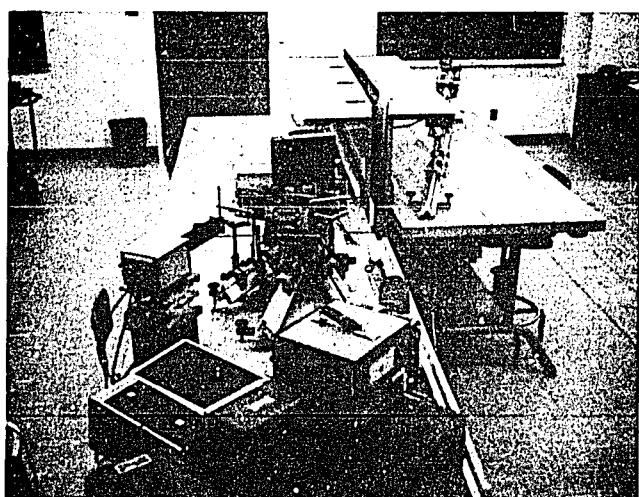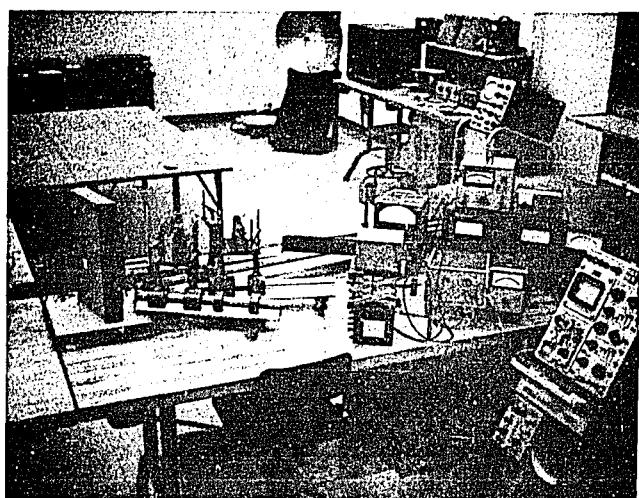
Figure 39. Photographs of the LDSV Experimental Setup
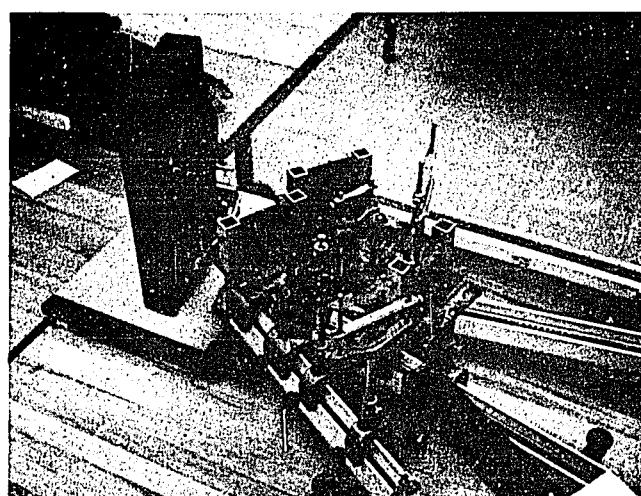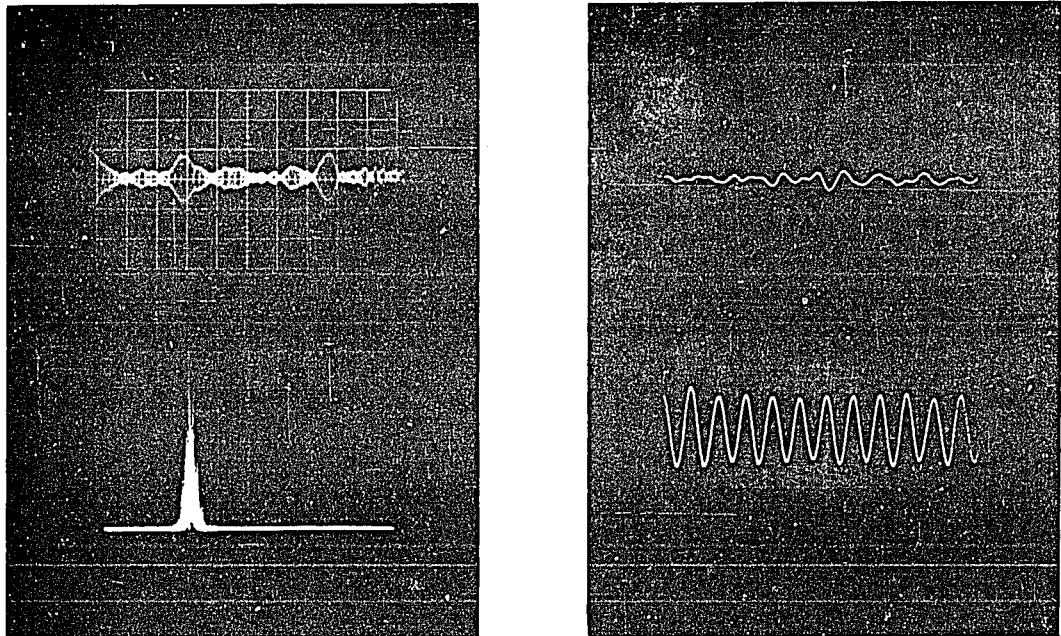
Figure 39. Photographs of the LDSV Experimental Setup
(Continued)

Upper: Video--Signal + Noise

        h = 1 msec./div.
        v = 0.5 V/div.

Lower: Spectrum--Signal + Noise

        h = 10 kHz./div.
        v = 0.05 V/div.

Left = 250 kHz; Right = 150 kHz.

Upper: Video-Noise Alone

Lower: Video--Signal + Noise

        h = 5 μsec./div.
        v = 0.5 V/div.

Figure 40. Typical Scope Waveforms

$$r_A = \frac{R_A}{0.88 \text{ mm}} \ .$$

4. The same as 3.

The rough surface used was not perfectly flat causing the scattered beam to be angularly misaligned with the local oscillator at the receiving aperture by varying degrees as the surface rotated. This, of course, caused a reduction in average signal power. The misalignment was taken into account, theoretically, by the use of an average misalignment angle between the signal wave and to the photo-surface. Referring to Figure 16, we see that fluctuations in the x_p direction will cause a misalignment in signal field along the y'' axis. For a small misalignment angle $\Delta\theta$, the scattered field will be

$$E_s'(y'',z'') = E_s(y'',z'')e^{-jk_s\Delta\theta y''} ,$$

where E_s is the field for no misalignment. The degree of coherence γ_s' will be

$$\gamma_s'(y_1'',z_1'',y_2'',z_2'') = \gamma_s(y_1'',z_1'',y_2'',z_2'')e^{jk_s\Delta\theta(y_2''-y_2'')}$$

or in the normalized variables $Y = y''/R\theta$

$$= \gamma_s(y_1'',z_1'',y_2'',z_2'')e^{j\ 2R\Delta\theta/w_o\ (Y_2-Y_1)} ,$$

where $\gamma_s(y_1'',z_1'',y_2'',z_2'')$ is given by equation 4-8.

The misalignment angle $\Delta\theta$ is determined from the arrangement in Figure 41. In this arrangement, the scattering region was imaged at a distance of 15.73 m from a collecting lens and the transverse motion distance of the image was measured visually with a traverse. This distance was found to be approximately 1.4 mm ± 0.1 mm so the misalignment angle $\Delta\theta$ was approximately 40 μ radians ± 5 μ radians for $\theta = 39°$. The misalignment angle for $\theta = 60°$ was likewise found to be approximately 50 μ radians ± 5 μ radians.

The results of the measurements for cases 1 through 4 are given in Table 1 through 8 and plotted in Figures 42 through 45. The SNR was normalized with respect to that at the greatest aperture diameter. In each case, close agreement is found between the theoretical curves (solid lines) and actual measurements of η_h and SNR (circled points).

The maximum error bounds on these measurements and the theoretical curves are shown in Figures 46 through 49. These bounds were calculated with the use of the bounds on the measurements of a, w_o, and $\Delta\theta$ previously mentioned and a ± 2 per cent of full scale error for the RMS and DC voltage measurements. The upper and lower bounds were calculated using maximum values in the numerators and minimum values in the denominator of the expression in one case, and the opposite in the other.

The close agreement tends to lend support to assumptions made in modeling the LDSV system in Chapter IV. In addition, it verifies the applicability of the equations for η_h and SNR as a useful method of studying heterodyne system performance.
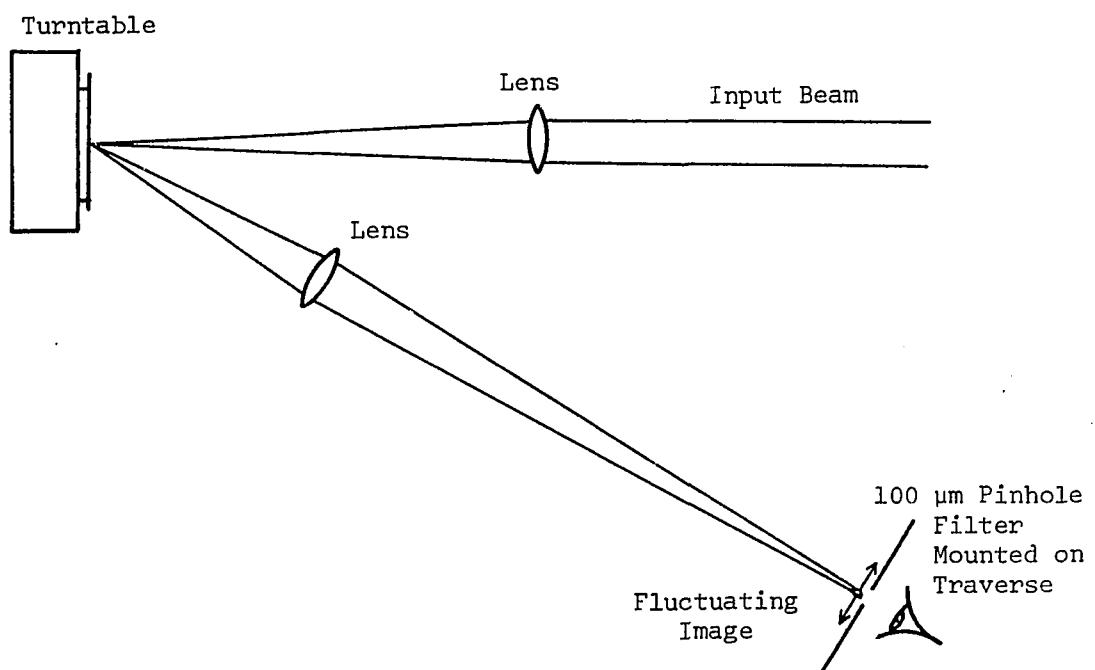
Figure 41. The Experimental Setup for Determining Δθ

Table 1. Data for the LDSV Experiments for Case 1

Aperture Radius	v_{DC_L}	v_{DC_s}	$v_{s+n_{rms}}$	$v_{n_{rms}}$
225 μm	10 V	0.50 mV	315 mV	145 mV
0.5 mm	10 V	0.51 mV	285 mV	88 mV
1.0 mm	10 V	0.61 mV	280 mV	38 mV
1.5 mm	10 V	0.73 mV	290 mV	29 mV
2.0 mm	10 V	1.10 mV	310 mV	26 mV
2.5 mm	10 V	1.37 mV	310 mV	25 mV
3.0 mm	10 V	1.82 mV	315 mV	24.5 mV

Doppler frequency f_D = 256 kHz.

Filter Bandwidth = 120 kHz.

Table 2. Calculations for the LDSV Experiments for Case 1

Aperture Radius	n_h	SNR	Normalized SNR
225 μm	0.995	3.71	0.02
0.5 mm	0.918	9.65	0.06
1.0 mm	0.804	53.3	0.31
1.5 mm	0.737	99	0.58
2.0 mm	0.577	141	0.83
2.5 mm	0.496	153	0.91
3.0 mm	0.437	170	1.00

Figure 42. Plots of the Data for Case 1 (7/22/69)

Table 3. Data for the LDSV Experiments for Case 2

Aperture Radius	v_{DC_L}	v_{DC_s}	$v_{s+n_{rms}}$	$v_{n_{rms}}$
0.5 mm	10 V	0.17 mV	190 mV	115 mV
1.0 mm	10 V	0.21 mV	165 mV	47 mV
1.5 mm	10 V	0.27 mV	160 mV	34 mV
2.0 mm	10 V	0.33 mV	160 mV	28.5 mV
2.5 mm	10 V	0.47 mV	160 mV	27 mV
3.0 mm	10 V	0.69 mV	170 mV	26 mV

Doppler frequency f_D = 428 kHz.

Filter Bandwidth = 200 kHz.

Table 4. Calculations for the LDSV Experiments for Case 2

Aperture Radius	η_h	SNR	Normalized SNR
0.5 mm	0.998	1.77	0.042
1.0 mm	0.860	11.4	0.269
1.5 mm	0.670	21.2	0.500
2.0 mm	0.571	30.7	0.725
2.5 mm	0.433	34.1	0.805
3.0 mm	0.370	42.5	1.000
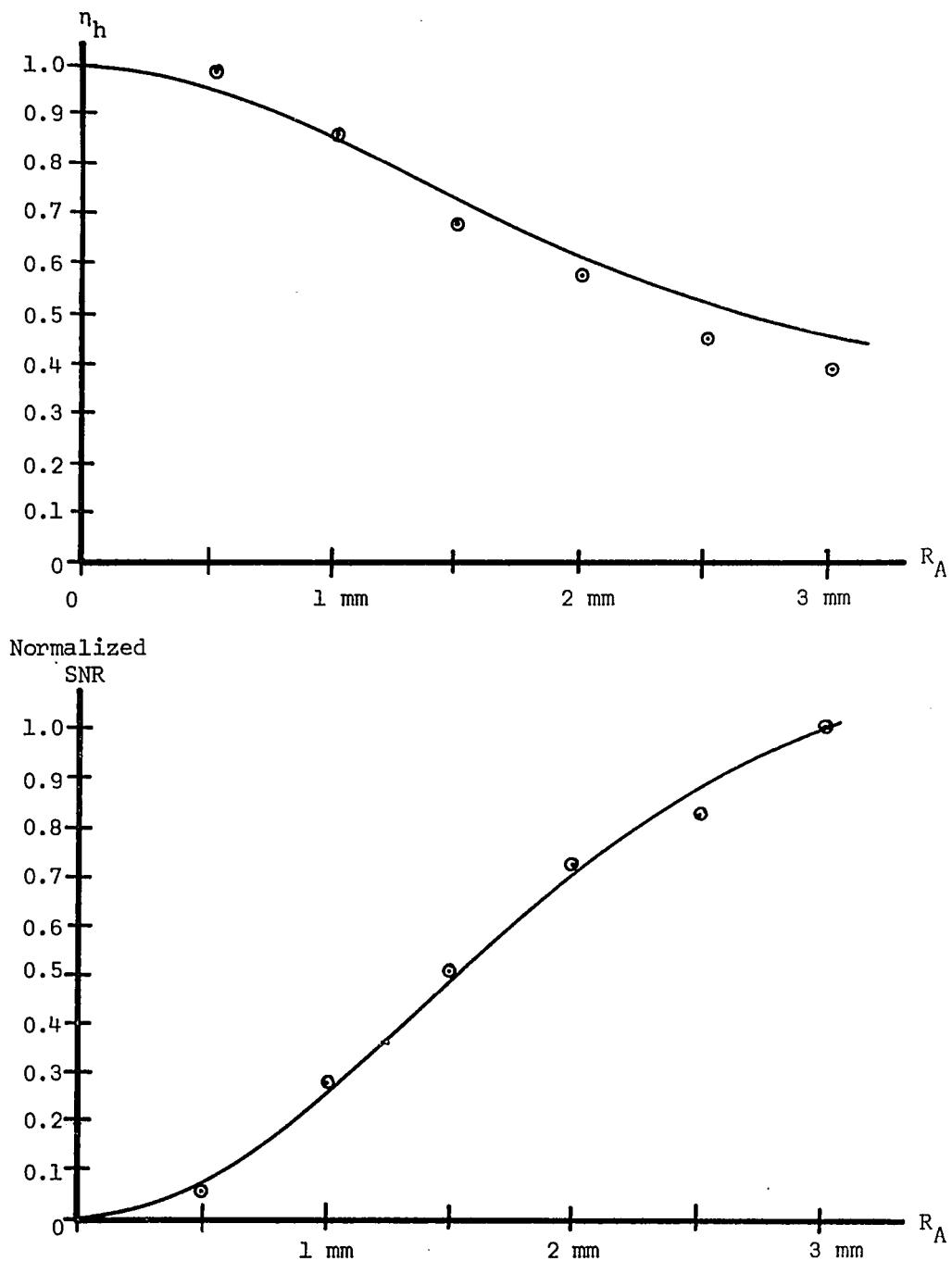
Figure 43. Plots of the Data for Case 2 (8/22/67)

Table 5. Data for the LDSV Experiments for Case 3

Aperture Radius	v_{DC_L}	v_{DC_s}	$v_{s+n_{rms}}$	$v_{n_{rms}}$
225 μm	10 V	0.04 mV	105 mV	75 mV
0.5 mm	10 V	0.05 mV	90 mV	50 mV
1.0 mm	10 V	0.09 mV	90 mV	28.5 mV
1.5 mm	10 V	0.13 mV	95 mV	22.5 mV
2.0 mm	10 V	0.24 mV	95 mV	20.5 mV

Doppler frequency f_D = 434 kHz.

Filter Bandwidth = 200 kHz.

Table 6. Calculations for the LDSV Experiments for Case 3

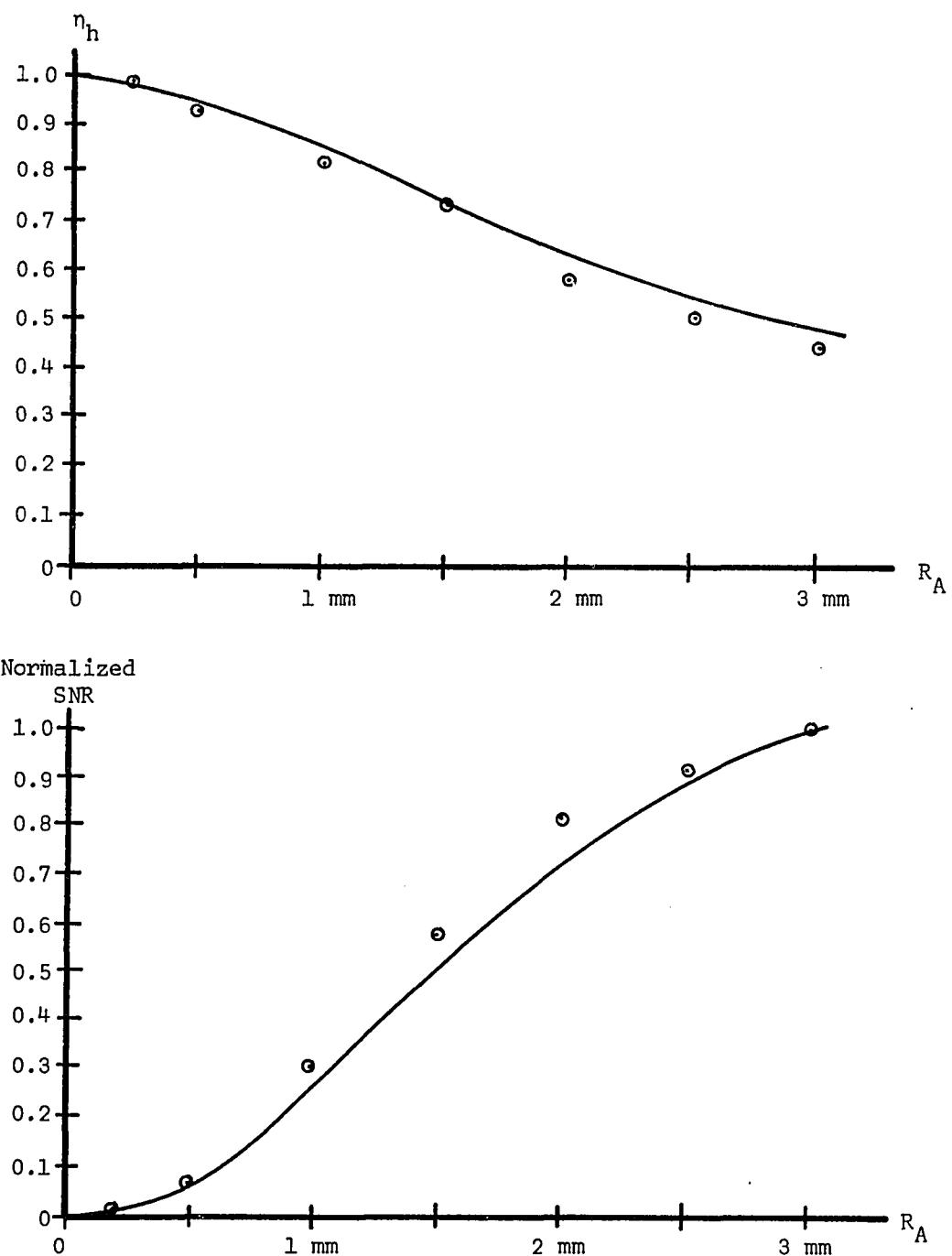| Aperture Radius	n_h	SNR	Normalized SNR
225 μm	0.976	0.96	0.047
0.5 mm	0.810	2.24	0.110
1.0 mm	0.606	8.96	0.442
1.5 mm	0.460	14.90	0.738
2.0 mm	0.380	20.30	1.000
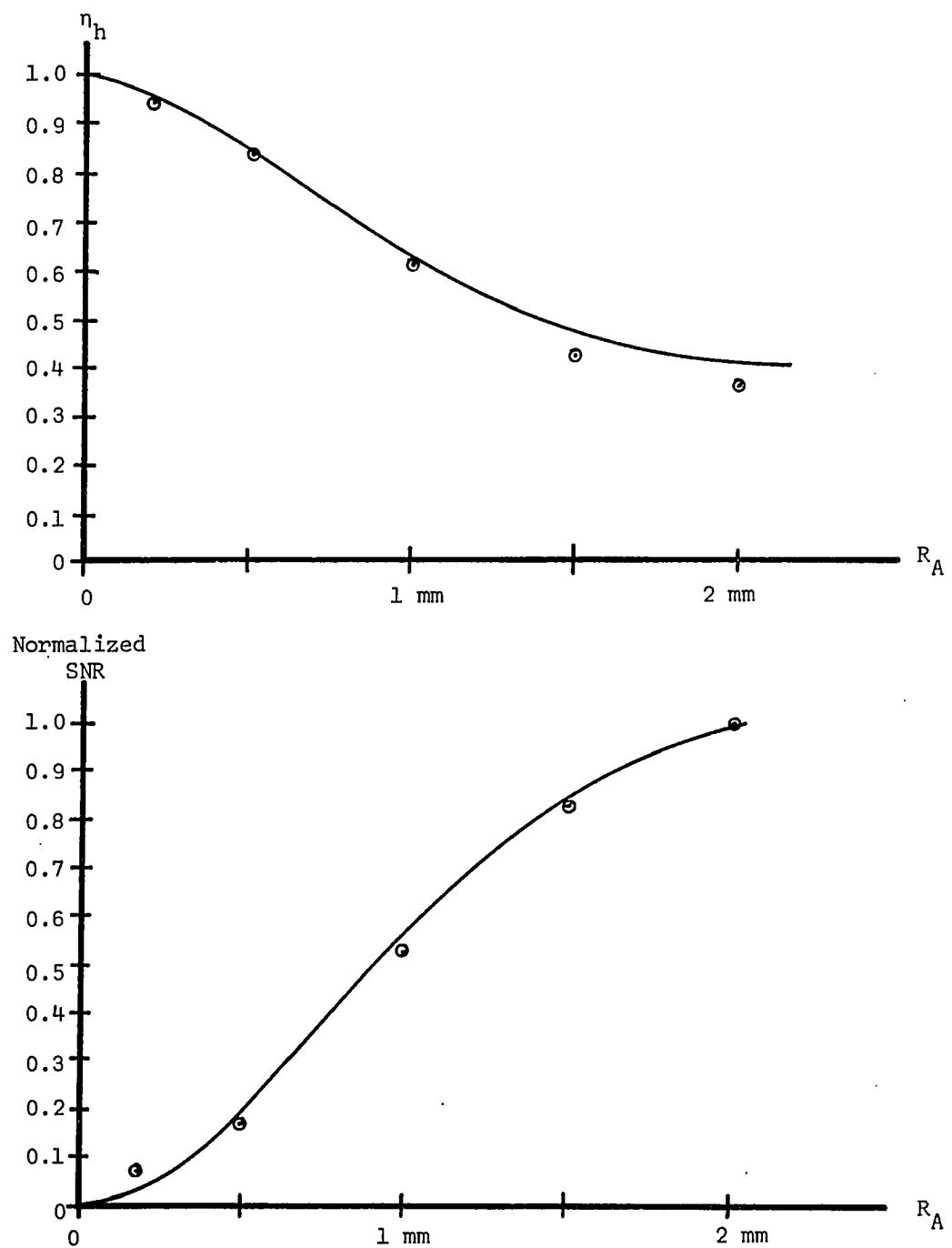
Figure 44. Plots of the Data for Case 3 (8/26/69)

Table 7. Data for the LDSV Experiments for Case 4

Aperture Radius	v_{DC_L}	v_{DC_s}	$v_{s+n_{rms}}$	$v_{n_{rms}}$
225 μm	10 V	0.125 mV	150 mV	67.5 mV
0.5 mm	10 V	0.20 mV	160 mV	52.0 mV
1.0 mm	10 V	0.23 mV	140 mV	26.5 mV
1.5 mm	10 V	0.42 mV	150 mV	21.5 mV
2.0 mm	10 V	0.77 mV	160 mV	21.0 mV

Doppler Frequency f_D = 315 kHz.

Filter Bandwidth = 160 kHz.

Table 8. Calculations for the LDSV Experiments for Case 4

Aperture Radius	η_h	SNR	Normalized SNR
225 μm	0.940	4.9	0.084
0.5 mm	0.837	9.5	0.164
1.0 mm	0.620	29.5	0.515
1.5 mm	0.410	47.7	0.820
2.0 mm	0.322	58.2	1.000
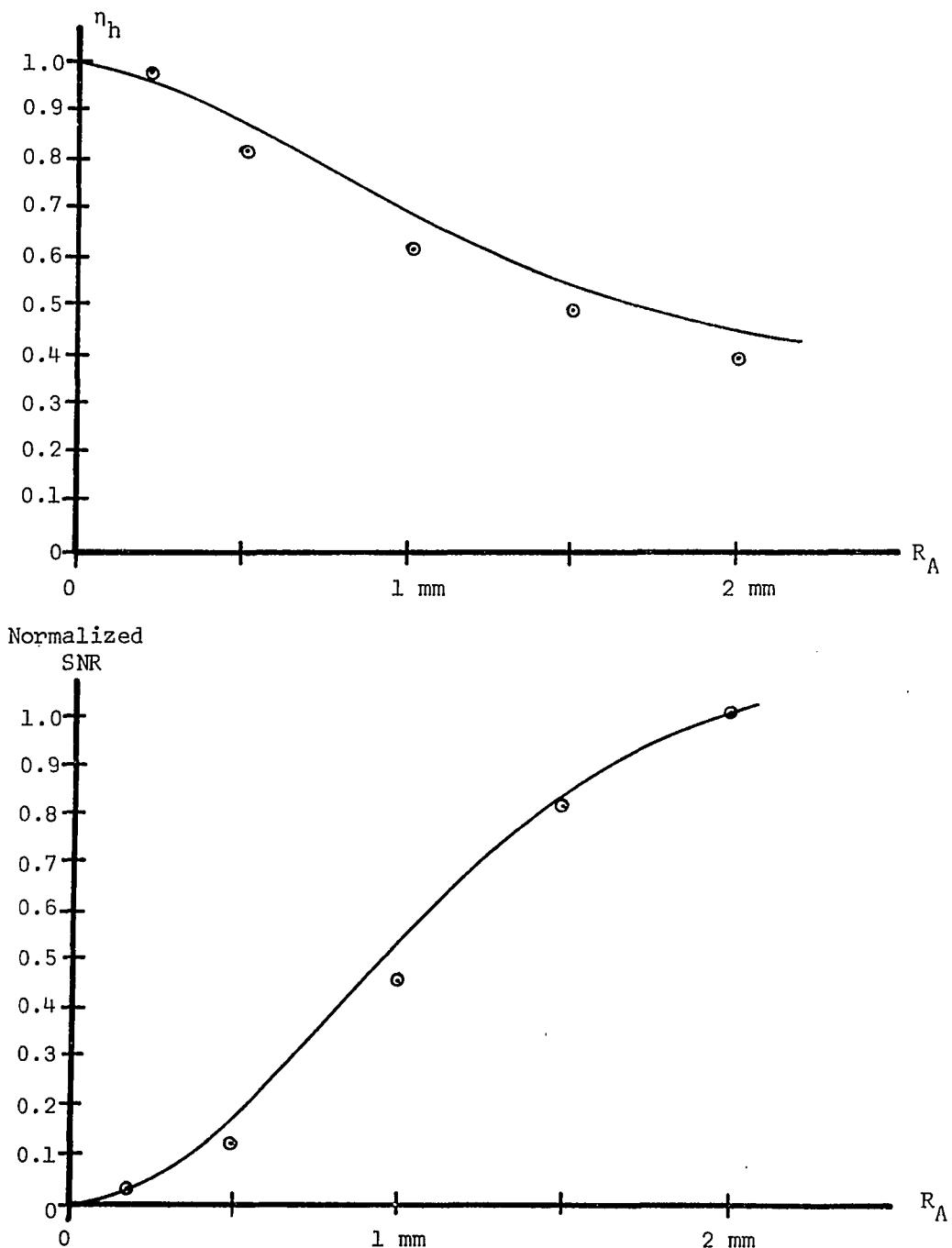
Figure 45. Plots of the Data for Case 4 (8/27/69)
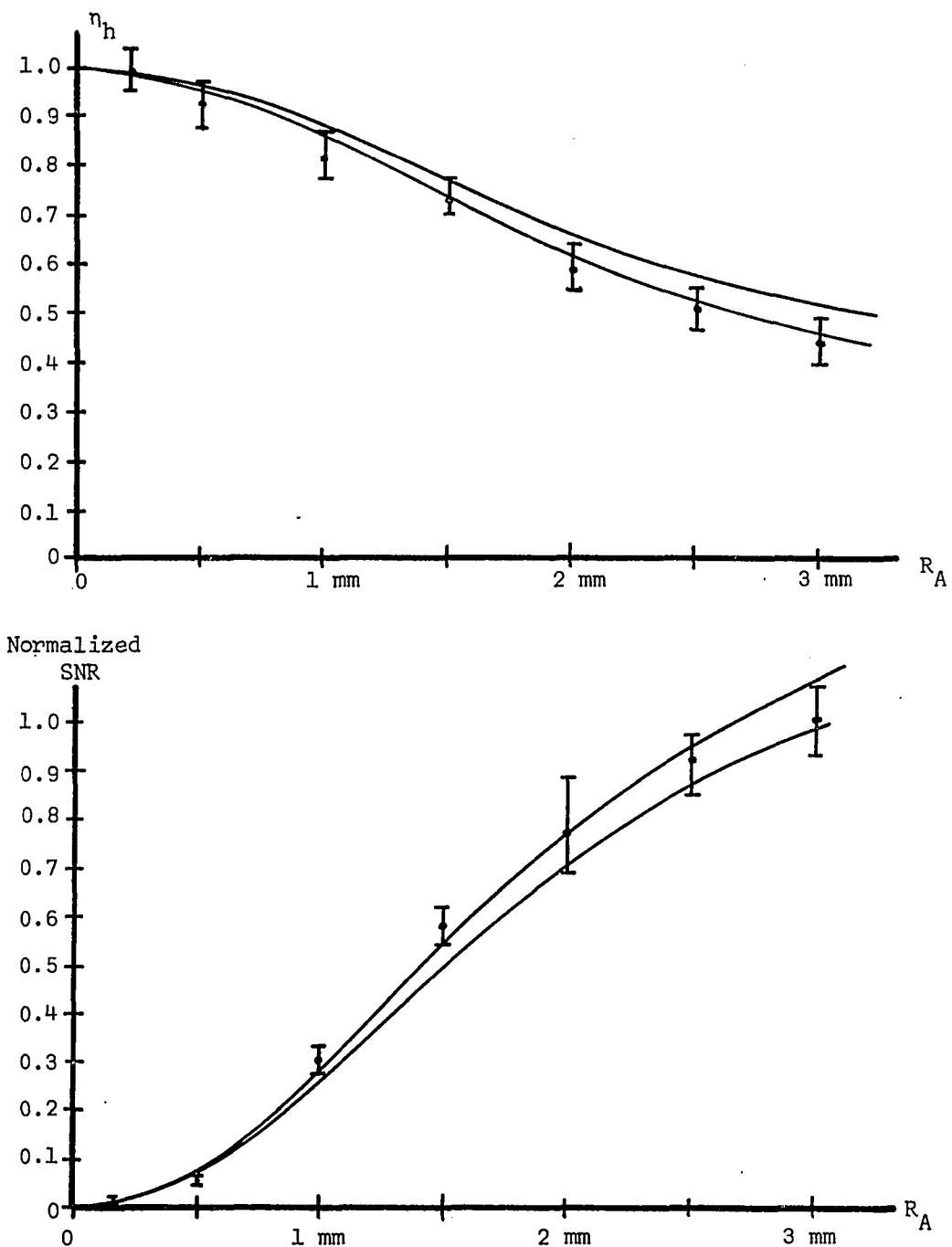
Figure 46. Error Bounds for Case 1
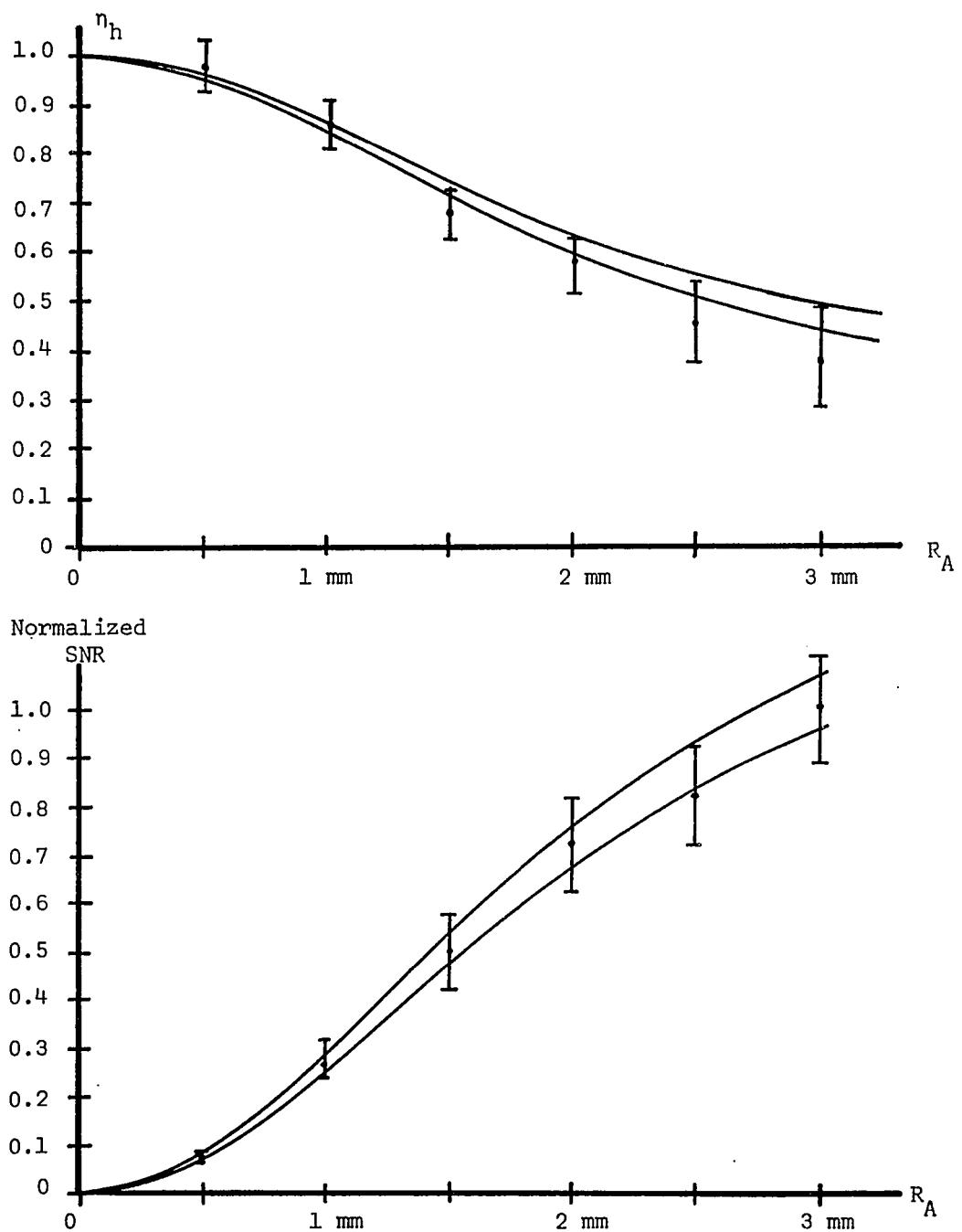
Figure 47.   Error Bounds for Case 2
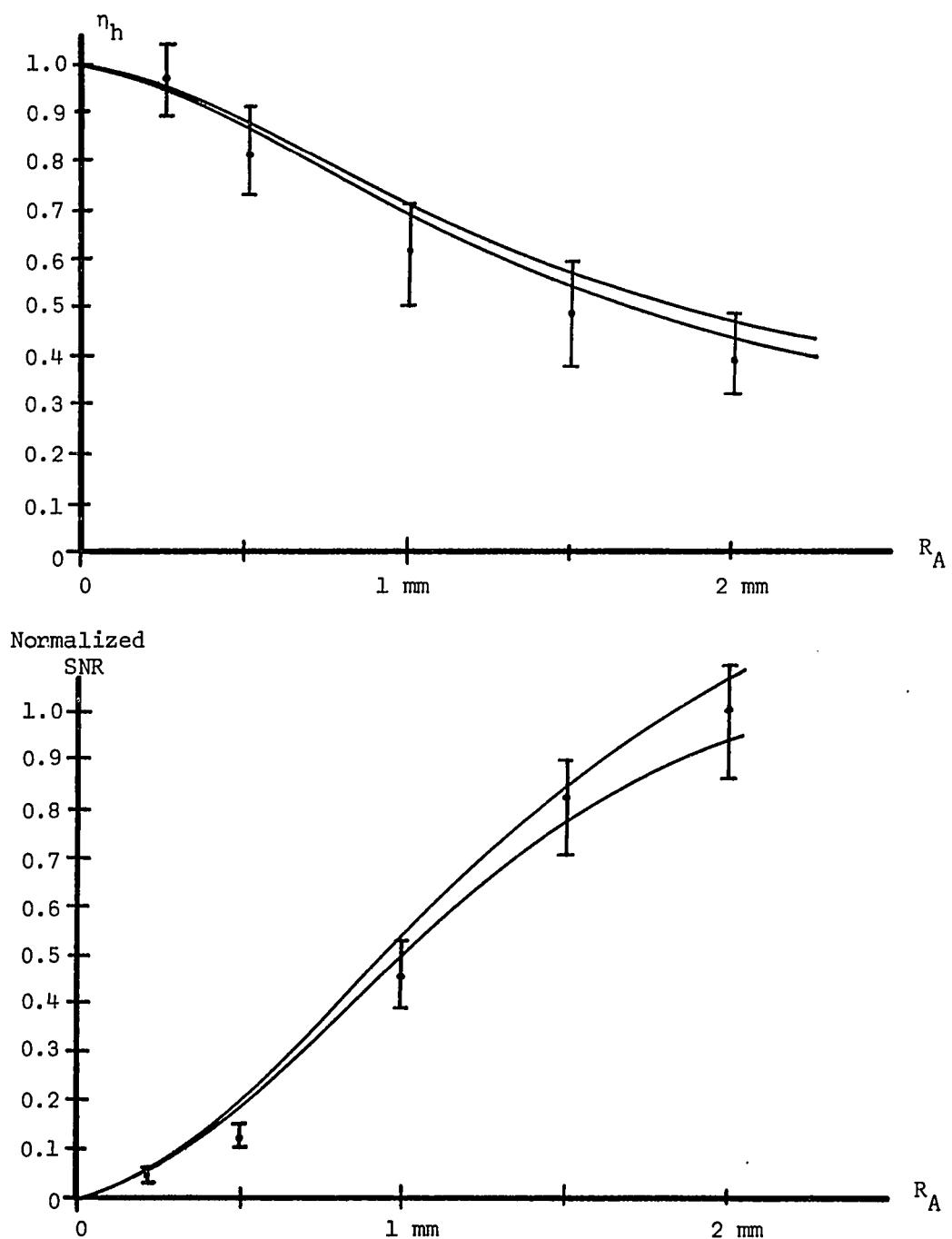
Figure 48. Error Bounds of Case 3
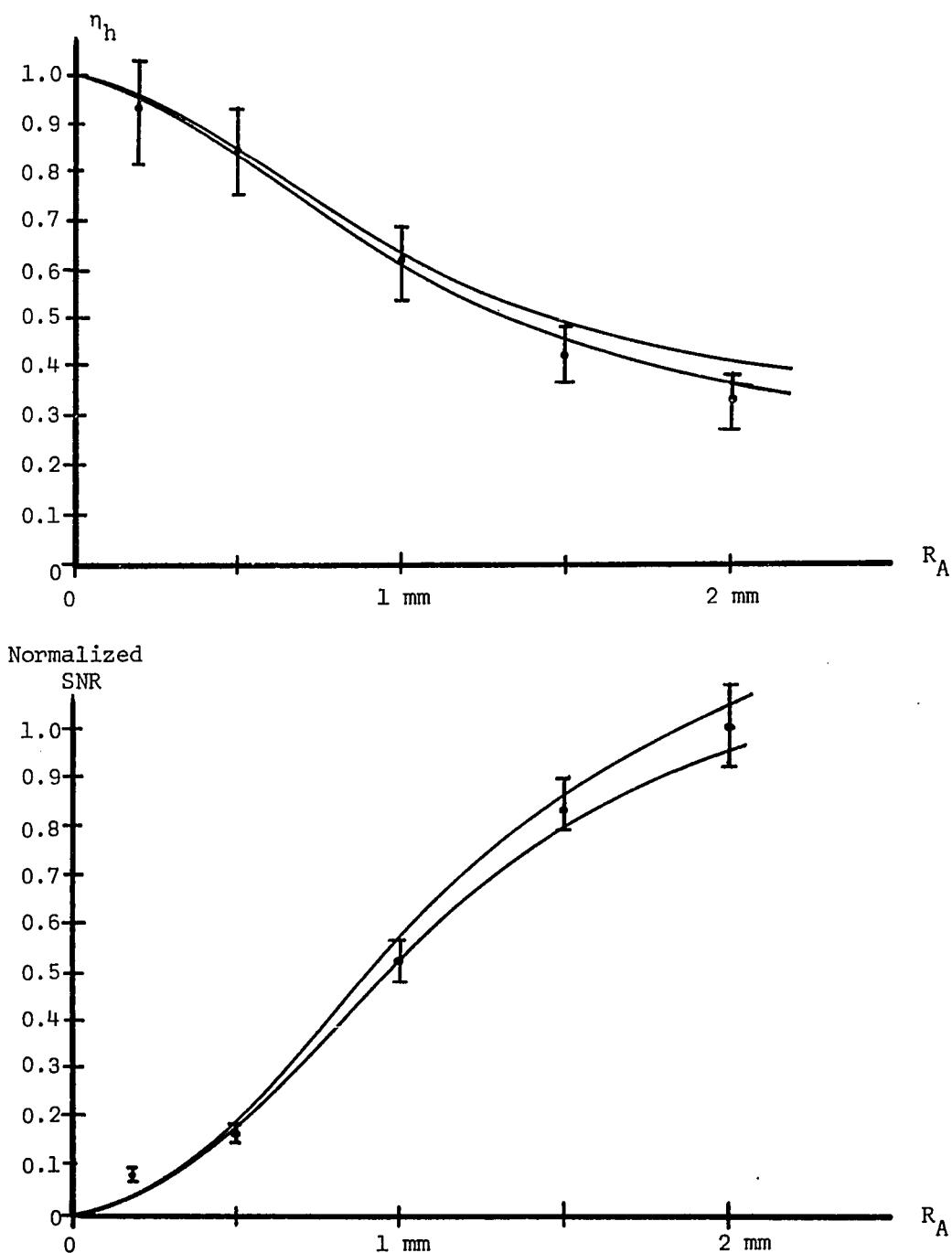
Figure 49. Error Bounds for Case 4

The Laser Doppler Flowmeter

The following three cases were studied:

1. Kaolinite scattering particles, R = 40 cm, ψ = 77°, θ = 25°, a = 2.42 mm ± 0.1 mm, w_o = 50 μm ± 5 μm. Slit width = 2W' = 1.02 mm ± 0.1 mm (in channel), $v_{DC_{s\parallel}}$ = 0.945 v_{DC_s}.

2. Pollen scattering particles, R = 40 cm, ψ = 77°, θ = 25°, a = 2.42 mm ± 0.1 mm, w_o = 50 μm ± 5 μm, 2W' = 1.02 mm ± 0.1 mm (in channel), $v_{DC_{s\parallel}}$ = 0.975 v_{DC_s}.

3. Pollen scattering particles, R = 40 cm, ψ = 77°, θ = 25°, a = 1.2 mm ± 0.1 mm, w_o = 75 μm ± 5 μm, 2W' = 1.02 mm ± 0.1 mm (in channel), $v_{DC_{s\parallel}}$ = 0.980v_{DC_s}.

These measurements reported here were made from October 27, 1969 through October 31, 1969. Photographs of the experimental arrangement are shown in Figure 50. The signal and noise waveforms along with their frequency spectra are shown in Figure 51 for a typical case.

The theoretical curves were again calculated with the use of the equations for the LDF system, developed in Chapter IV, i.e. equations 4-14 through 4-18 with the number 3.1 in equation 4-15 replaced again by 4.5. The normalized parameters used are as follows for each case:

1.   Rθ = 1.57 mm

so

$$A = \frac{2.42 \text{ mm}}{1.57 \text{ mm}} = 1.55, \quad W = \frac{2W'}{2w_o} = 20.4,$$
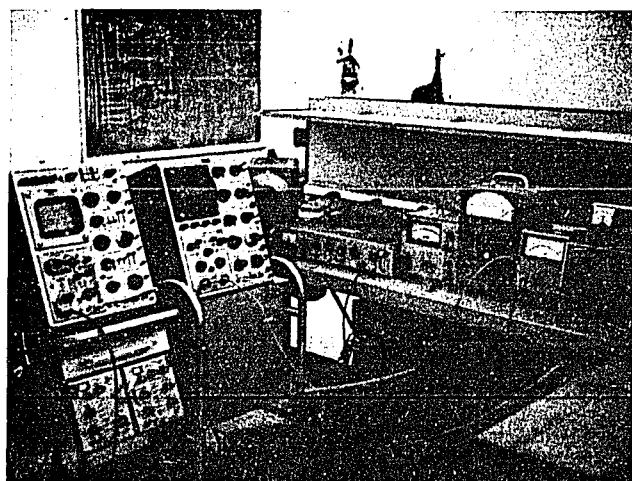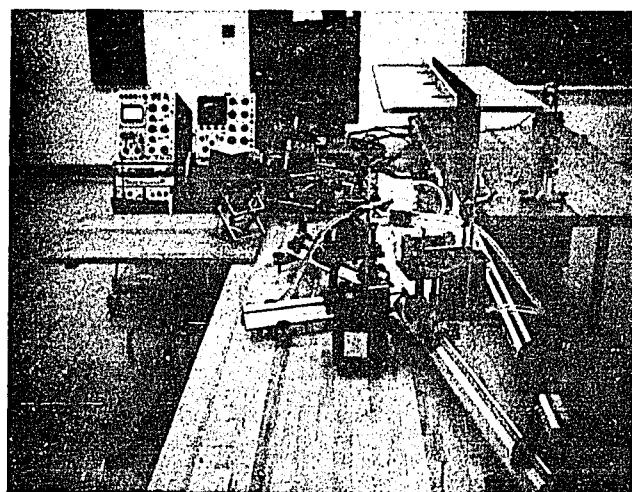
Figure 50. Photographs of the LDF Experimental Setup
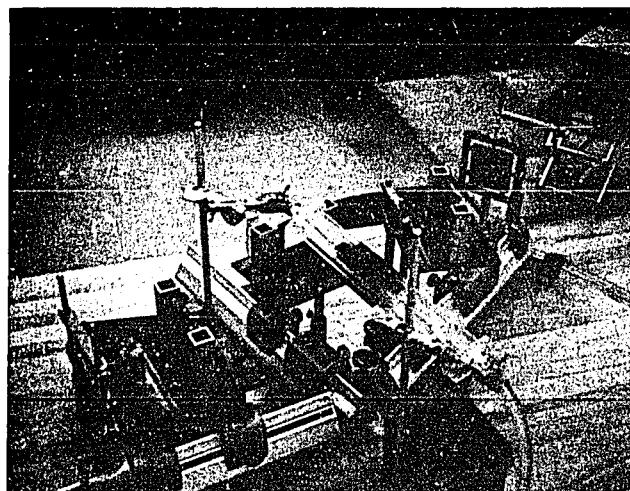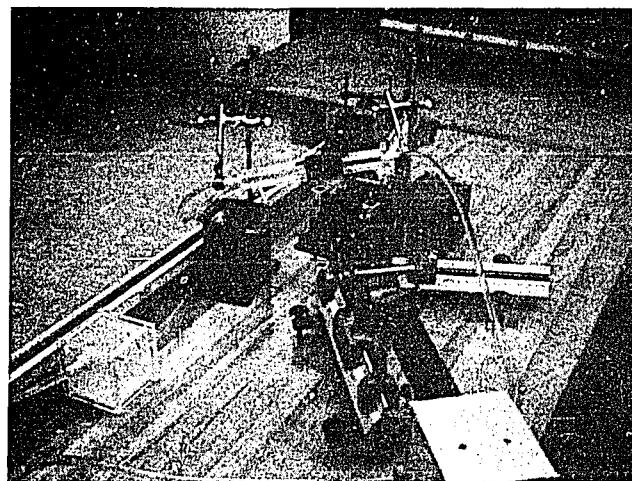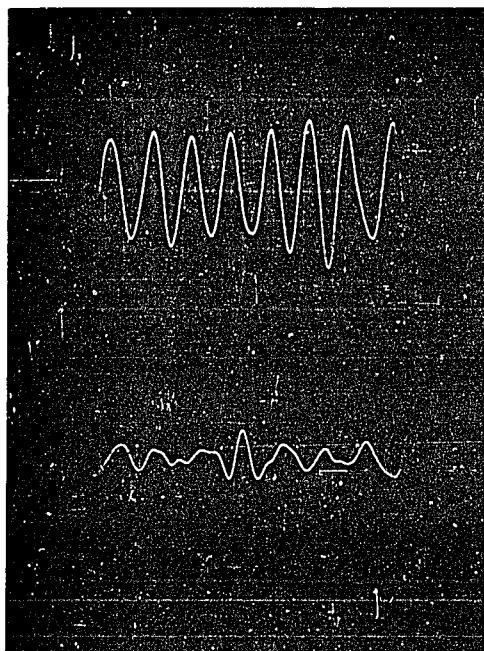
Figure 50. Photographs of the LDF Experimental Setup
(Continued)

Upper: Video--Signal + Noise   Upper: Spectrum--Noise Alone

       h = 2 μsec./div.   Lower: Spectrum--Signal + Noise
       v = 0.05 V/div.
                                         h = 100 kHz/div.

Lower: Video-Noise Alone   v = 0.005 V/div.

       h = 2 μsec./div.   Left = 1 MHz, Right = 0Hz.
       v = 0.05 V/div.
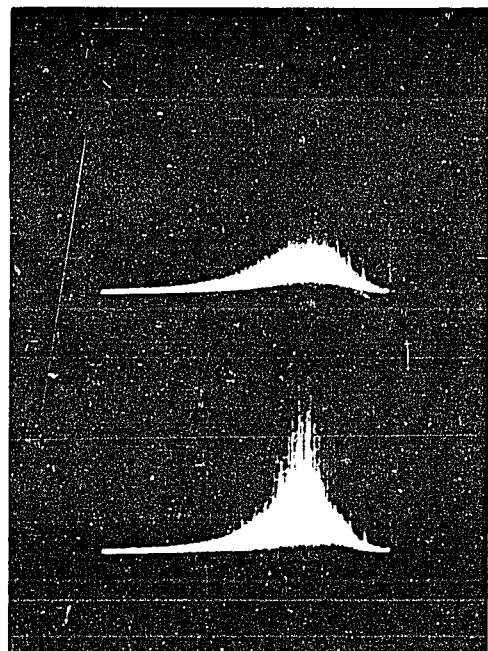
Figure 51. Typical Scope Waveforms

and

$$r_A = \frac{R_A}{1.57 \text{ mm}} .$$

2. Same as 1.

3. $R\Theta = 1.03$ mm

so

$$A = \frac{1.2 \text{ mm}}{1.03 \text{ mm}} = 1.17, \quad W = 13.6,$$

and

$$r_A = \frac{R_A}{1.03 \text{ mm}} .$$

The results of the measurements for these cases are given in Tables 9 through 14 and plotted in Figure 52 and 53. The SNR was again normalized with respect to that at the greatest aperture diameter. The voltage, v_{DC_s}, under normal measurement conditions turned out to be much too small to be measured. The photomultiplier dark current completely masked this voltage. An increase in the applied voltage to the photomultiplier to 1500V brought the voltage v_{DC_s} up to a level where it could be measured. The gain characteristics of the photomultiplier versus applied voltage was measured and plotted in Figure 54.

In each case, close agreement is again found between the theoretical curves and actual measurements but not as good as in the LDSV

Table 9. Data for the LDF Experiments for Case 1

Aperture Radius	PM Supply Voltage	v_{DC_L}	v_{DC_S} @ 1500 V	$v_{s+n_{rms}}$	$v_{n_{rms}}$
0.5 mm	812 V	10 V	1.55 mV	91 mV	79 mV
1.0 mm	630 V	10 V	9.1 mV	38 mV	31 mV
1.5 mm	578 V	10 V	19.1 mV	27.5 mV	22 mV
2.0 mm	550 V	10 V	35.2 mV	23.5 mV	18 mV

Filter Bandwidth = 350 kHz.

Doppler Frequency f_D between 250 kHz. and 350 kHz.

Table 10. Calculations for the LDF Experiments for Case 1

Aperture Radius	v_{DC_S} @ PM Supply Voltage	η_h	SNR	Normalized SNR
0.5 mm	20.2 µV	0.546	0.327	0.465
1.0 mm	16.4 µV	0.159	0.499	0.709
1.5 mm	17.9 µV	0.084	0.570	0.810
2.0 mm	23.2 µV	0.056	0.704	1.000

Table 11. Data for the LDF Experiments for Case 2

Aperture Radius	PM Supply Voltage	v_{DC_L}	v_{DC_S} @ 1500 V	$v_{s+n_{rms}}$	$v_{n_{rms}}$
0.5 mm	833 V	10 V	1.34 mV	95 mV	85 mV
1.0 mm	643 V	10 V	11.4 mV	43 mV	34 mV
1.5 mm	567 V	10 V	34 mV	28 mV	21 mV
2.0 mm	542 V	10 V	18.5 mV	23 mV	17 mV

Doppler Frequency f_D from 250 kHz. to 350 kHz.

Filter Bandwidth = 350 kHz.

Table 12. Calculations for the LDF Experiments for Case 2

Aperture Radius	v_{DC_S} @ PM Supply Voltage	n_h	SNR	Normalized SNR
0.5 mm	19.4 μV	0.512	0.249	0.300
1.0 mm	25.2 μV	0.170	0.686	0.826
1.5 mm	27.8 μV	0.068	0.780	0.940
2.0 mm	29.1 μV	0.047	0.830	1.000
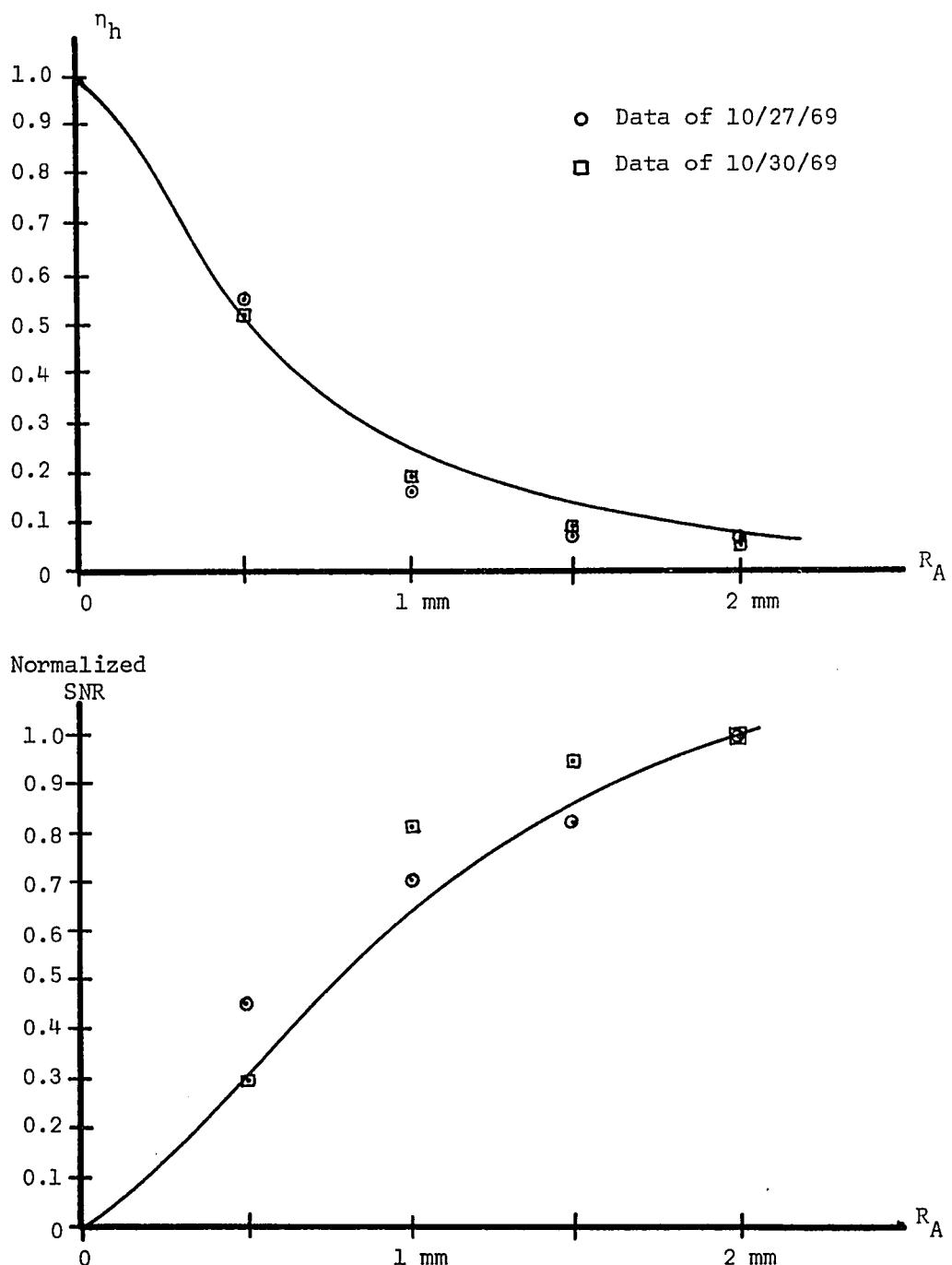
Figure 52. Plots of the Data for Cases 1 and 2

Table 13. Data for the LDF Experiments for Case 3

Aperture Radius	DM Supply Voltage	v_{DC_L}	v_{DC_s} @ 1500 V	$v_{s+n_{rms}}$	$v_{n_{rms}}$
225 μm	770 V	10 V	0.31 mV	68 mV	65 mV
0.5 mm	657 V	10 V	1.4 mV	39 mV	34.5 mV
1.0 mm	550 V	10 V	8.3 mV	25 mV	20 mV
1.5 mm	527 V	10 V	18.8 mV	18.5 mV	14.5 mV

Doppler Frequency from 250 kHz. to 350 kHz.

Filter Bandwidth = 350 kHz.

Table 14. Calculations for the LDF Experiments for Case 3

Aperture Radius	v_{DC_s} @ PM Supply Voltage	η_h	SNR	Normalized SNR
225 μm	2.60 μV	0.850	0.095	0.150
0.5 mm	3.50 μV	0.519	0.277	0.438
1.0 mm	5.48 μV	0.241	0.564	0.895
1.5 mm	9.40 μV	0.094	0.630	1.000
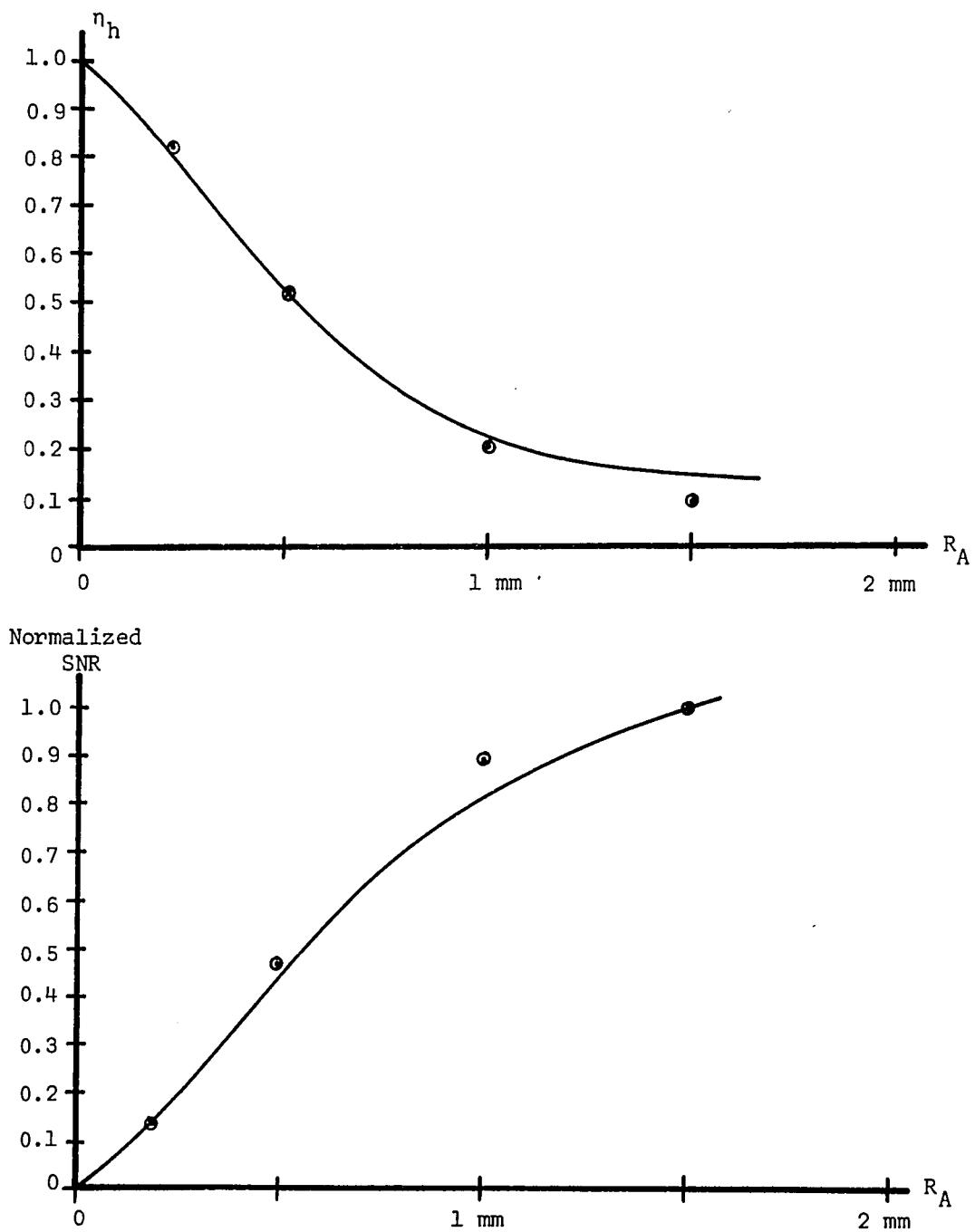
Figure 53. Plots of the Data for Case 3 (10/29/69)
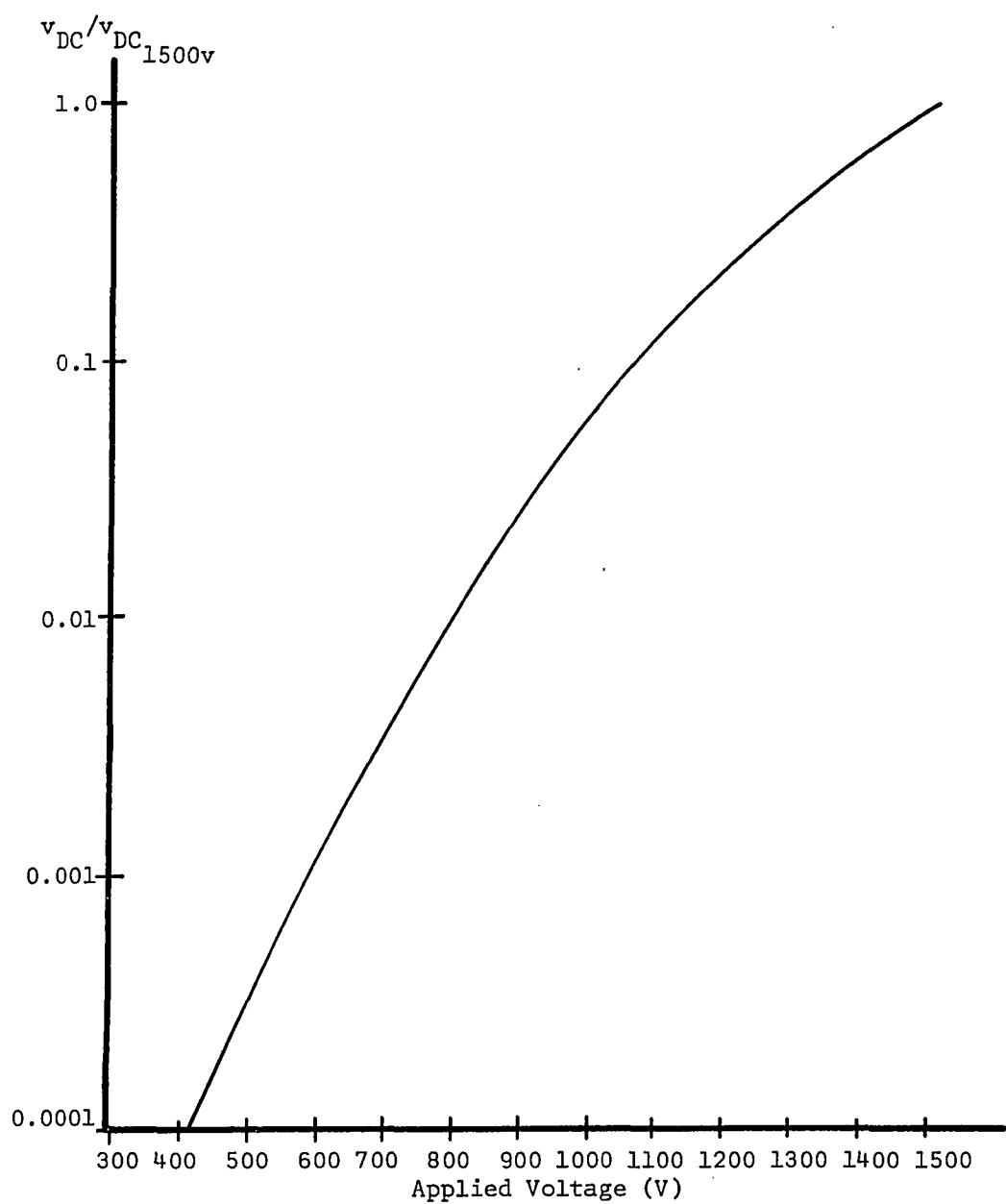
Figure 54. Photomultiplier Gain Curve

system. This is due to the much lower SNR's encountered in this system than in the LDSV system.

The maximum error bounds on the measurements and theoretical curves are shown in Figures 55 through 57. These bounds are calculated in the same manner as in the LDSV system.

The close agreement again lends support to the assumption made in modeling the LDF system in Chapter IV. The results verify the applicability of the equations for η_h and SNR for studying heterodyne system performance.
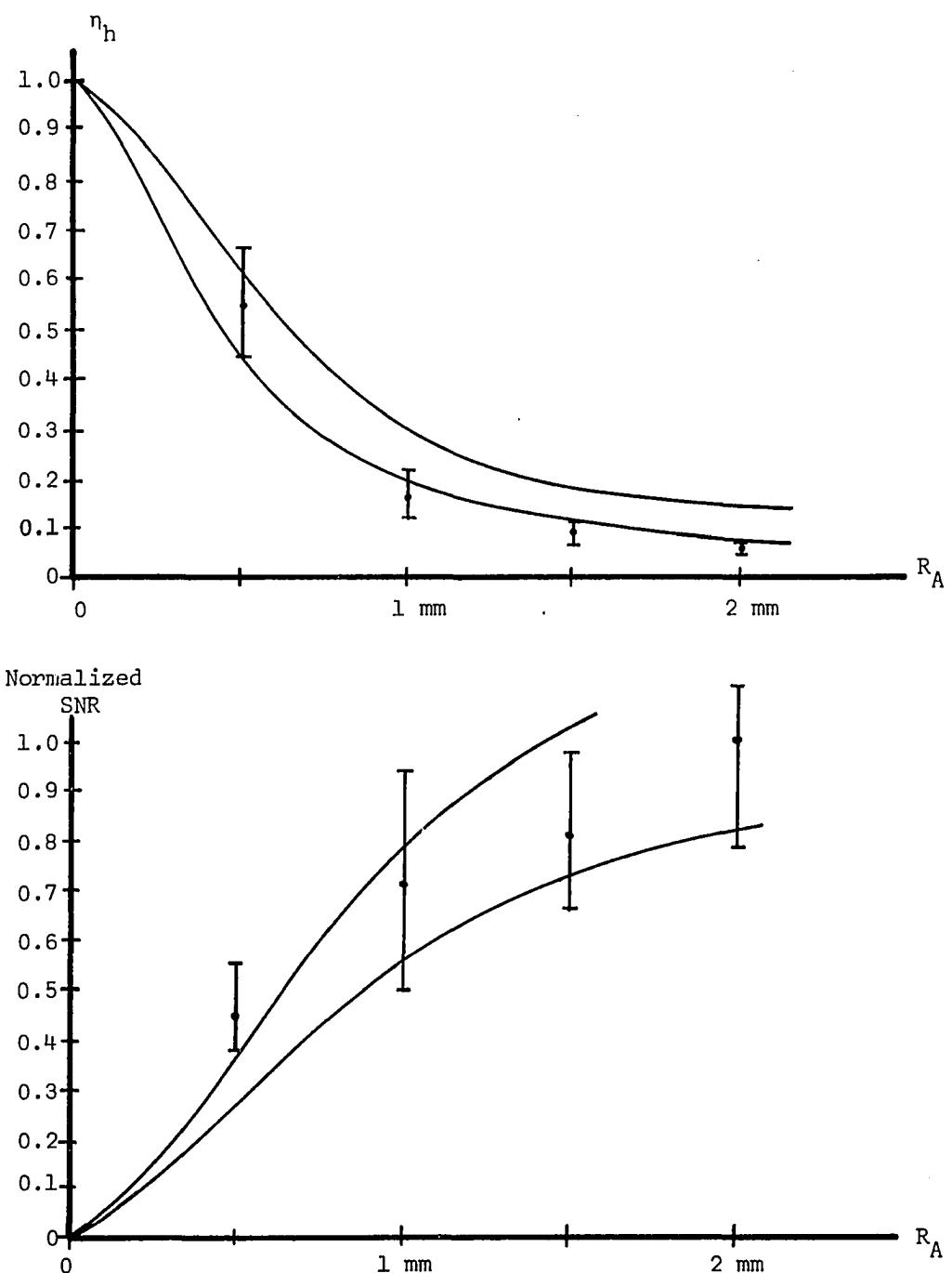
Figure 55. Error Bounds for Case 1
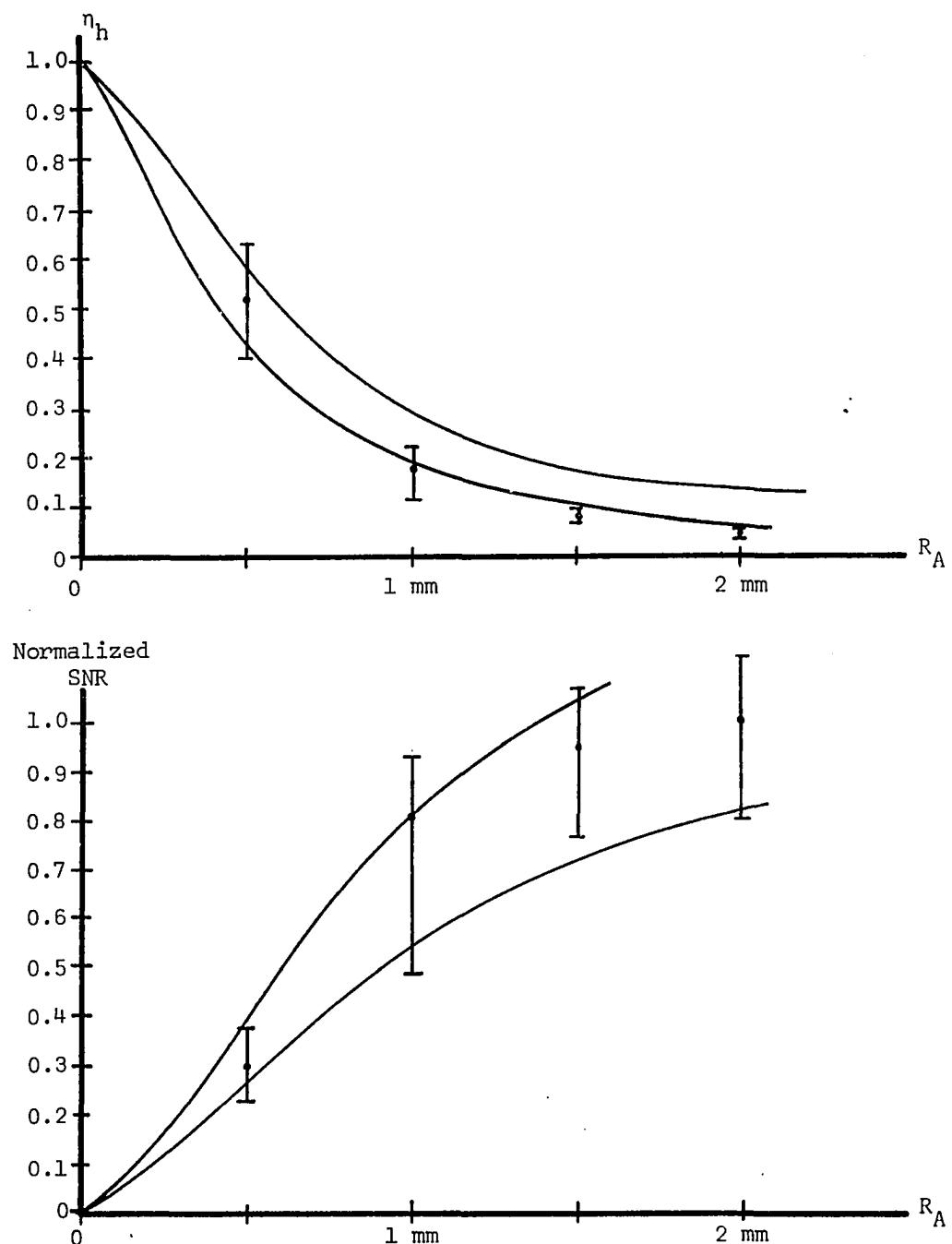
Figure 56. Error Bounds for Case 2
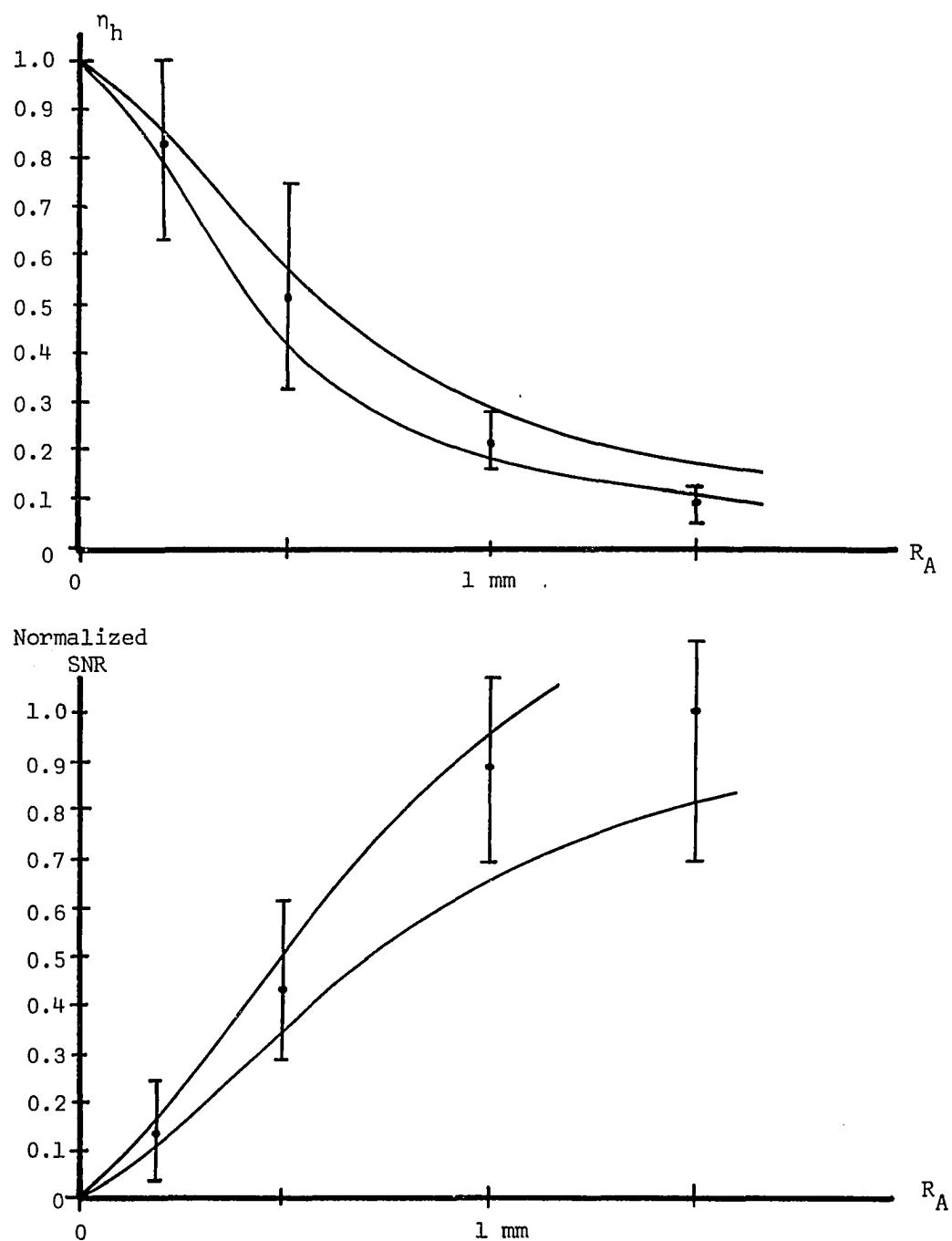
Figure 57. Error Bounds for Case 3

CHAPTER VI

CONCLUSIONS

The following general conclusions are made for the cases studied here:

1. The assumptions made and models used for the system studied analytically are accurate enough to predict experimental performance.

2. The local oscillator beam radius and the receiving aperture size have the greatest effect on system performance and are, therefore, the most important parameters to be considered.

3. Small changes in local oscillator coherence and intensity distribution consistent with most available local oscillator sources, along with small changes in the shape of the receiving aperture have no significant effect on system performance.

4. We can improve the efficiency by making the local oscillator beam radius as small as possible so that only the coherent part of the signal is used. We can achieve relative maximum in SNR for this case by making the aperture radius approximately equal to twice the local oscillator beam radius.

5. We can obtain a maximum SNR by making the local oscillator beam radius as large as possible and letting the aperture radius again be equal to twice the beam radius. There is signal power in the incoherent part and the use of this is necessary for maximum SNR.

6. As a result of numbers 4 and 5, we may conclude that efficient operation and maximum SNR cannot be obtained simultaneously in these cases.

7. The results and predictions of the systems studied here were independent of system. The same criteria may therefore, be used in design and evaluation of each of these heterodyne systems.

This study has been concerned mainly with the effects of receiver parameters on heterodyne system performance given a certain set of signal parameters, i.e. coherence function, intensity distribution, etc. If the signal parameters were varied as well, the results might be different. If, for example, a Gaussian signal intensity distribution was used instead of a constant, it might be possible to obtain both good efficiency and maximum SNR, simultaneously.

This study has been concerned with an otherwise perfectly aligned system. It is important to know the effects of partial coherence of the signal and local oscillator on the alignment requirements, most notably, the angular alignment requirement between the signal and local oscillator propagation. This directivity property is often used to advantage in an optical heterodyne system and these effects should be studied.

In addition, the effects of relaxing some of the conditions placed on the heterodyne systems studied as examples here should be investigated. In the LDSV system, the effects of other types of rough surface should be studied to determine if the system is insensitive to the type of rough surface used. In the LDF system, the effects

of multiple scattering and flow turbulence on the signal coherence and system performance should be understood.

APPENDIX

APPENDIX I

SAMPLE COMPUTER PROGRAMS

This appendix contains some samples of the computer programs used for calculating heterodyne efficiency and SNR. These were written in Fortran and executed on a Univac 1108 digital computer. The programs presented here are for the following cases:

(1) the communications link study for a Gaussian I_L, circular aperture, and perfect local oscillator coherence;

(2) the communications link study for a rectangular I_L, circular aperture, and "nearly" perfect local oscillator coherence;

(3) the LDSV study for a Gaussian I_L, elliptic aperture, and perfect local oscillator coherence;

(4) the LDSV study for a rectangular I_L, circular aperture, and "nearly" perfect local oscillator coherence;

(5) the LDF study for a Gaussian I_L, circular aperture, and perfect local oscillator coherence; and

(6) the LDF study for a rectangular I_L, circular aperture, and "nearly" perfect local oscillator coherence.

1. COMMUNICATIONS LINK STUDY

```
      DIMENSION  LN1(51),EXIFN(51),RA(8),EXCFL1(51),
     1           FNI(51,51),CFN(51,51)
      READ 5, A, THETA, PSI, (RA(K),  K = 1,8)
    5 FORMAT(F5.2,2F5.1,8F5.2)
      PRINT 6
    6 FORMAT(1H1)
      PRINT 10,A,THETA,PSI
   10 FORMAT(5H A =  F5.2,11H , THETA =  F5.1,9H , PSI =   F5.1///)
      PRINT 20
   20 FORMAT(55H      R       SIGPWR  IDEALSIGPWR   NOISEPWR   HETEFF
     1     SNR ///)
      DO 200 K = 1,8
      R = RA(K)
      PWRS = 0.0
      PWRN = 0.0
      PWRI = 0.0
      DELA = R**2 * 1.6E-3
      DO 50 I = 1,51
      LN1(I) = INT(SQRT(FLOAT(25**2 - (I-26)**2))+0.5)
      EXIFN(I) = EXP((-1.0)*(FLOAT(I-26)*R/25.0)**2/A**2)
      EXCFL1(I) = 1.0
   50 CONTINUE
      DO 60 I = 1,51
      L2 = LN1(I)
      L1 = (-1)*L2
      DO 60 J = L1, L2
   60 FNI(I,J+26) = EXIFN(I)*EXIFN(J+26)*DELA
      Y = (-1.0)*((R/25.0)**(1.666666))
      DO 70 I = 1,51
      DO 70 J = I,51
      CFN(I,J) = EXP(Y*((FLOAT((I-1)**2+(J-1)**2))**(0.833333)))
     1          *EXCFL1(I)*EXCFL1(J)
   70 CFN(J,I) = CFN(I,J)
      DU 100 I2 = -25, 25
      L2 = LN1(I2+26)
      L1 = (-1)*L2
      DO 100 J2 = L1,L2
      PWRN = PWRN + FNI(I2+26,J2+26)**2/DELA
      DO 100 I1 = -25, 25
      N2 = LN1(I1+26)
      N1 = (-1)*N2
      DO 100 J1 = N1,N2
      M1 = ABS(I1-I2)+1
      M2 = ABS(J1-J2)+1
      DELTAP = FNI(I1+26,J1+26)*FNI(I2+26,J2+26)
      PWRS = PWRS + DELTAP*CFN(M1,M2)
```

```
100 PWRI = PWRI + DELTAP
    HETEFF = PWRS/PWRI
    SNR = PWRS/PWRN
200 PRINT 30,R,PWRS,PWRI,PWRN,HETEFF,SNR
 30 FORMAT(2H  F5.2,2H  F7.3,4H     F7.3,6H        F7.3,3H   F5.3,
   1         2H  F7.3//)
    END
```

2. COMMUNICATIONS LINK STUDY

```
    DIMENSION  LN1(51),RA(8),EXCFL1(51),FNI(51,51),CFN(51,51)
    READ 5, A, THETA, PSI, (RA(K),  K = 1,8)
  5 FORMAT(F5.2,2F5.1,8F5.2)
    PRINT 6
  6 FORMAT(1H1)
    PRINT 10,A,THETA,PSI
 10 FORMAT(5H A =  F5.2,11H , THETA =  F5.1,9H , PSI =  F5.1///)
    PRINT 20
 20 FORMAT(55H   R      SIGPWR  IDEALSIGPWR   NOISEPWR  HETEFF
   1     SNR ///)
    DO 200 K = 1,8
    R = RA(K)
    PWRS = 0.0
    PWRN = 0.0
    PWRI = 0.0
    DELA = R**2 * 1.6E-3
    DO 50 I = 1,51
    LN1(I) = INT(SQRT(FLOAT(25**2 - (I-26)**2))+0.5)
    EXCFL1(I) = EXP((-1.0)*(FLOAT(I-1)*R/25.0)**2/((3.1)*A)**2)
 50 CONTINUE
    RADN = (25.0)*A/R
    DO 60 I = 1,51
    L2 = LN1(I)
    L1 = (-1)*L2
    DO 60 J = L1,L2
    RAD = SQRT((I-26)**2 + J**2)
    IF (RAD - RADN)  61,62,62
 61 FNI(I,J+26) = DELA
    GO TO 60
 62 FNI(I,J+26) = 0
 60 CONTINUE
    Y = (-1.0)*((R/25.0)**(1.666666))
    DO 70 I = 1,51
    DO 70 J = I,51
    CFN(I,J) = EXP(Y*((FLOAT((I-1)**2+(J-1)**2))**(0.833333)))
   1           *EXCFL1(I)*EXCFL1(J)
```

```
   70 CFN(J,I) = CFN(I,J)
      DO 100 I2 = -25, 25
      L2 = LN1(I2+26)
      L1 = (-1)*L2
      DO 100 J2 = L1,L2
      PWRN = PWRN + FNI(I2+26,J2+26)**2/DFI A
      DO 100 I1 = -25, 25
      N2 = LN1(I1+26)
      N1 = (-1)*N2
      DO 100 J1 = N1,N2
      M1 = ABS(I1-I2)+1
      M2 = ABS(J1-J2)+1
      DELTAP = FNI(I1+26,J1+26)*FNI(I2+26,J2+26)
      PWRS = PWRS + DELTAP*CFN(M1,M2)
  100 PWRI = PWRI + DELTAP
      HETEFF = PWRS/PWRI
      SNR = PWRS/PWRN
  200 PRINT 30,R,PWRS,PWRI,PWRN,HETEFF,SNR
   30 FORMAT(2H  F5.2,2H  F7.3,4H    F7.3,6H       F7.3,3H  F5.3,
     1      2H  F7.3//)
      END



                         3. LDSV STUDY


      DIMENSION  LN1(51),EXIFN(51),EXCFS1(51),EXCFS2(51),RA(8),
     1           FNI(51,51),CFN(51,51),EXCFL1(51)
      READ 5, A, THETA, PSI, (RA(K),  K = 1,8)
    5 FORMAT(F5.2,2F5.1,8F5.2)
      PRINT 6
    6 FORMAT(1H1)
      PRINT 10,A,THETA,PSI
   10 FORMAT(5H A =  F5.2,11H , THETA =  F5.1,9H , PSI =  F5.1///)
      PRINT 20
   20 FORMAT(55H     R      SIGPWR  IDEALSIGPWR   NOISEPWR   HETEFF
     1     SNR ///)
      DO 200 K = 1,8
      R = RA(K)
      ANGF = ((SIN((0.01745329)*(THETA+PSI)))**2)
     1       /((SIN((0.01745329)*PSI))**2)
      PWRS = 0.0
      PWRN = 0.0
      PWRI = 0.0
      DELA = R**2 * 1.6E-3
      DO 50 I = 1,51
      LN1(I) = INT(SQRT(FLOAT(25**2 - (I-26)**2)*ANGF) + 0.5)
      EXIFN(I) = EXP((-1.0)*(FLOAT(I-26)*R/25.0)**2/A**2)
```

```
      EXCFS1(I) = EXP((-0.5)*(FLOAT(I-1)*R/25.0)**2 * ANGF)
      EXCFS2(I) = EXP((-0.5)*(FLOAT(I-1)*R/25.0)**2)
      EXCFL1(I) = 1.0
   50 CONTINUE
      DO 60 I = 1,51
      L2 = LN1(I)
      L1 = (-1)*L2
      DO 60 J = L1, L2
   60 FNI(I,J+26) = EXIFN(I)*EXIFN(J+26)*DFLA
      DO 70 I = 1,51
      DO 70 J = 1,51
   70 CFN(I,J) = EXCFL1(I)*EXCFL1(J)*EXCFS1(I)*EXCFS2(J)
      DO 100 I2 = -25, 25
      L2 = LN1(I2+26)
      L1 = (-1)*L2
      DO 100 J2 = L1,L2
      PWRN = PWRN + FNI(I2+26,J2+26)**2/DFIA
      DO 100 I1 = -25, 25
      N2 = LN1(I1+26)
      N1 = (-1)*N2
      DO 100 J1 = N1,N2
      M1 = ABS(I1-I2)+1
      M2 = ABS(J1-J2)+1
      DELTAP = FNI(I1+26,J1+26)*FNI(I2+26,J2+26)
      PWRS = PWRS + DELTAP*CFN(M1,M2)
  100 PWRI = PWRI + DELTAP
      HETEFF = PWRS/PWRI
      SNR = PWRS/PWRN
  200 PRINT 30,R,PWRS,PWRI,PWRN,HETEFF,SNR
   30 FORMAT(2H  F5.2,2H  F7.3,4H     F7.3,6H        F7.3,3H   F5.3,
     1        2H  F7.3//)
      END
```

4. LOSv STUDY

```
      DIMENSION  LN1(51),EXCFS1(51),EXCFS2(51),RA(8),
     1           FNI(51,51),CFN(51,51),EXCFL1(51)
      READ 5, A, THETA, PSI, (RA(K),  K = 1,8)
    5 FORMAT(F5.2,2F5.1,8F5.2)
      PRINT 6
    6 FORMAT(1H1)
      PRINT 10,A, THETA, PSI
   10 FORMAT(5H A =  F5.2,11H , THETA =  F5.1,9H , PSI =  F5.1///)
      PRINT 20
   20 FORMAT(55H     R     SIGPWR  IDEALSIGPWR   NOISEPWR   HETEFF
     1     SNR ///)
```

```
      DO 200 K = 1,8
      R = RA(K)
      ANGF = ((SIN((0.01745329)*(THETA+PSI)))**2)
     1           /((SIN((0.01745329)*PSI))**2)
      PWRS = 0.0
      PWRN = 0.0
      PWRI = 0.0
      DELA = R**2 * 1.6E-3
      DO 50 I = 1,51
      LN1(I) = INT(SQRT(FLOAT(25**2 - (I-26)**2)) + 0.5)
      EXCFS1(I) = EXP((-0.5)*(FLOAT(I-1)*R/25.0)**2 * ANGF)
      EXCFS2(I) = EXP((-0.5)*(FLOAT(I-1)*R/25.0)**2)
      EXCFL1(I) = EXP((-1.0)*(FLOAT(I-1)*R/25.0)**2/((3.1)*A)**2)
   50 CONTINUE
      RADN = (25.0)*A/R
      DO 60 I = 1,51
      L2 = LN1(I)
      L1 = (-1)*L2
      DO 60 J = L1, L2
      RAD = SQRT((I-26)**2 + J**2)
      IF (RAD - RADN) 61,62,62
   61 FNI(I,J+26) = DELA
      GO TO 60
   62 FNI(I,J+26) = 0
   60 CONTINUE
      DO 70 I = 1,51
      DO 70 J = 1,51
   70 CFN(I,J) = EXCFL1(I)*EXCFL1(J)*EXCFS1(I)*EXCFS2(J)
      DO 100 I2 = -25, 25
      L2 = LN1(I2+26)
      L1 = (-1)*L2
      DO 100 J2 = L1,L2
      PWRN = PWRN + FNI(I2+26,J2+26)**2/DELA
      DO 100 I1 = -25, 25
      N2 = LN1(I1+26)
      N1 = (-1)*N2
      DO 100 J1 = N1,N2
      M1 = ABS(I1-I2)+1
      M2 = ABS(J1-J2)+1
      DELTAP = FNI(I1+26,J1+26)*FNI(I2+26,J2+26)
      PWRS = PWRS + DELTAP*CFN(M1,M2)
  100 PWRI = PWRI + DELTAP
      HETEFF = PWRS/PWRI
      SNR = PWRS/PWRN
  200 PRINT 30, R, PWRS, PWRI, PWRN, HETEFF, SNR
   30 FORMAT(2H  F5.2,2H  F7.3,4H    F7.3,6H      F7.3,3H  F5.3,
     1        2H  F7.3//)
      END
```

```
                         5. LDF STUDY
      DIMENSION   LN1(51),EXIFN(51),EXCFS1(51),EXCFS2(51),RA(8),
     1            FNI(51,51),CFN(51,51),EXCFL1(51)
      READ 5, A, THETA, PSI, (RA(K),  K = 1,8)
    5 FORMAT(F5.2,2F5.1,8F5.2)
      PRINT 6
    6 FORMAT(1H1)
      PRINT 10,A, THETA, PSI
   10 FORMAT(5H A =  F5.2,11H , THETA =  F5.1,9H , PSI =   F5.1///)
      PRINT 20
   20 FORMAT(55H     R        SIGPWR   IDEALSIGPWR    NOISEPWR   HETEFF
     1     SNR ///)
      DO 200 K = 1,8
      R = RA(K)
      ANGF = COS((0.01745329)*THETA)**2
      STHETA = SIN((0.01745329)*THETA)
      PWRS = 0.0
      PWRN = 0.0
      PWRI = 0.0
      DELA = R**2 * 1.6E-3
      DO 50 I = 1,51
      LN1(I) = INT(SQRT(FLOAT(25**2 - (I-26)**2))+0.5)
      EXIFN(I) = EXP((-1.0)*(FLOAT(I-26)*R/25.0)**2/A**2)
      IF (I-1)  40,40,41
   40 EXCFS1(1) = 1.0
      GO TO 42
   41 EXCFS1(I) = EXP((-0.5)*(FLOAT(I-1)*R/25.0)**2*ANGF)*
     1    SIN((10.0)*STHETA*FLOAT(I-1)*R/25.0)/((10.0)*STHETA*
     2    FLOAT(I-1)*R/25.0)
   42 CONTINUE
      EXCFS2(I) = EXP((-0.5)*(FLOAT(I-1)*R/25.0)**2)
      EXCFL1(I) = 1.0
   50 CONTINUE
      DO 60 I = 1,51
      L2 = LN1(I)
      L1 = (-1)*L2
      DO 60 J = L1, L2
   60 FNI(I,J+26) = EXIFN(I)*EXIFN(J+26)*DELA
      DO 70 I = 1,51
      DO 70 J = 1,51
   70 CFN(I,J) = EXCFL1(I)*EXCFL1(J)*EXCFS1(I)*EXCFS2(J)
      DO 100 I2 = -25, 25
      L2 = LN1(I2+26)
      L1 = (-1)*L2
      DO 100 J2 = L1,L2
      PWRN = PWRN + FNI(I2+26,J2+26)**2/DELA
      DO 100 I1 = -25, 25
```

```
      N2 = LN1(I1+26)
      N1 = (-1)*N2
      DO 100 J1 = N1,N2
      M1 = ABS(I1-I2)+1
      M2 = ABS(J1-J2)+1
      DELTAP = FNI(I1+26,J1+26)*FNI(I2+26,J2+26)
      PWRS = PWRS + DELTAP*CFN(M1,M2)
100   PWRI = PWRI + DELTAP
      HETEFF = PWRS/PWRI
      SNR = PWRS/PWRN
200   PRINT 30, R, PWRS, PWRI, PWRN, HETEFF, SNR
30    FORMAT(2H  F5.2,2H  F7.3,4H     F7.3,6H       F7.3,3H   F5.3,
     1          2H  F7.3//)
      END
```

6. LDF STUDY

```
      DIMENSION   LN1(51),EXCFS1(51),EXCFS2(51),RA(8),
     1            FNI(51,51),CFN(51,51),EXCFL1(51)
      READ 5, A, THETA, PSI, (RA(K),  K = 1,8)
5     FORMAT(F5.2,2F5.1,8F5.2)
      PRINT 6
6     FORMAT(1H1)
      PRINT 10,A,THETA,PSI
10    FORMAT(5H A =   F5.2,11H , THETA =  F5.1,9H , PSI =  F5.1///)
      PRINT 20
20    FORMAT(55H    R      SIGPWR  IDEALSIGPWR   NOISEPWR   HETEFF
     1     SNR ///)
      DO 200 K = 1,8
      R = RA(K)
      ANGF = COS((0.01745329)*THETA)**2
      STHETA = SIN((0.01745329)*THETA)
      PWRS = 0.0
      PWRN = 0.0
      PWRI = 0.0
      DELA = R**2 * 1.6E-3
      DO 50 I = 1,51
      LN1(I) = INT(SQRT(FLOAT(25**2 - (I-26)**2))+0.5)
      IF (I-1) 40,40,41
40    EXCFS1(1) = 1.0
      GO TO 42
41    EXCFS1(I) = EXP((-0.5)*(FLOAT(I-1)*R/25.0)**2*ANGF)*
     1     SIN((10.0)*STHETA*FLOAT(I-1)*R/25.0)/((10.0)*STHETA*
     2     FLOAT(I-1)*R/25.0)
42    CONTINUE
```

```
      EXCFS2(I) = EXP((-0.5)*(FLOAT(I-1)*R/25.0)**2)
      EXCFL1(I) = EXP((-1.0)*(FLOAT(I-1)*R/25.0)**2/((3.1)*A)**2)
   50 CONTINUE
      RADN = (25.0)*A/R
      DO 60 I = 1,51
      L2 = LN1(I)
      L1 = (-1)*L2
      DO 60 J = L1,L2
      RAD = SQRT((I-26)**2 + J**2)
      IF (RAD - RADN)  61,62,62
   61 FNI(I,J+26) = DELA
      GO TO 60
   62 FNI(I,J+26) = 0
   60 CONTINUE
      DO 70 I = 1,51
      DO 70 J = 1,51
   70 CFN(I,J) = EXCFL1(I)*EXCFL1(J)*EXCFS1(I)*EXCFS2(J)
      DO 100 I2 = -25, 25
      L2 = LN1(I2+26)
      L1 = (-1)*L2
      DO 100 J2 = L1,L2
      PWRN = PWRN + FNI(I2+26,J2+26)**2/DELA
      DO 100 I1 = -25, 25
      N2 = LN1(I1+26)
      N1 = (-1)*N2
      DO 100 J1 = N1,N2
      M1 = ABS(I1-I2)+1
      M2 = ABS(J1-J2)+1
      DELTAP = FNI(I1+26,J1+26)*FNI(I2+26,J2+26)
      PWRS = PWRS + DELTAP*CFN(M1,M2)
  100 PWRI = PWRI + DELTAP
      HETEFF = PWRS/PWRI
      SNR = PWRS/PWRN
  200 PRINT 30,R,PWRS,PWRI,PWRN,HETEFF,SNR
   30 FORMAT(2H  F5.2,2H  F7.3,4H     F7.3,6H        F7.3,3H   F5.3,
     1         2H  F7.3//)
      END
```

APPENDIX II

A STATISTICAL DESCRIPTION OF THE FIELD SCATTERED

FROM A RANDOM COLLECTION OF SCATTERERS[*]

In this appendix, the statistical description of a coherent
field scattered from a three dimensional random distribution of
particles is discussed and the correlation function for the field is
derived. This topic has been discussed previously; Twersky[34] presents
a general but very tedious approach to the problem valid regardless
of particle concentration. In most cases, however, the concentration
is assumed large so that Gaussian statistics may be used. In the last
two examples presented in the thesis, the large concentration assump-
tion is not always valid, particularly in the LDF system where the
average number of particles in the scattering region is quite small.
A more general approach is, therefore, taken.

In this thesis, the scattering particles are assumed to be
distributed at random in a Poisson way; that is, the probability
of finding N particles in a volume V is given by

$$P(N,V) = \frac{(MV)^N}{N!} e^{-(MV)}$$

[*]Preliminary phases of this work were done jointly with W. T.
Mayo.[26]

where M is the average number of particles per unit volume and is a
constant. The position of each particle is completely independent of
all the others.

In addition, single scattering results are used; any fields
present due to multiple scattering are neglected. The scattering
particle size is uniform; the field scattered by each particle is also
assumed to be linearly polarized. The scattered field at a point $\bar{R}$ is,
therefore, given by

$$E_s(\bar{R}) = \sum_{k}^{\substack{\text{all}\\\text{particles}}} E_{s_k}(\bar{r}_k, \bar{R}),$$

where $E_{s_k}(\bar{r}_k, \bar{R})$ is the field at $\bar{R}$ due scattering from the kth particle
located at $\bar{r}_k$.

The correlation between variation in the field at points $\bar{R}_1$ and
$\bar{R}_2$ is given by

$$\Gamma_s(\bar{R}_1, \bar{R}_2) = E[E_s(\bar{R}_1)E_s^*(\bar{R}_2)]$$

$$= E[\sum_i \sum_j E_{s_i}(\bar{r}_1, \bar{R}_1)E_{sj}^*(\bar{r}_j, \bar{R}_2)]$$

$$= E[\sum_k E_{s_k}(\bar{r}_k, \bar{R}_1)E_{s_k}^*(\bar{r}_k, \bar{R}_2)]$$

$$+ E[\sum_{i \neq j} \sum E_{s_i}(\bar{r}_i, \bar{R}_1)E_{s_j}(\bar{r}_j, \bar{R}_2)].$$

For a Gaussian incident field, the scattering will be confined for the

most part to some particular region. Now consider a larger but finite

volume V. At some time t_1, this volume contains n particles (a dis-

crete random variable from system to system in the ensemble of all pos-

sible system) with a probability of P(n). The correlation function for

this case is

$$\Gamma_s(\bar{R}_1,\bar{R}_2) = E[E_s(\bar{R}_1)E_s^*(\bar{R}_2)|n]$$

$$= E[\sum_{k=1}^{n} E_{s_k}(\bar{r}_k,\bar{R}_1)E_{s_k}^*(\bar{r}_k,\bar{R}_2)]$$

$$+ E[\sum_{k\neq}^{n}\sum_{j=1}^{n} E_{s_i}(\bar{r}_i,\bar{R}_1)E_{s_j}^*(\bar{r}_j,\bar{R}_2)]$$

$$= \sum_{k=1}^{n} E[E_{s_k}(\bar{r}_k,\bar{R}_1)E_{s_k}^*(\bar{r}_k,\bar{R}_2)]$$

$$+ \sum_{i\neq}^{n}\sum_{j=1}^{n} E[E_{s_i}(\bar{r}_i,\bar{R}_1)E_{s_j}^*(\bar{r}_j,\bar{R}_2)]. \qquad \text{(A-1)}$$

Consider for the moment the average

$$E[E_{s_k}(\bar{r}_k,R_1)E_{s_k}^*(\bar{r}_k,R_2)] = \int_V E_{s_k}(\bar{r},\bar{R}_1)E_{s_k}^*(\bar{r},\bar{R}_2)p(\bar{r})dV,$$

where $p(\bar{r})$ is the probability density function for $\bar{r}$ in the volume

V. Since each particle is distributed completely at random in the

volume, the probability of finding the kth particle in a volume element

dV_k is given by

$$P(\bar{r}_k \in dV) = p(\bar{r})dV = \frac{dV}{V},$$

so that

$$p(\bar{r}) = \frac{1}{V}.$$

This average, therefore, becomes

$$E[E_{s_k}(\bar{r}_k,\bar{R}_1)E_{s_k}^*(\bar{r}_k,\bar{R}_2)] = \frac{1}{V}\int_V E_{s_k}(\bar{r},\bar{R}_1)E_{s_k}^*(\bar{r},\bar{R}_2)dV \qquad (A-2)$$

and is independent of k since the particle size is uniform. Next consider the average.

$$E[E_{s_i}(\bar{r}_i,\bar{R}_1)E_{s_j}^*(\bar{r}_j,\bar{R}_2)]_{i\neq j} = \int_V \int_{V'} E_{s_i}(\bar{r},\bar{R}_1)E_{s_j}^*(\bar{r}',\bar{R}_2)p(\bar{r},\bar{r}')dVdV',$$

where $p(\bar{r},\bar{r}')$ is the joint density function for $\bar{r}$ and $\bar{r}'$ in $V = V'$. Since the position of each particle is completely independent of all the others, we have

$$p(\bar{r},\bar{r}') = p(\bar{r})p(\bar{r}') = \frac{1}{V^2},$$

so that

$$E[E_{s_i}(\bar{r}_i,\bar{R}_1)E_{s_j}^*(\bar{r}_j,\bar{R}_2)] = \frac{1}{V^2}\int_V \int_{V'} E_{s_i}(\bar{r},\bar{R}_1)E_{s_j}^*(\bar{r}',R_2)dVdV'$$

$$= \frac{1}{V^2}\int_V E_{s_k}(\bar{r},\bar{R}_1)dV \int_V E_{s_k}^*(\bar{r},\bar{R}_2)dV, \qquad (A-3)$$

and is independent of i and j since the particle size is uniform.

Using equation A-2 and A-3 in A-1, we get

$$E[E_s(\bar{R}_1)E_s^*(\bar{R}_2)|n] = \frac{n}{V} \int_V E_{s_k}(\bar{r},R_1)E_{s_k}^*(\bar{r},\bar{R}_2)dV$$

$$+ \frac{(n^2-n)}{V^2} \int_V E_{s_k}(\bar{r},\bar{R}_1)dV \int_V E_{s_k}^*(\bar{r},\bar{R}_2)dV.$$

Since the number of scatterers is independent of their positions, we have

$$\Gamma_s(\bar{R}_1,\bar{R}_2) = E[E_s(\bar{R}_1)E_s^*(\bar{R}_2)]$$

$$= \sum_{n=1}^{\infty} E[E_s(\bar{R}_1)E_s^*(\bar{R}_2)|n]P(n)$$

$$= \sum_{n=1}^{\infty} nP(n) \frac{1}{V} \int_V E_{s_k}(\bar{r},\bar{R}_1)E_{s_k}^*(\bar{r},\bar{R}_2)dV$$

$$+ \sum_{n=1}^{\infty} (n^2-n)P(n) \frac{1}{V^2} \int_V E_{s_k}(\bar{r},\bar{R}_1)dV \int_V E_{s_k}^*(\bar{r},\bar{R}_2)dV$$

$$= \frac{E[n]}{V} \int_V E_{s_k}(\bar{r},\bar{R}_1)E_{s_k}^*(\bar{r},\bar{R}_1)dV$$

$$+ \frac{E[n]^2}{V^2} \int_V E_{s_k}(\bar{r},\bar{R}_1)dV \int_V E_{s_k}^*(\bar{r},\bar{R}_2)dV$$

$$= M \int_V E_{s_k}(\bar{r},\bar{R}_1)E_{s_k}^*(\bar{r},\bar{R}_2)dV$$

$$+ M^2 \int_V E_{s_k}(\bar{r},\bar{R}_1)dV \int_V E^{*}_{s_k}(\bar{r},\bar{R}_2)dV.$$

Letting V increase adds only a negligible amount to the integrals so we have

$$\Gamma_s(\bar{R}_1,\bar{R}_2) = M \int_{\text{all space}} E_{s_k}(\bar{r},\bar{R}_1)E^{*}_{s_k}(\bar{r},\bar{R}_2)dV$$

$$+ M^2 \int_{\text{all space}} E_{s_k}(\bar{r},\bar{R}_1)dV \int_{\text{all space}} E^{*}_{s_k}(\bar{r},\bar{R}_2)dV. \quad (A-4)$$

Equation A-4 in terms of the complex envelope of E_{s_k} is

$$\Gamma_s(\bar{R}_1,\bar{R}_2) = M \int_{\text{all space}} A_{s_k}(\bar{r},\bar{R}_1)A^{*}_{s_k}(\bar{r},\bar{R}_2)dV$$

$$+ M^2 \int_{\text{all space}} A_{s_k}(\bar{r},\bar{R}_1)dV \int_{\text{all space}} A^{*}_{s_k}(\bar{r},\bar{R}_2)dV.$$

Consider the relative magnitude of the two terms in this equation. The phase term in the integrand of the first integral is proportional to the difference in distance from $\bar{r}$ to $\bar{R}_1$ to $\bar{r}$ to $\bar{R}_2$. The phase term in each of the integrand of the integrals in the second term are pro- portional to distance from $\bar{r}$ to $\bar{R}_1$ and $\bar{r}$ to $\bar{R}_2$. Over the region of $\bar{r}$ where the magnitude of E_s is significantly greater than zero, the phase of the first integrand varies only over a few cycles so that the magnitude varies a great deal over a single cycle. The integral over one cycle will, therefore, be nonzero. The phase of the second

term varies over many cycles, however, so the magnitude does not change significantly over a single cycle. The integral over one cycle will, therefore, be approximately zero. The second term, then, will be much less in value than the first so it adds little to the correlation function. Equation A-4 thus becomes

$$\Gamma_s(\bar{R}_1,\bar{R}_2) \cong M \int_{all\ space} E_{s_k}(\bar{r},\bar{R}_1) E_{s_k}^*(\bar{r},\bar{R}_2) dV \qquad (A-5)$$

If the scattering particles are confined to a plane, the correlation function is given by

$$\Gamma_s(\bar{R}_1,\bar{R}_2) \cong M \int_{scattering\ plane} E_{s_k}(\bar{r},\bar{R}_1) E_{s_k}^*(\bar{r},\bar{R}_2) dV$$

where M is the average number of particles per unit area.

Next consider a single system and look at $E_s(\bar{R}_1) E_s^*(\bar{R}_2)$ at many time instances t_1, t_2, etc. The average over a larger and larger number of these specific time instances approaches the infinite time average. At each time instance, we see a random number of particles in the volume V at random location. For a large number of time instances, it is reasonable to expect to see almost all the members of the ensemble of all possible configurations of particles in V at some time t_1. The average over all possible time instances and the average over all members of the ensemble will, therefore, be equal; i.e. the system is stationary and ergodic.

APPENDIX III

THE EFFECTS OF A POLYDISPERSION OF SCATTERING PARTICLES

ON THE CORRELATION FUNCTION FOR THE SCATTERED FIELD

In this appendix, the effects of relaxing the monodispersion requirement on the scattering particles is considered. The correlation function for the field scattered from a polydispersed collection of spherical particles is calculated.

The scattered field in some fixed direction from each particle will be a function of particle diameter a_k denoted by $m(a_k)$. The function m is also a function of direction of scattering but as long as most of the scattering takes place over a small region, the field at some point R will be essentially constant and m is independent of scattering angle. Under these conditions, the total scattered field at $\bar{R}$ is given by

$$E_s(\bar{R}) = \sum_k m(a_k) E_{s_k}(\bar{r}_k, \bar{R}),$$

where E_{s_k} is the scattered field from a particle of referenced diameter, i.e. m = 1. The diameter of each particle is a random variable independent of particle position.

The correlation function for the field is given by

$$\Gamma_s(\bar{R}_1, \bar{R}_2) = E[E_s(\bar{R}_1) E_s^*(\bar{R}_2)]$$

$$= E[\sum_i \sum_j m(a_i)m^*(a_j)E_{s_i}(\bar{r}_i,\bar{R}_1)E_{s_j}^*(\bar{r}_j,\bar{R}_2)]$$

$$= E[\sum_k |m(a_k)|^2 E_{s_k}(\bar{r}_k,R_1)E_{s_k}^*(\bar{r}_k,\bar{R}_2)]$$

$$+ E[\sum_{i \neq j} \sum m(a_i)m^*(a_j)E_{s_i}(\bar{r}_i,\bar{R}_1)E_{s_j}^*(\bar{r}_j,\bar{R}_2)]$$

In Appendix II, the second term is shown to be negligible with respect to the first terms so

$$\Gamma_s(\bar{R}_1,\bar{R}_2) \doteq E[\sum_k |m(a_k)|^2 E_{s_k}(\bar{r}_k,\bar{R}_1)E_{s_k}^*(\bar{r}_k,\bar{R}_2)]$$

Consider again a large volume V from which essentially all the scattering takes place. At some time t_1, it contains n particles. In this case

$$\Gamma_s(\bar{R}_1,\bar{R}_2) = E[E_s(\bar{R}_1)E_s^*(\bar{R}_2)|n]$$

$$= \sum_{k=1}^{n} E[|m(a_k)|^2 E_{s_k}(\bar{r}_k,\bar{R}_1)E_{s_k}^*(\bar{r}_k,\bar{R}_2)]$$

Using the results developed in Appendix II and the fact that a_k and $\bar{r}_k$ are independent, we have

$$E[|m(a_k)|^2 E_{s_k}(\bar{r}_k,\bar{R}_1)E_{s_k}^*(\bar{r}_k,\bar{R}_2)]$$

$$= E[|m(a_k)|^2]E[E_{s_k}(\bar{r}_k,\bar{R}_1)E_{s_k}^*(\bar{r}_k,\bar{R}_2)]$$

$$= \frac{1}{V} \int_{\text{all } a} |m(a)|^2 p(a)da \int_V E_{s_k}(\bar{r},\bar{R}_1)E^*_{s_k}(\bar{r},\bar{R}_2)dV$$

where p(a) is the probability density function for the particle diameters.

Averaging over the number of particles in V, we get

$$\Gamma_S(\bar{R}_1,\bar{R}_2) = \sum_{n=1}^{\infty} E[E_s(\bar{R}_1)E^*_s(\bar{R}_2)|n]P(n)$$

$$= \sum_{n=1}^{\infty} \sum_{k=1}^{n} E[|m(a)|^2]E[E_{s_k}(\bar{r}_k,\bar{R}_1)E^*_{s_k}(\bar{r}_k,\bar{R}_2)]P(n)$$

$$= \sum_{n=1}^{\infty} nP(n)E[|m(a)|^2]E[E_{s_k}(\bar{r}_k,\bar{R}_1)E^*_{s_k}(\bar{r}_k,\bar{R}_2)]$$

$$= E[n]E[|m(a)|^2]E[E_{s_k}(\bar{r}_k,\bar{R}_1)E^*_{s_k}(\bar{r}_k,\bar{R}_2)]$$

$$= \frac{E[n]}{V} E[|m(a)|^2] \int_V E_{s_k}(\bar{r},\bar{R}_1)E^*_{s_k}(\bar{r},\bar{R}_2)dV$$

$$= ME[|m(a)|^2] \int_V E_{s_k}(\bar{r},\bar{R}_1)E^*_{s_k}(\bar{r},\bar{R}_2)dV$$

Again, letting V approach infinity, we get

$$\Gamma_s(\bar{R}_1,\bar{R}_2) = ME[|m(a)|^2] \int_{\text{all space}} E_{s_k}(\bar{r},\bar{R}_1)E^*_{s_k}(\bar{r},\bar{R}_2)dV \qquad (A-6)$$

In normalized form, the correlation function is given by

$$\gamma_s(\bar{R}_2,\bar{R}_2) = \frac{\Gamma_s(\bar{R}_1,\bar{R}_2)}{[\Gamma_s(\bar{R}_1,\bar{R}_1)\Gamma_s(\bar{R}_2,\bar{R}_2)]^{\frac{1}{2}}}$$

$$\frac{ME[|m(a)|^2]\int E_{s_k}(\bar{r},\bar{R}_1)E_{s_k}^*(\bar{r},\bar{R}_2)dV}{ME[|m(a)|^2][\int E_{s_k}(\bar{r},\bar{R}_1)E_{s_k}^*(\bar{r},\bar{R}_1)dV \int E_{s_k}(\bar{r},\bar{R}_2)E_{s_k}^*(\bar{r},\bar{R}_2)dV]^{\frac{1}{2}}}$$

This last expression when $E[|m(a)|^2]$ is divided out is just the normalized correlation function for a monodispersed distribution. Under the stated conditions, the normalized correlation function (degree of coherence) for a polydispersed system is the same as a monodispersed system.

BIBLIOGRAPHY

1. M. Born and E. Wolf, *Principles of Optics*, Pergamon Press, New York, N. Y., 1964.

2. L. Mandel and E. Wolf, "Coherence Properties of Optical Fields," *Reviews of Modern Physics*, *37*, 291, April, 1965.

3. M. Beran and G. B. Parent, *Theory of Partial Coherence*, Prentice Hall, Inc., 1964.

4. R. M. Fano, L. J. Chu, and R. B. Adler, *Electromagnetic Fields, Energy, and Forces*, John Wiley and Sons, New York, N. Y., 1963.

5. D. L. Fried, "Optical Heterodyne Detection of an Atmospherically Distorted Signal Wave Front," *Proceedings of the IEEE*, *55*, 57, January, 1967.

6. S. Gardner, "Some Effects of Atmospheric Turbulence on Optical Heterodyne Communications," *1964 IEEE International Convention Record*, *12*, Part 6, 337.

7. V. J. Corcoran and Y. Pao, "Detection of Laser Radiation," *Journal of the Optical Society of America*, *52*, 1341, December, 1962.

8. C. Q. Lee, "B. An Investigation of Photoelectrically Heterodyning Coherent Light," Astrionics Research and Development Report No. 2, p. 92.

9. J. W. Foreman, Jr., A personal discussion at Brown Engineering, Huntsville, Alabama, December, 1966.

10. I. T. T. Federal Laboratories Staff, "Coherent Optical Propagation Study," Rome Air Development Center Report No. RADC-TR-65-313, November, 1965.

11. M. P. Warden, "Experimental Study of the Theory of Optical Superheterodyne Reception," *Proceedings of the IEEE*, *133*, 997, June, 1966.

12. V. J. Corcoran, "Directional Characteristics in Optical Heterodyne Detection Processes, I and II," *Journal of Applied Physics*, *36*, 1819, June, 1965, and *38*, 3117, July, 1967.

13. A. E. Siegman, "The Antenna Properties of Optical Heterodyne Receivers," *Proceedings of the IEEE, 54,* 1350, October, 1966.

14. B. M. Oliver, "Thermal and Quantum Noise," *Proceedings of the IEEE, 53,* 37, May, 1965.

15. R. D. Rosner, "Performance of an Optical Heterodyne Receiver for Various Receiving Apertures," *IEEE Transactions on Antennas and Propagation, AP-17,* 324, May, 1969.

16. A. Kolmogoroff, in *Turbulence, Classic Papers on Statistical Theory,* S. K. Friedlander and L. Topper, Eds., Interscience, New York, N. Y., 1961, p. 151.

17. V. I. Tatarski, *Wave Propagation in a Turbulent Medium,* McGraw-Hill, New York, N. Y., 1961.

18. R. D. Kroeger, "Motion Sensing by Optical Heterodyne Doppler Detection from Diffuse Surfaces," *Proceedings of the IEEE, 53,* 211, February, 1965.

19. M. C. Teich, "Homodyne Detection of Infrared Radiation from a Moving Diffuse Target," *Proceedings of the IEEE, 57,* 786, May, 1969.

20. J. W. Foreman, Jr., E. W. George, J. L. Jetton, R. D. Lewis, J. R. Thornton, and H. J. Watson, "Fluid Flow Measurements with a Laser Doppler Velocimeter," *IEEE Journal of Quantum Electronics, QE-2,* 260, August, 1966.

21. H. Kogelnik and T. Li, "Laser Beams and Resonators," *Proceedings of the IEEE, 54,* 1312, October, 1966.

22. Y. Yeh and H. Z. Cummins, Localized Fluid Flow Measurements with an He-Ne Laser Spectrometer," *Applied Physics Letters, 4,* 176, May 15, 1964.

23. J. W. Foreman, Jr., E. W. George, and R. D. Lewis, "Measurements of Localized Flow Velocities in Gases with a Laser Doppler Flow-meter," *Applied Physics Letters, 7,* 77, August 15, 1965.

24. J. W. Foreman, Jr., R. D. Lewis, J. R. Thornton, and H. J. Watson, "Laser Doppler Velocimeter for Measurements of Local Flow Veloci-ties in Liquids," *Proceedings of the IEEE, 54,* 424, March, 1966.

25. E. Rolfe, J. K. Silk, S. Booth, K. Meister, and R. M. Young, "Laser Doppler Velocity Instrument," NASA Report CR-119.

26. W. T. Mayo, Jr., "Laser Doppler Flowmeters--A Spectral Analysis," Ph.D. Thesis, Georgia Institute of Technology, May, 1969.

27. N. E. Welch and W. T. Tomme, "The Analysis of Turbulence from Data Obtained with a Laser Velocimeter," AIAA Fifth Aerospace Sciences Meeting, New York, N. Y., January 23-26, 1967.

28. R. J. Goldstein and D. K. Kreid, "Measurement of Laminar Flow Development in a Square Duct Using a Laser-Doppler Flowmeter," *Journal of Applied Mechanics, 34,* 813, December, 1967.

29. R. J. Goldstein and W. F. Hagen, "Turbulent Flow Measurements Utilizing the Doppler Shift of Scattered Laser Radiation," *The Physics of Fluids, 10,* 1349, June, 1967.

30. J. W. Foreman, Jr., "Optical Path Length Difference Effects in Photomixing with Multimode Gas Laser Radiation," *Applied Optics, 6,* 821, May, 1967.

31. A. C. Holland and J. S. Draper, "Analytical and Experimental Investigation of Light Scattering from Polydispersions of Mie Particles," *Applied Optics, 6,* 511, March, 1967.

32. H. Z. Cummins, N. Knable, and Y. Yeh, "Observation of Diffusion Broadening of Rayleigh Scattered Light," *Physical Review Letters, 12,* 150, February 10, 1964.

33. G. A. Korn and T. M. Korn, *Mathematical Handbook for Scientists and Engineers,* McGraw-Hill, New York, N.Y., 1961.

34. V. Twersky, "Signals, Scatterers, and Statistics," *IEEE Transactions on Antennas and Propagation,* AP-11, 688, November, 1963.

VITA

Charles Franklin Morris, Jr. was born in Century, Florida, on July 30, 1942. He is the son of the late Charles Franklin Morris and Ruth McPhail Morris. He was married to Elizabeth Brahm of LaGrange, Georgia, on September 12, 1964 and has one daughter, Martha Marie.

He attended public schools in Jay, Milton, and Tallahassee, Florida, and he graduated from Florida High School in Tallahassee in 1960. He attended Florida State University from 1960 to 1962, then transferred to Georgia Institute of Technology, where he received his B.E.E. Degree in 1964 and M.S.E.E. Degree in 1965. He is a member of Eta Kappa Nu and Tau Beta Pi.

He held a NASA fellowship for the first three years of graduate school, and from September, 1967, until December, 1969, he held a Graduate Teaching/Research Assistantship in the School of Electrical Engineering, Georgia Tech.